AD-A243 991 BEST AVAILABLE COPY

SECURITY CLASSIFICATION OF THIS PAGE

REPORT DOCUMENTATION PAGE

DEC 2 6 1991

1a. REPORT SECURITY CLASSIFICATION: Unclassified	1b. RESTRICTIVE MARKINGS: None
2a. SECURITY CLASSIFICATION AUTHORITY	3. DISTRIBUTION/AVAILABILITY OF REPORT: Unclassified; Approved for public release; distribution unlimited
2b. DECLASSIFICATION/DOWNGRADING SCHEDULE	
4. PERFORMING ORGANIZATION REPORT NUMBER(S): ISI Report #5733-05	5. MONITORING ORGANIZATION REPORT NUMBER(S): AFOSR-TR- 91 0971
6a. NAME OF PERFORMING ORGANIZATION: Integrated Systems Inc.	6b. OFFICE SYMBOL (If applicable):
7a. NAME OF MONITORING ORGANIZATION: USAF, AFOSR	
6c. ADDRESS (City, State and ZIP Code): 3260 Jay Street, Santa Clara, CA 95054	7b. ADDRESS (City, State and ZIP Code): Building 410, Bolling AFB, DC 20332
8a. NAME OF FUNDING/SPONSORING ORGANIZATION: AFOSR	8b. OFFICE SYMBOL (If applicable): NM
9. PROCUREMENT INSTRUMENT IDENTIFICATION NUMBER: F49620-88-C-0012	
8c. ADDRESS (City, State and ZIP Code): Bolling AFB, DC 20332 AFOSR/NM Bolling AFB DC 20332-6448	10. SOURCE OF FUNDING NOS. — PROGRAM ELEMENT NO.: 61102F; PROJECT NO.: 2312; TASK NO.: A1; WORK UNIT NO.:
11. TITLE (Include Security Classification): Adaptive and Non-Linear Control for Rapid Maneuvering of Flexible Structures	
12. PERSONAL AUTHOR(S): Robert L. Kosut, Guntekin M. Kabuli	
13a. TYPE OF REPORT: Final Report	13b. TIME COVERED: FROM 9/87 TO 6/91
14. DATE OF REPORT (Yr., Mo., Day): 1 Oct, 1991	15. PAGE COUNT:
16. SUPPLEMENTARY NOTATION	

17. COSATI CODES			18. SUBJECT TERMS (Continue on reverse if necessary and identify by block number)
FIELD	GROUP	SUB. GR.	

19. ABSTRACT (Continue on reverse if necessary and identify by block number)

This report describes research results on the design of feedback controllers for rapid slewing of flexible space structures, such as optical tracking systems. Two approaches evolved during this research. The first approach modifies the exact rigid-body time-optimal control as to account for chattering near zero tracking error and robustness to flexible modes close to the controller bandwidth. Efforts to make this controller adaptive are also presented. The second approach uses a combination of feed forward trajectory generation with a standard linear feedback in the inner loop. The feed-forward generator is designed by solving a convex optimization problem which is an approximation to the time-optimal problem. The latter approach is effective for multiple input multiple output systems with independent actuator saturation constraints.

20 DISTRIBUTION/AVAILABILITY OF ABSTRACT: UNCLASSIFIED/UNLIMITED [X] SAME AS RPT [ ] DTIC USERS [ ]	21. ABSTRACT SECURITY CLASSIFICATION	
22a. NAME OF RESPONSIBLE INDIVIDUAL: Robert L. Kosut	22b. TELEPHONE NUMBER (Include Area Code): 408-980-1500	22c. OFFICE SYMBOL:

DD FORM 1473, 83 APR EDITION OF BEST AVAILABLE COPY

Final Report

Contract No: F49620-88-C-0012

Adaptive and Nonlinear Control for Rapid Maneuvering of Flexible Structures

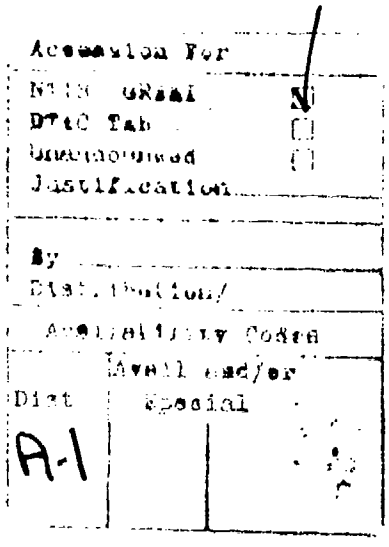

Prepared by:

Dr. Robert L. Kosut
Dr. M. Güntekin Kabuli
Integrated Systems Inc.
3260 Jay Street
Santa Clara, California 95054-3309

Prepared for:

USAF, AFSC
Air Force Office of Scientific Research
Building 410
Bolling AFB , DC 20332-6448

ISI Report No. 5733-05

October 1, 1991

Contents

1 Introduction 1

1.1 Problem Description 1

1.2 Overview of Results 1

2 Approach 1 5

3 Approach 2 7

3.1 Introduction 7

3.2 Motivation 8

3.3 Finite-Time Tracking of Reference Signals 9

3.3.1 $\mathcal{U}_T$ 9

3.3.2 T-track 9

3.3.3 $\mathcal{R}_T$ 10

3.3.4 Decomposition in $\mathcal{R}_T$ 10

3.3.5 $\mathcal{P}_T$ 10

3.3.6 Standard Minimum-Energy Solution 10

3.4 Transfer Function Approach 12

3.4.1 Complete Solution to $\mathcal{P}_T$ 12

3.4.2 A Convex Approximation to the Minimum-Time Tracking Problem . 13

3.4.3 A Particular Choice for $U_p(z)$ 14

3.4.4 An Approximation by a Sequence of Linear Programs 16

3.4.5 T-Polytopes and T-isochrones 16

3.4.6 A Simple Approximation to $\mathcal{S}_T$ 17

3.4.7 A Map from the Residue-Space to the Input Space 17

3.5 Example 19

3.5.1 Plant Model 20

3.5.2 Admissible Reference Signals and Matching Conditions 20

3.5.3 e_1-Maximum-Performance Curve 23

3.5.4 e_2-Maximum-Performance Curves 28

3.5.5 $\bar{\mathcal{S}}_T$ 29

3.5.6 A Fast T-Tracking Example 32

3.6 Robustness Considerations 32

3.7 Closing the Loop 36

3.7.1 Signal Generator 36

3.7.2 Unity-Feedback System 37

References 43

Appendix A 45

Appendix B 53

Appendix C 61

Appendix D 75

Appendix E 83

1 Introduction

1.1 Problem Description

The motivation for this research arises from the maneuvering and target tracking functions currently envisioned for large space structure (LSS) optical tracking systems. Such systems consist of lightweight structures which are mounted on, or articulated with respect to, heavier less flexible structures. Within the lightweight structure is an optical system, and within that system there are subsystems having similar further divisions. For example, a typical LSS optical system might consist of the following subsystems, listed here in order of increasing bandwidth: (1) coarse tracking of rigid body dynamics via gimbals, CMG's, reaction jets, and isolation devices; (2) beam pointing via mirror actuators; (3) wavefront and focus via secondary mirror control; and (4) fine tracking via fast mirrors and track illumination. Due to the natural frequency separation between each descending subsystem, it is possible to view each as essentially an independent tracking problem.

With this view in mind our reasearch has concentrated on a more generic and fundamental objective, namely, feedback control for rapid precision maneuvering of flexible structures. This objective encompasses any or all of the typical subsystems involved in an LSS optical tracking system. Our specific aims were as follows:

(1) Determine the performance limitations for rapid slewing.

(2) Develop methodologies to implement feedback slewing controllers which achieve specified performance goals.

1.2 Overview of Results

The limitations of tracking performance, particularly target acquisition, arise principally from actuator saturation. Since saturation is a nonlinear function, it is not surprising that high performance slewing controllers are nonlinear. The rapid slewing problem, which is perhaps more well known as the time-optimal control problem, has been the subject of research for very many years. Mathematically, a complete formulation of this problem can be obtained using Pontryagin's Maximum Principle, e.g., [Ath1]. However, in only the simplest cases has it been possible to obtain a solution. The general solution requires solving a two-point boundary value problem. In addition, for practical reasons, such as robustness and disturbance attenuation, it is necessary to implement the time-optimal control as a feedback system. However, such an implementation requires determining very complicated multi-dimensional switching surfaces. This is not a solved problem except for some very simple cases, e.g., rigid body dynamics. As a result, the research challenge undertaken here is the design and feedback implementation of time-optimal control for systems with the complexity of typical LSS optical tracking systems.

Within the setting of linear (time-invariant finite-dimensional) control design and analysis, there exists a considerable amount of theory as well as complementary, very efficient computational tools. Many classes of performance specifications can be included in the design

methodology, e.g., minimum energy, worst-case gain, etc. Nonlinear control design, however, is at its infancy, and except for very specific cases, a performance specification other than stability is very hard to incorporate.

The minimum-time control design problem is a *nonlinear* control design problem. This is due to the fact that the solution relies on maximizing the available actuation energy over the finite duration of actuation. As is well known from Pontryagin's Maximum Principle, for a given reference the actuation is bang-bang, i.e., saturating at the two extremes. Clearly a scalar multiple of the reference will yield a similar actuation sequence over a different duration. Observe that a closed-loop implementation is acceptable provided that it generates the (open-loop) time-optimal solution at the plant input.

For a given plant model and reference trajectory, if one could solve the associated minimum-time problem, one would obtain the description of the input in terms of the costate. This costate-to-input map would in turn describe a closed-loop implementation. Such a point of view, apart from the nontrivial issue of solving the minimum-time problem, has two other major drawbacks:

i) A time-optimal maneuver requires an actuation sequence which does not excite the structural modes. Since the structural modes can only be determined within some tolerance, what is optimal for the design model may not prove to be satisfactory for the perturbations of the design model. In other words, the complete solution lacks information on the achieved robustness in performance.

ii) Regardless of the plant model, the solution is necessarily bang-bang. Hence, one requires switching logic (sign functions) to implement the costate-to-input map. Such an implementation is known to chatter for small error signals.

These drawbacks imply that one should step back from the minimum-time and seek approximate solutions which will make the closed-loop implementation feasible and achieve performance degradation which is acceptable. Within the scope of this project, two distinct approaches have been taken in the course of seeking an approximate solution:

- Approach 1 .
  Start with a representative problem for which the complete analytical solution can be obtained. Modify the solution to obtain an implementable fast tracking closed-loop system. Such an approach restricts the set of allowable models. However, the existence of an analytical solution provides a variety of extensions to be made, e.g., adaptation. Section 2 focuses on the results obtained using this particular approach.

- Approach 2 .
  Instead of modifying the solution to a specific problem, pose the original minimum-time problem as the limit of a sequence of easy to solve convex optimization problems. For a fixed member of this sequence, determine a closed-loop design scheme based on the solution. Such an approach increases computational complexity in the design

stage. However, for a satisfactory approximation to the original minimum-time problem, the closed-loop design makes intensive use of existing linear (time-invariant finite-dimensional) design tools. The closed-loop design relies on a model follower scheme. Section 3 focuses on the results obtained using this particular approach.

2 Approach 1

This phase of the project consists of the research leading to the following three publications which are reprinted in Appendices B through D . Part of this research was motivated by the publication in Appendix A (under an NSF grant), which is included for completeness.

1. M. L. Workman, R. L. Kosut and G. F. Franklin,
   "Adaptive Proximate Time-Optimal Control: Discrete-Time Case,"
   Proceedings of the IEEE Conference on Decision and Control, pp. 1548-1553,
   Los Angeles, California, December 1987.

2. R. L. Kosut , A. M. Pascoal, M. L. Workman and G. F. Franklin,
   "Minimum-Time Control of Large Space Structures,"
   Proceedings of the SPIE Conference,
   Los Angeles, California, January 1988.

3. A. M. Pascoal, R. L. Kosut, G. F. Franklin, D. R. Meldrum and M. L. Workman,
   "Adaptive Time-Optimal Control of Flexible Structures,"
   Proceedings of the American Control Conference,
   Pittsburgh, Pennsylvania, June 1989.

During this period Dr. Kosut collaborated with Prof. Franklin from the EE Dept. at Stanford University and his graduate students M.L. Workman and D.R. Meldrum. Dr. Pascoal was employed by ISI.

3 Approach 2

3.1 Introduction[1]

Within the setting of finite-dimensional linear time-invariant multi-input multi-output plant modeling/identification and control design, increased computational power allows higher order nominal plant models to be incorparated in the designs in order to meet stringent performance demands. Currently used design methodologies include minimum-energy, worst-case energy-gain and peak-gain designs. In the case of actuator saturation, even if a globally stabilizing compensator is designed, saturation of the actuators may significantly degrade the overall performance. Typically, one forces sufficient conditions to guarantee that the actuator signals do not saturate over the region of operation.

The minimum-time tracking (of a fixed or moving target) on the other hand becomes an ill-posed problem if the saturation of the actuators is not incorporated in the problem description. Subject to the specified saturation limits, minimum-time solutions are necessarily bang-bang; hence, a linear control design will prove to be unsatisfactory. Closing the loop aside, solving for the (or a, as the case might be) time-optimal input is a nontrivial task. Pontryagin's Maximum Principle (see e.g., [Ath1]) brings a complete solution to the problem, using the calculus of variations. Solving for the equivalent nonlinear (non-convex) non-differentiable programming problem brings up all the associated hardships. In order for such an approach to be implementable, one requires a characterization of the switching surfaces in the state-space. Complete solutions for single-input single-output low order models have been derived in the literature; these results are extremely case specific and they are derivations for the complete solution for the case at hand. Regardless of what the solution is, the result requires a relay in the closed-loop; hence, chattering subject to disturbances. The way to overcome this difficulty is to approximate the infinite-gain nonlinearity (namely, the relay) with a finite-gain nonlinearity. Hence one is bound to step back from the time-optimal result for the sake of implementation. Even if one reformulates the open-loop minimum-time problem as a fast finite-time tracking problem (for a given reference trajectory, determine an input (subject to actuator saturation) so that the tracking error remains at zero after a finite time-instant) a feasible solution method for a closed-loop design goal remains a challenge.

Fast finite-time tracking of reference signals with saturating actuators has been a benchmark control problem since the complete solution method to the open-loop problem has been derived using Pontryagin's Maximum Principle. Solutions for the rigid body approximations have been used in different control strategies in applications areas such as the control of disk drives and precise maneuvering of flexible systems. The demand for fast tracking with saturating actuators has produced a variety of closed-loop implementations ranging from using idealized relays, finite-gain relays, adaptation methods, etc. [Wor1, Wor2, Wor3] . In the meantime, openloop solution to the problem with flexible modes has been studied in detail, for specific cases with no damping. The resulting proposed nonlinear optimization problems are derived using the necessary optimality conditions posed by the Maximum Principle, for specific plant models [Ben1, Sin1] .

In this report, an approximation to the time-optimal tracking problem under actuator

[1] An abridged version of a subset of the following results is to appear in the *Proceedings of the IEEE Conference on Decision and Control*, Brighton, United Kingdom, December 1991 (see Appendix E) .

saturation constraints is proposed for linear time-invariant finite-dimensional multi-input multi-output plants. The approximation relies on a transfer function approach to formulating constraints on the set of admissible finite-duration signals that achieve precise point-to-point positioning of flexible structures [Bha1] . The results are used to design fast finite-time tracking closed-loop feedback systems using only linear time-invariant design tools; the design replicates the open-loop behaviour with the added advantages of feedback. An example illustrates the feasibility of the approach.

3.2 Motivation

Consider a linear time-invariant finite-dimensional multi-input multi-output plant P . For preliminary arguments, consider the continuous-time case (the solution method proposed relies on transfer function descriptions; hence it naturally extends to the discrete-time case). Consider the following optimal control problem:

- For a given reference r , find the minimum time T such that a T-duration control input u ($\|u\|_\infty \leq 1$) achieves $(P * u)(t) = r(t)$ for all $t \geq T$.

Clearly, not all signals r can be tracked in such manner. Once the right class of r is described, this problem boils down to the standard time-optimal intercept problem. As is well known, Pontryagin's Maximum Principle sets up the necessary conditions to solve this problem; however, literally computing the control u turns out to be a nasty nonlinear optimization problem. Even if we had the the time-optimal u_r that tracked r in T_r seconds, trying this input on an open-loop plant is a futile attempt. Consider a simple double integrator plant with r as a step input. The time-optimal u_r clearly satisfies $\int_0^\infty u_r(\tau)d\tau = 0$; otherwise the plant would start to tumble. If one had an actuation disturbance (say a short duration pulse with a DC component) there would be no way to implement a time-optimal slew in open-loop without *exact* knowledge of the input disturbance. Clearly, one requires a feedback configuration.

For the double integrator plant, for *any* stabilizing compensator (in the unity-feedback system) , the sensitivity map has a zero at $s = 0$; hence, any additive DC disturbance at the input is asymptotically rejected at the true plant input.Instead of choosing any stabilizing compensator, if we designed an ℓ_1-optimal compensator, we will have a worst-case amplitude gain from the input disturbance to the plant input. Using this headroom, we could solve the time-optimal problem with the actuation constraint modified to $\|u\|_\infty \leq (1 - \varepsilon)$, where $\varepsilon \in (0, 1)$, is the discount factor keeping the worst case disturbance contribution. In other words, the closed-loop design (how sophisticated one desires to get) can be decoupled from the time-optimal problem by presetting ε . Clearly, any stable unity-feedback system can be used to track r once the time-optimal (or as close as one can get) u_r is determined (inject u_r at the plant input and use Pu_r as the reference and let the compensator work on the output measurement error); see Figure 1 . This line of reasoning works fine as long as one has the suitable u_r ; in other words, the open-loop solution.

So, a feasible closed-loop (robust, disturbance rejecting, ...) design problem boils down to computing u_r in a fast manner; possibly, after certain simplifications and getting sub-optimal results within a reasonable headroom.

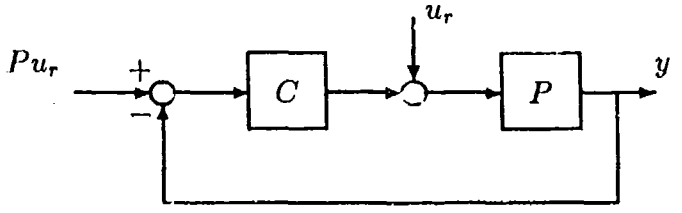

Figure 1: Stable unity-feedback system with zero initial conditions that achieves $y = Pu_r$

This report focuses on an approximation to the time-optimal tracking problem. The result can be expressed in terms of a sequence of linear programs, where the number of variables is fixed throughout. The results are applicable to any multi-input multi-output P with a minimal state-space description (A, B, C) . Time-suboptimal tracking is achieved for the set of admissible reference signals associated with P . The results are incorporated in a closed-loop design procedure. An example illustrates the feasibility of the approach.

3.3 Finite-Time Tracking of Reference Signals

Let the plant, P , be strictly proper and have a minimal state-space description (A, B, C) , with n_i inputs, n_o outputs and n_s states. The state-space description can be in continuous-time or discrete-time. For the sake of illustration, the results will be exclusively stated for the continuous-time strictly proper multi-input multi-output plant P . Since the approach relies on a rational transfer function description, with appropriate modifications, discrete-time setting can also be handled.

3.3.1 Definition: $(\mathcal{U}_T)$

For a given $T \in (0, \infty)$, $\mathcal{U}_T$ denotes the set of all bounded[2] inputs of duration T , where

$$\mathcal{U}_T := \{ u : \mathbb{R}_+ \to \mathbb{R}^{n_i} \mid u(t) = 0 \text{ for } t > T \ , \ \|u\|_\infty < \infty \} \quad . \square$$

Typically, the actuators have saturation limits. After appropriate normalization of the input u to the plant, we assume that the saturation constraints are expressed as $\|u\|_\infty \leq 1$.

3.3.2 Definition: (T-track)

For a given $T \in (0, \infty)$, y is said to T-track r iff $y(t) = r(t)$ for all $t \geq T$. $\square$

For a given reference signal r , the minimum-time tracking problem is to determine the minimum time T and an input $u \in \mathcal{U}_T$, such that $\|u\|_\infty \leq 1$ and $(P * u)$ T-tracks r . Since the inputs are restricted to $\mathcal{U}_T$, the reference should T-track a zero-input response of P .

[2] with respect to the norm $\| \cdot \|_\infty$. For $u : \mathbb{R}_+ \to \mathbb{R}^{n_i}$, $\|u\|_\infty := \sup_{t \in \mathbb{R}_+} \max_{1 \leq i \leq n_i} |u_i(t)|$.

3.3.3 Fact:

For a given plant P with a minimal description (A, B, C) , and a reference r , there exists an input $u \in \mathcal{U}_T$ such that $(P * u)$ T-tracks r if and only if $r \in \mathcal{R}_T$, where

$$\mathcal{R}_T := \left\{ r : \mathbb{R}_+ \to \mathbb{R}^{n_o} \mid r(t) = Ce^{At}x_0 \ , \ x_0 \in \mathbb{R}^{n_s} \ , \ t \geq T \right\} \quad . \square \qquad (1)$$

Note that (1) is a complete description of reference trajectories that the plant output can T-track with inputs in $\mathcal{U}_T$. From now on, we will refer to the set $\mathcal{R}_T$ as the set of admissible reference trajectories. Using the description in (1) , any $r \in \mathcal{R}_T$ has a unique decomposition as stated in the following fact.

3.3.4 Fact:

For a given plant P with a minimal description (A, B, C) , let $r \in \mathcal{R}_T$. Then there exists a unique $r_T \in \mathcal{U}_T$ and a unique $x_r \in \mathbb{R}^{n_s}$ such that

$$r(t) \ = \ r_T(t) \ + \ Ce^{At}x_r \quad . \square$$

3.3.5 Finite-Time Tracking Problem $\mathcal{P}_T$:

For a given $r \in \mathcal{R}_T$, determine a $u \in \mathcal{U}_T$ such that $(P * u)$ T-tracks r . $\square$

Clearly, the problem $\mathcal{P}_T$ has always a solution, since there is no constraint on the actuator signal. The standard analytical solution method for $\mathcal{P}_T$ is outlined in order to motivate the results.

3.3.6 Finite-time tracking with unconstrained actuation:

Let (A, B, C) be minimal; without loss of generality, set initial time instant to zero. We now briefly state the standard solution method.

1. Fix $T \in (0, \infty)$.
2. Fix $r \in \mathcal{R}_T$.
3. Determine the unique $x(T)$ described by the constraint

$$r(t) \ = \ Ce^{A(t-T)}x(T) \ , \ t \geq T \quad ;$$

i.e.,

$$\begin{bmatrix} C \\ CA \\ \vdots \\ CA^{n-1} \end{bmatrix} x(T) \ = \ \begin{bmatrix} r(T) \\ r^{(1)}(T) \\ \vdots \\ r^{(n-1)}(T) \end{bmatrix} \quad .$$

4. Solve for $W_C(T)$ where $W_C(t)$ satisfies

$$\dot{W}_C \ = \ AW_C \ + \ W_C A^T \ + \ BB^T \ , \ W_C(0) = 0 \quad .$$

5. Compute the finite-duration minimum energy control that steers x_0 to $x(T)$, namely

$$u(t) \;=\; \begin{cases} B^T e^{A^T(T-t)} W_C^{-1}(T)[x(T) - e^{AT}x_0] & t \in [0,T] \\ 0 & t > T \end{cases} \quad . \; \square \qquad (2)$$

Recall that the minimum energy solution in (2) is a solution of the linear equation

$$x_T \;=\; \widehat{\mathcal{L}}_T(u) \quad , \qquad (3)$$

where

$$\begin{aligned} x_T \;&:=\; x(T) \;-\; e^{AT}x(0) \\ \widehat{\mathcal{L}}_T(u) \;&:=\; \int_0^T e^{A(T-\tau)} B u(\tau) \mathrm{d}\tau \quad . \end{aligned}$$

If one obtains a parametrization of the null-space of $\widehat{\mathcal{L}}_T$, together with the minimum energy solution in (2) , one obtains a parametrization of all solutions to (3) . Note that, the resulting parametrization is a parametrization of all inputs that achieve T-tracking of the reference r . One could then search over the subspace of solutions for an input that satisfied the maximum bounds.

A straightforward approach would be to introduce sampling at a fixed rate and zero-order hold. Instead of keeping the input value at each sampling instant as an independent parameter (which would increase the complexity of the optimization problem considerably), hold the input signal constant over a fixed amount of sampling instants so that the number of free parameters is reasonable. The equation in (3) would then be a linear equation in finite number of parameters; together with the parameter bounds imposed by the saturation limits, one ends up with a standard linear programming problem. There is one major drawback of this approach: setting up the approximate linear programming problem requires considerable amount of computation (discretization, time-domain convolutions, state-transition matrix evaluations, etc.) .

The proposed solution method, sets up another linear programming problem using transfer function description and partial fraction expansions.

Before we start describing another way of parametrizing inputs in $\mathcal{U}_T$ that achieve T-tracking of r , we point out the fact that the standard minimum energy solution to $\mathcal{P}_T$ can be used to determine a lower bound on the T's the search is based on.

For a signal $u \in \mathcal{U}_T$, $\|u\|_\infty \leq 1$ implies that the energy[3] $\|u\|_2^2 \leq T n_i$. We know that the minimum energy needed to steer x_0 to $x(T)$ is given by

$$\|\hat{u}\|_2^2 \;=\; \zeta^T W_C^{-1}(T)\zeta \quad ,$$

where $\zeta \;=\; x(T) - e^{AT}x_0$. Clearly, if $\|\hat{u}\|_2^2$ is greater than $T n_i$, there cannot be a bounded signal in $\mathcal{U}_T$ that can do the job. Later, during the detailed description of an example, we will use this energy bound condition in order to show the effect of the proposed approximations to the minimum-time reachability problem.

[3] For $u \;:\; \mathbb{R}_+ \rightarrow \mathbb{R}^{n_i}$, $\|u\|_2^2 := \int_0^\infty u^T(\tau)u(\tau)d\tau$.

3.4 Transfer Function Approach

Although time-domain solutions and necessary conditions of optimality formulate the complete solution to the minimum-time tracking problem, it requires considerable computational effort to solve the resulting nonlinear problem. What we propose is to approximate the problem as a sequence of finite-time tracking problems in terms of linear programming. The finite-time tracking problems are formulated in terms of partial fraction expansions; hence they require no time-domain simulations. We now describe the procedure.

What we mean by the poles of a function of time are the poles of the Laplace-transform of the function. Note that a signal in $\mathcal{U}_T$ is entire; hence, it does not have any poles.

Recall that for a given minimal (A, B, C) , the set of all reference signals that can be tracked in finite time is given by (1) . From Fact 3.3.4 , we conclude that the reference signal can have poles at the plant poles and nowhere else.

Let $r \in \mathcal{R}_T$ and the plant be at an initial state x_0 at $t = 0$. Let r_T and x_r describe the unique decomposition of r as in Fact 3.3.4 . The goal is to find a $u \in \mathcal{U}_T$ such that

$$R_T(s) + C(sI - A)^{-1}x_r \;=\; C(sI - A)^{-1}\left(x_0 \;+\; BU(s)\right) \quad .$$

Since signals in $\mathcal{U}_T$ do not have any poles, the set of all signals that achieve T-tracking is described by partial fraction expansion matching conditions. From now on, without loss of generality, we will assume that x_0 (the initial condition) is zero. If x_0 is not zero, one can redefine x_r as $(x_r - x_0)$.

3.4.1 Proposition:

Let the plant P have the expansion

$$P(s) = \sum_{i=1}^{k}\sum_{j=1}^{m_i} \frac{K_{ij}}{(s - s_i)^j} \quad ,$$

where $K_{ij} \in \mathbb{R}^{n_o \times n_i}$. Let $r \in \mathcal{R}_T$. Consider the unique decomposition

$$r \;=:\; r_T \;+\; r_{exp} \quad ,$$

where $r_T \in \mathcal{U}_T$ and $r_{exp} = Ce^{At}x_r$ (see Fact 3.3.4) . Under these assumptions,

1. $r_{exp} \in \mathcal{R}_T$; moreover,

$$R_{exp}(s) \;=\; \sum_{i=1}^{k}\sum_{j=1}^{m_i} \frac{\widehat{K}_{ij}}{(s - s_i)^j} \quad ,$$

   where $\widehat{K}_{ij} \in \mathbb{R}^{n_o}$.

2. The set of all signals $u \in \mathcal{U}_T$ such that $(P * u)$ T-tracks r is given by

$$\left\{ u \in \mathcal{U}_T \;\mid\; \widehat{K}_{i,(m_i - j + 1)} \;=\; \frac{1}{(j-1)!}\left[\frac{d^{j-1}}{ds^{j-1}}\left[(s - s_i)^{m_i}P(s)U(s)\right]\right]_{s=s_i} \right.$$
$$\left. i = 1, \ldots, k\,;\; j = 1, \ldots, m_i \right\} \quad .\square \qquad (4)$$

3.4.2 A Convex Approximation to the Minimum-Time Tracking Problem

In order to use the results mentioned above in a finite-dimensional optimization problem, choose a basis of $\mathcal{U}_T$ (preferably, one for which the Laplace transforms can be easily calculated) . Truncate this basis down to a finite collection $\{h_i\}_{i=1}^N$, for a specified N . Consider the subclass of signals in $\mathcal{U}_T$ whose Laplace transforms are of the form

$$U_p(s) \;=\; \sum_{i=1}^{N} p_i H_i(s) \quad .$$

Clearly, all of the matching constraints in (4) translate into a *linear* equation in terms of $p \in \mathbb{R}^N$, say

$$\Gamma(T)p \;=\; \gamma \quad . \tag{5}$$

Note that $\gamma \in \mathbb{R}^n$, where

$$n \;:=\; n_o \cdot \sum_{i=1}^{k} m_i \quad .$$

The entries of γ are solely determined by the entries of $\widehat{K}_{ij}$ corresponding to r_{exp} (see Proposition 3.4.1) . We will refer to the space γ is in as the residue-space (an abuse of notation; after all, not all entries of γ correspond to the residues in the partial fraction expansion) . For the specified expansion $U_p(s)$ and specified T , (4) determines a unique $\Gamma(T)$. Solving (5) for different vectors γ in the residue-space, one obtains solutions to $\mathcal{P}_T$ for different admissible reference signals

As we have seen before, there is no loss of generality when the reference trajectory r is expressed in terms of r_{exp} only. The finite duration portion has no contribution to the matching constraints in (4) . We now point out an observation that may further simplify setting up the problem. Typically, the reference r_{exp} does not have nonzero coefficients at each and every single pole of P , i.e., not all entries of γ are nonzero. The desired reference is usually T-tracked by exciting a subset of the plant poles. Note that if none of the plant poles are excited, the plant output will also be in $\mathcal{U}_T$.

Suppose that one has a model of P of the form

$$P(s) \;=\; \frac{K_0}{s^2} \;+\; \sum_{i=1}^{m} \frac{K_i}{s^2 + 2\zeta_i\omega_i s + \omega_i^2} \quad ,$$

where the desired performance is to achieve rigid body performance with minimal residual vibration due to the rest of the flexible modes. Note that the results mentioned so far are quite general, not specifically derived with this simplification in mind. Carrying on with the observation, since the flexible modes are distinct, zero residual vibration at s_i is achieved if $U(s_i) = 0$, provided that the plant is initially at rest. Since the rank of K_i is nonzero (otherwise the mode would not show up in the model), $U(s_i)$ has to be in the null-space of K_i . Definitely, chosing $U(s_i) = 0$ is a sufficient condition; however, the results considerably simplify since the performance boils down to step and ramp constraints on $U(s)$. The null-space description for the residual vibration portion can be replaced by setting the input to zero at those poles. Clearly, for single input systems, this sufficient condition is also necessary. Note that, when one seeks an input that steers any state to a terminal state, $U(s_i)$ will not necessarily be zero, in order to suppress the corresponding mode.

Provided that (5) has a solution, one brings another way of solving the finite-time tracking problem $\mathcal{P}_T$. Introducing the actuation saturation constraints, we end up with a convex feasibility problem:

$$\text{Find } p \in \mathbb{R}^N \text{ such that } \Gamma(T)p \;=\; \gamma \text{ and } \|p^T h\|_\infty \leq 1 \quad ,$$

where $h(t) := [h_1(t) \quad \ldots \quad h_N(t)]^T$. As it will be explained later on, by suitably choosing the finite collection of functions in $\mathcal{U}_T$, the convex problem becomes a linear programming problem.

Instead of solving a sequence of convex feasibility problems and seek answers of the form yes or no, one can form a slight variation to extract the most from each optimization run. For a fixed T and N , γ denotes the desired direction and magnitude; instead of solving for γ solve for a scaled version:

$$\begin{array}{c} \max \qquad \lambda \quad . \\ p \in \mathbb{R}^N, \lambda \in \mathbb{R} \\ \Gamma(T)p = \lambda\gamma \\ \|p^T h\|_\infty \leq 1 \end{array} \tag{6}$$

Solving the convex minimization problem (6) , one obtains the maximum performance along the direction γ for a specified T and N . Clearly, one can then solve a sequence of convex minimization problems by varying T (and N) to sweep a maximum performance curve; hence, obtaining an approximation to the minimum-time problem. In the rest of this report, we will fix N and vary T . The implications of this approach will be discussed in detail for the specific convex setting: linear program. Such a choice is made only for making sure that the complexity of the sequence of convex optimization problems stays the same throughout the whole sweep. If one is not interested in further simplifying this convex program (6) to a linear program, one could apply all of the topics discussed under the linear program setup to this general convex setting.

3.4.3 A Particular Choice for $U_p(s)$

A time-optimal input signal is necessarily bang-bang; i.e., it is piecewise constant (with values ± 1 , for a detailed treatment of the solution technique using calculus of variations, see e.g., [Ath1]) . While there is no upper-bound on the finite number of switchings in general, for a fixed number of switchings, say N , one can choose a sequence of N pulses (with alternating amplitudes) with varying widths as a family of functions in $\mathcal{U}_T$. One can then solve for the constraints in (4) to obtain a family of nonlinear (non-convex) algebraic equations [Sch1] . Similar algebraic equations are obtained by applying the Pontryagin's Maximum Principle to specific cases of P, using state-space computations [Ben1, Sin1] . Since the signals (by construction) , do not violate the specified actuation bounds, solving for the minimum width pulse sequence brings an approximation to the solution of the minimum-time problem. In order to avoid local minima problems, we choose a linear combination of functions in $\mathcal{U}_T$.

For a fixed T , consider the weighted sum of a sequence of N pulses with uniform widths (T/N) ; i.e., choose $U_p(s)$ as

$$U_p(s) \;=\; \mathcal{L}\left\{ \sum_{k=1}^{N} \mathbb{1}\left(t-(k-1)\frac{T}{N}\right) \;-\; \mathbb{1}\left(t-k\frac{T}{N}\right) \right\}$$

$$= \frac{e^{sT/N}-1}{s}\sum_{k=1}^{N} p_k e^{-ksT/N} \quad , \tag{7}$$

$\mathcal{L}$ denotes the Laplace-transform and $\mathbb{1}$ denotes the unit-step function.[4] Since the input signal is piecewise constant, the actuation bounds can be expressed as

$$-1 \leq p \leq 1 \quad ,$$

where $p \in \mathbb{R}^N$ is to be determined.[5] Recall that, the general convex approximation was in fact a linear equation with convex constraint on the parameters. Now that the input constraint can be equivalently represented as a parameter bound, we end up with a linear program setup.

Before proceeding with the sequence of linear programs, we comment on the choice of N .

The matching conditions in (4) yield n equations in N unknowns. In order not to have a trivial null-space, N should be greater than n . Note that the null-space solution will be used to find a solution in the hypercube $-1 \leq p \leq 1$. If the time-optimal switchings were at integer multiples of T/N , the resulting linear program would return a solution at one of the corners of the hypercube. Hence the specific approximation as a linear program will consistently come up with solutions trying to reach a corner, but not necessarily get there. Clearly, the finer the pulse width, the higher the number of pulses that attain the maximum bounds. In the detailed treatment of an example, we will comment on the improvements of the solutions with respect to N .

There is another way of interpreting this specific choice of input. Since the pulses are uniform, one could view the coefficient matching in (4) as matching the output of the discrete-time plant (namely, P sampled at N/T Hz) . This dictates that the choice of N should be so that

$$\text{Imag}(s_i)T \ \leq 2\pi N \quad , \quad i = 1, \ldots, k \quad , \tag{8}$$

(preferably, $\ll$ rather than $\leq$) , where s_i denotes the ith pole of P .

Typically, one has energy constraints on the actuators,

$$\|u\|_2^2 \ \leq \ E_{max} \quad ,$$

where E_{max} denotes an upper bound on the actuation energy. Note that this brings an upper bound on T since the inputs satisfy $\|u\|_\infty \leq 1$.

$$\|u\|_2^2 \ \leq \ n_i T \ \leq \ E_{max} \quad .$$

Denote the upper bound on T as T_{max} .

Hence, once the poles of P are determined, one can choose such an N and fix the order of the linear program throughout the solution.

---

[4] $\mathbb{1} \ : \ \mathbb{R} \rightarrow \mathbb{R} \ , \ \mathbb{1}(t) = \begin{cases} 0 & , \ t < 0 \\ 1 & , \ t \geq 0 \end{cases}$.

[5] For $p \in \mathbb{R}^N$, $-1 \leq p \leq 1$ denotes $-1 \leq p_k \leq 1$, for $1 \leq k \leq N$.

3.4.4 An Approximation by a Sequence of Linear Programs

For a given plant P and N , the maximum performance function

$$\Psi \ : \ (0,\infty) \times \mathbb{R}^n \ \rightarrow \ \mathbb{R}_+$$

is defined in terms of the following linear program.

$$\Psi(T,\gamma) \ := \ \max_{\substack{p \in \mathbb{R}^N, \lambda \in \mathbb{R} \\ \Gamma(T)p = \lambda\gamma \\ -1 \leq p \leq 1}} \lambda \quad , \tag{9}$$

where $\Gamma(T)$ is obtained by the matching conditions (4) . Any $\hat{p} \in \mathbb{R}^N$ for which the linear program in (9) returns the value $\Psi(T,\gamma)$, is used to define the relation Φ ,

$$\Phi \ : \ (0,\infty) \times \mathbb{R}^n \ \rightarrow \ \mathbb{R}^N \quad ,$$

where

$$\Phi(T,\gamma) \ := \ \hat{p} \quad .$$

For a specified time-instant T , $\Psi(T,\gamma)$ determines the maximum-performance one can achieve along the specified direction γ . For a fixed direction γ , by sweeping over T , one obtains the γ-maximum-performance curve

$$(\, T \, , \, \Psi(T,\gamma) \,) \quad , \quad T \in \mathbb{R}_+ \quad .$$

Instead of generating the γ-maximum-performance curve for $T \in \mathbb{R}_+$, introduce a time-resolution of ΔT and discretize the curve; i.e., for a pre-determined k_{max} , evaluate the curve at integer multiples of ΔT :

$$(\, T \, , \, \Psi(T,\gamma) \,) \quad , \quad T = k\Delta T \quad , \quad 0 \leq k \leq k_{max} \quad .$$

The sub-optimal (due to the approximations) time-instant $\widehat{T}$ for which the residue γ is achieved is in the interval

$$\widehat{T} \in [T_l, T_l + \Delta T] \quad ,$$

where

$$\begin{aligned} \Psi(T_l,\gamma) \ &\leq \ 1 \ , \\ \Psi(T_l + \Delta T,\gamma) \ &\geq \ 1 \ . \end{aligned}$$

3.4.5 T-Polytopes and T-isochrones

Consider the maximum-performance function Ψ defined in (9) . The T-polytope $\mathcal{S}_T$,

$$\mathcal{S}_T \ := \ \{ \ \lambda\gamma \ \mid \ \gamma \in \mathbb{R}^n \ , \ \|\gamma\|_2 = 1 \ , \ \lambda \ \in \ [0, \Psi(T,\gamma)] \ \} \quad . \tag{10}$$

is the set of all points in the residue-space that can be reached in T seconds. The boundary of this set, denoted by $\partial\mathcal{S}_T$, is referred to as the T-isochrone.

Let $\widehat{\mathcal{S}}_T$ denote the set of all residues that can be reached in T seconds when inputs are restricted to bounded (by one) signals in $\mathcal{U}_T$; i.e., the T-optimal-polytope. In other words, $\widehat{\mathcal{S}}_T$ is "the" complete result if we were not to restrict the inputs as we did in (9) .

We have the following simple yet crucial properties:

- $\mathcal{S}_T \subseteq \hat{\mathcal{S}}_T$.
- $\mathcal{S}_T$ and $\hat{\mathcal{S}}_T$ are convex.

Hence, $\mathcal{S}_T$ is a convex approximation to $\mathcal{S}_T$.

3.4.6 A Simple Approximation to $\mathcal{S}_T$

Consider the following T-polytope $\tilde{\mathcal{S}}_T$ which is a subset of $\mathcal{S}_T$ in (10) .

$$\tilde{\mathcal{S}}_T := \left\{ \sum_{i=1}^{n} \lambda_i \Psi(T, e_i) e_i \mid \|\lambda\|_1 \leq 1 \right\} \quad , \tag{11}$$

where $\{e_1, \ldots, e_n\}$ is a basis in $\mathbb{R}^n$.

3.4.7 A Map from the Residue-Space to the Input Space

Our goal is to construct a map, possibly using look-up tables, such that given a desired reference signal and the states of the plant, an input signal is generated so that the plant output T-tracks the reference signal as fast as possible.

The desired reference signal (which should be in $\mathcal{R}_T$) and the initial state determines the amount of change necessary in the residues of the output signal. For this reason, we will focus on the following subproblem: For a given γ in the residue-space determine an input signal such that the output of the plant achieves the residues specified by γ as fast as possible.

In the rest of this report, we will use the standard orthonormal basis $\{e_1, \ldots, e_n\}$ in $\mathbb{R}^n$. In order to cut down on the storage space, we will identify $\tilde{\mathcal{S}}_T$ with its "positive orthant":

$$\tilde{\mathcal{S}}_T := \left\{ \sum_{i=1}^{n} \lambda_i \Psi(T, e_i) e_i \mid \|\lambda\|_1 \leq 1 \ , \ \lambda \geq 0 \right\} \quad . \tag{12}$$

Let the signum function $SGN : \mathbb{R}^n \rightarrow \mathbb{R}^n$ be defined as

$$e_i^T SGN(\gamma) := \begin{cases} 1 & \text{if } e_i^T \gamma > 0 \\ 0 & \text{if } e_i^T \gamma = 0 \\ -1 & \text{if } e_i^T \gamma < 0 \end{cases} .$$

Let the operator $.*$ denote element-by-element product in $\mathbb{R}^n$; i.e.,

$$e_i^T (\gamma_1 .* \gamma_2) := (e_i^T \gamma_1)(e_i^T \gamma_2) \quad .$$

Suppose that $\gamma \in \partial \tilde{\mathcal{S}}_T$. Let $\hat{\gamma}$ be defined by

$$\gamma =: SGN(\gamma) .* \hat{\gamma} \quad .$$

Clearly, $\gamma \in \partial \tilde{\mathcal{S}}_T$ if and only if $\hat{\gamma} \in \partial \tilde{\mathcal{S}}_T$. Since $\hat{\gamma}$ can be expressed as a convex combination

$$\hat{\gamma} =: \sum_{i=1}^{n} \hat{\lambda}_i \Psi(T, e_i) e_i \ , \ \hat{\lambda} \geq 0 \ , \ \|\hat{\lambda}\|_1 = 1 \quad ,$$

we conclude that the input that achieves $\hat{\gamma}$ residue in T seconds is represented by

$$\hat{p} \;=\; \sum_{i=1}^{n} \hat{\lambda}_i \Phi(T, e_i) \quad .$$

The input that achieves γ residue in T seconds is represented by

$$p \;=\; \sum_{i=1}^{n} \hat{\lambda}_i \left(e_i^T SGN(\gamma) \right) \Phi(T, e_i) \quad .$$

Note that

$$-1 \leq p \leq 1 \quad .$$

Since the input is assumed to be piecewise-constant over T/N second durations, suppose that (with respect to the underlying sampling rate) there are M points per pulse. For the sake of illustration, assume that $n_i = 1$; let $\hat{u} \in \mathbb{R}^M$ be the vector will all entries equal to one. The input sequence that is compactly represented by $p \in \mathbb{R}^N$ is given by the following sequence (from 0 to T) $u \in \mathbb{R}^{MN}$:

$$u \;=\; p \otimes \hat{u} \quad ,$$

where the operator $\otimes$ denotes the tensor product. Hence the underlying idea, is to express a given residue vector γ as a convex combination; we choose to do this on one of the T-isochrones.

We now outline the procedure:

1. Fix N and T_{max} , following the points mentioned above.

2. Determine a time resolution ΔT . Suppose that $N_T := \text{round}(T_{max}/\Delta T)$ points sweep the desired range over which the actuation is considered. Note that, with respect to this quantization, for any $T \in (T_0 - \Delta T, T_0]$, T-tracking is indistinguishable from T_0-tracking.

3. Solve $(n \cdot N_T)$ linear programs; i.e., for the N_T time points solve for and store

$$\Psi(T, e_i) \quad , \quad \Phi(T, e_i) \quad , \quad i = 1, \ldots, n \quad .$$

   Note that if steady-state to steady-state T-tracking is to be desired, one need not span all n directions, as it will become apparent later on in the detailed example.

4. So far, the storage space needed is $(n \cdot N_T \cdot (N+1))$. This data represents the N_T isochrones, i.e., the boundaries $\partial \bar{\mathcal{S}}_T$. This completes all preprocessing that is necessary to construct the desired map. Note that along each direction e_i , we have reached out as much as possible. Hence, for residues which are close to the directions, the convex approximation will yield the best possible result subject to the linear program approximation to the time-optimal problem.

5. The domain of the desired map is

$$\tilde{\mathcal{S}}_{T_{max}} \quad .$$

That is, for any $\gamma \in \tilde{\mathcal{S}}_{T_{max}}$, we will generate an input that achieves that residue as fast as possible. Recalling the discussion above, we will identify γ with $\hat{\gamma} \in \bar{\mathcal{S}}_{T_{max}}$, by keeping track of $SGN(\gamma)$, to cut down on storage space.

6. For a given $\hat{\gamma}$ determine the smallest T such that $\hat{\gamma} \in \bar{\mathcal{S}}_T$. We propose the following procedure: Let $\eta \in \mathbb{R}^{N_T}$ be defined as

$$e_k^T \eta \;:=\; 1/\left(\sum_{i=1}^{n} \frac{e_i^T \hat{\gamma}}{\Psi(T_k, e_i)}\right) \quad , \quad k = 1, \ldots, N_T \quad .$$

Let the ℓth entry of η be the first entry which is less than or equal to one. Since $\hat{\gamma}$ was in $\bar{\mathcal{S}}_{t_{max}}$ to start with, such an ℓ exists. Hence, we conclude that, among the family of T-isochrones, $\hat{\gamma}$ can be achieved no faster than T_ℓ seconds.

7. Once the index ℓ and the multiplier $e_\ell^T \eta$ is determined, assign $p \in \mathbb{R}^N$:

$$p \;:=\; \sum_{i=1}^{n} \frac{(e_\ell^T \eta)(e_i^T \gamma)}{\Psi(T_\ell, e_i)} \Phi(T_\ell, e_i) \quad . \tag{13}$$

Note that p in (13) satisfies $-1 \leq p \leq 1$, moreover, the input that is compactly represented by p achieves the specified γ residue in T_ℓ seconds, the fastest among the family of T-isochrones.

8. Extract the input sequence from p . Provided that there are n_i inputs, we have

$$N \;=:\; \hat{N} n_i \quad ,$$

for some integer $\hat{N}$. Partition p as

$$p \;=:\; [p_1 \quad \ldots \quad p_{n_i}]^T \quad , \quad p_k \in \mathbb{R}^{\hat{N}} \; , \; k = 1, \ldots, n_i \quad .$$

As mentioned before, (with respect to the sampling rate specified) suppose that there are M points per pulse width (of $T_\ell/\hat{N}$ seconds). Let $\hat{u} \in \mathbb{R}^M$ have entries equal to one. The input waveform over $T_\ell/\hat{N}$ is represented by

$$u_k \;=\; p_k \otimes \hat{u} \quad , \quad k = 1, \ldots, n_i \quad ,$$

where $u_k \in \mathbb{R}^{\hat{N}M}$.

3.5 Example

Recall that none of the results stated so far, put any constraints on (A, B, C) . In order to test out the proposed scheme, we focused on a specific siso plant, consisting of a double integrator and three damped flexible modes.

3.5.1 Plant Model

Consider the single-input single-output plant $P(s)$:

$$P(s) := \frac{1}{s^2} + \sum_{i=1}^{3} \frac{\alpha_i}{s^2 + 2\zeta_i\omega_i s + \omega_i^2} \quad , \tag{14}$$

where

$$\begin{aligned} [\alpha_1\ \alpha_2\ \alpha_3] &= [5\ 10\ 20] \\ [\omega_1\ \omega_2\ \omega_3] &= 2\pi\,[0.5\ 1\ 1.5]\ \text{rad/s} \\ [\zeta_1\ \zeta_2\ \zeta_3] &= [0.1\ 0.01\ 0.001] \quad . \end{aligned}$$

The Bode-plot of P is shown in Figure 2 ; note that the specified time interval corresponds to excitations with frequency content ranging over the band $[0.1, 1]$ Hz . The choice of the constants had no specific purpose other than making sure that the flexible modes significantly contribute to the position output. In order to show the efficiency of the proposed scheme, we will focus on actuation signals in $\mathcal{U}_T$, where $T \in [1, 10]s$. Standard bang-bang actuation relying on the rigid-body approximation of P for rest-to-rest slewing over the interval $[1, 10]$ s resulted in unsatisfactory outputs.

3.5.2 Admissible Reference Signals and Matching Conditions

For the plant model in (14) , admissible r_{exp}'s are linear combination of steps, ramps and lightly-damped sinusoids. The vast majority of tracking problems restricts the references to to a linear combination of steps and ramps:

$$\{\ r\ \mid\ r(t) = r_0\ +\ r_1 t\ ,\ r_0 \in \mathbb{R}\ ,\ r_1 \in \mathbb{R}\ ,\ t \geq 0\ \} \quad .$$

In terms of the previous notation, we have:

$$\begin{aligned} n_i = n_o &= 1\ , \\ n_s = n &= 8\ , \\ T_{max} &= 10\ , \\ k &= 7\ , \\ m_1 &= 2\ , \\ m_2 = m_3 = \ldots = m_7 &= 1\ , \end{aligned}$$

namely, one input, one output, eight states, eight parameters, a maximum of ten seconds of actuation, seven poles, one of multiplicity two and the rest of multiplicity one.

Following (8) , the constraint

$$\text{Imag}(s_i) T_{max} \leq 2\pi N \quad , \quad i = 1, \ldots, k$$

yields

$$N \geq \max\{\ 0\ ,\ 4.9749\ ,\ 9.9995\ ,\ 15\ \} = 15 \quad .$$

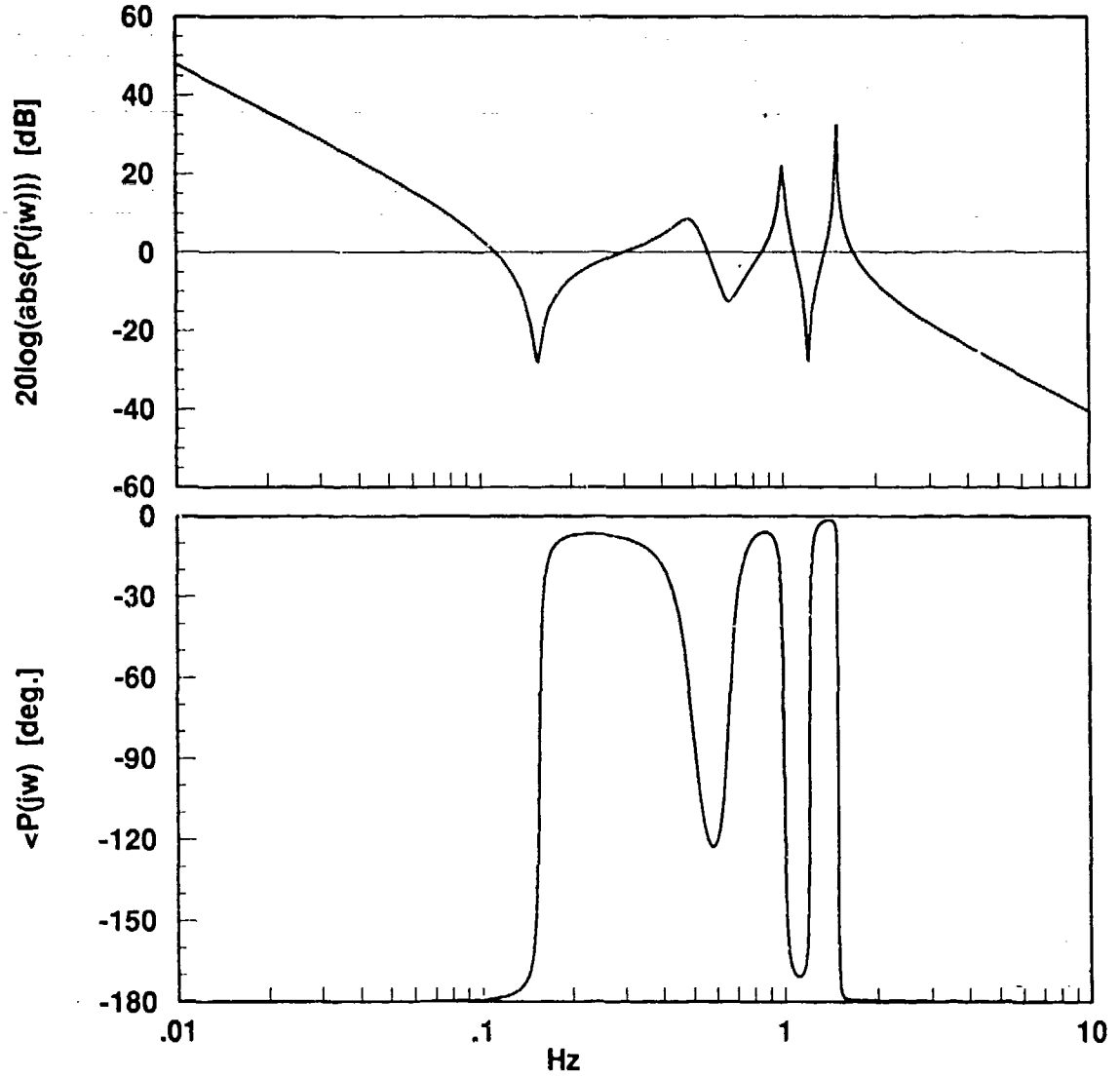

Figure 2: Bode-plot of P in (14)

We choose

$$N = 20 \quad .$$

All simulations were performed by sampling the plant P at 100 Hz . In order to have one sample instant added on for each time step ΔT , we choose

$$\begin{aligned} \Delta T &= 0.2 \ , \\ N_T &= 46 \quad . \end{aligned}$$

In order to set up the linear programming problem, we need to construct $\Gamma(T)$ from the matching conditions in (4) . For this example, we have

$$\begin{aligned} s_1 &= 0 \ , \\ s_2 = \bar{s}_3 &= -0.3142 + j3.1258 \ , \\ s_4 = \bar{s}_5 &= -0.0628 + j6.2829 \ , \\ s_6 = \bar{s}_7 &= -0.0094 + j9.4248 \quad . \end{aligned}$$

Expand P at its poles (three multiplicity one complex-conjugate pairs and two at zero) ,

$$P(s) =: \frac{k_0}{s} + \frac{k_1}{s^2} + \frac{k_2}{(s-s_2)} + \frac{\bar{k}_2}{(s-\bar{s}_2)} + \frac{k_4}{(s-s_4)} + \frac{\bar{k}_4}{(s-\bar{s}_4)} + \frac{k_6}{(s-s_6)} + \frac{\bar{k}_6}{(s-\bar{s}_6)} \ , \tag{15}$$

where

$$\begin{aligned} k_0 &= 0 \\ k_1 &= 1 \\ k_2 &= j0.7998 \\ k_4 &= j0.7958 \\ k_6 &= j1.0610 \quad . \end{aligned}$$

In general, admissible reference trajectories r will have the expansion

$$R(s) =: \frac{r_0}{s} + \frac{r_1}{s^2} + \frac{r_2}{(s-s_2)} + \frac{\bar{r}_2}{(s-\bar{s}_2)} + \frac{r_4}{(s-s_4)} + \frac{\bar{r}_4}{(s-\bar{s}_4)} + \frac{r_6}{(s-s_6)} + \frac{\bar{r}_6}{(s-\bar{s}_6)} \ . \tag{16}$$

Let the input be chosen as in (7) . Using the fact that signals in $\mathcal{U}_T$ do not have any poles, apply the matching conditions in (4 to

$$R(s) = P(s)U_p(s) \quad ,$$

where P and R are as in (15) and (16) , respectively. Equating the coefficients of the partial fraction expansions, we obtain

$$k_1 U_p(0) = r_1 \tag{17}$$

$$k_0 U_p(0) + k_1 U_p^{(1)}(0) = r_0 \tag{18}$$

$$k_2 U_p(s_2) = r_2 \tag{19}$$

$$k_4 U_p(s_4) = r_4 \tag{20}$$

$$k_6 U_p(s_6) = r_6 \quad . \tag{21}$$

Note that equations (17 – 21) describe $n = 8$ linear equations with real coefficients in $N = 20$ unknowns, namely

$$\Gamma(T)p \;=\; \gamma \;:=\; [r_0\; r_1\; \mathrm{Real}(r_2)\; \mathrm{Imag}(r_2)\; \mathrm{Real}(r_4)\; \mathrm{Imag}(r_4)\; \mathrm{Real}(r_6)\; \mathrm{Imag}(r_6)]^T \quad .$$

For ease of notation let $\mathrm{ones}(1, N)$ denote the row vector whose entries are all equal to 1 . Let $[1 : N]$ denote the row vector whose ith entry is equal to i . For $s \in \mathbb{C}$,

$$\phi(s, T) \;:=\; \nu(s, T) \left[\; e^{-sT/N}\; e^{-2sT/N}\; \ldots\; e^{-sT} \;\right] \quad ,$$

where

$$\nu(s, T) \;:=\; \frac{e^{sT/N} - 1}{s} \quad .$$

For $T = 1 + (m-1)\Delta T$, $\Gamma(T) \in \mathbb{R}^{n \times N}$ is given by :

$$\Gamma(T) \;:=\; \begin{bmatrix} (T/N)^2\,(0.5 \cdot \mathrm{ones}(1, N) \;-\; [1 : N]) \\ (T/N) \cdot \mathrm{ones}(1, N) \\ \mathrm{Real}(k_2 \nu(s_2, T) \phi(s_2, T)) \\ \mathrm{Imag}(k_2 \nu(s_2, T) \phi(s_2, T)) \\ \mathrm{Real}(k_4 \nu(s_4, T) \phi(s_4, T)) \\ \mathrm{Imag}(k_4 \nu(s_4, T) \phi(s_4, T)) \\ \mathrm{Real}(k_6 \nu(s_6, T) \phi(s_6, T)) \\ \mathrm{Imag}(k_6 \nu(s_6, T) \phi(s_6, T)) \end{bmatrix} \qquad (22)$$

For illustration purposes, we will assume that the flexible modes are not excited and the sequence of input signals achieve slewing and tumbling maneuvers; i.e., we will focus on T-tracking of steps and ramps only. Such an assumption is made so that the steps taken can be easily comprehended; by working on a two-dimensional subspace of the residue space, we can illustrate the T-isochrones and the T-tracking signal generation easily. However, as emphasized throughout the study, the results are general.

We now solve N_T linear programs along $\gamma = e_1$ and another N_T linear programs along $\gamma = e_2$.

The e_1-maximum-performance curve and e_2-maximum-performance curve are shown in Figure 3 .

3.5.3 e_1-Maximum-Performance Curve

In this section, we will evaluate the e_1-maximum-performance curve obtained by linear programs. For the plant model P in (14) , we do not have the exact "time-optimal" performance curve. Hence the true errors introduced in the approximation cannot be accounted for. However, a very useful comparison will be made instead, based on the rigid-body approximation to P .

Let

$$\hat{P} \;:=\; \frac{1}{s^2} \quad .$$

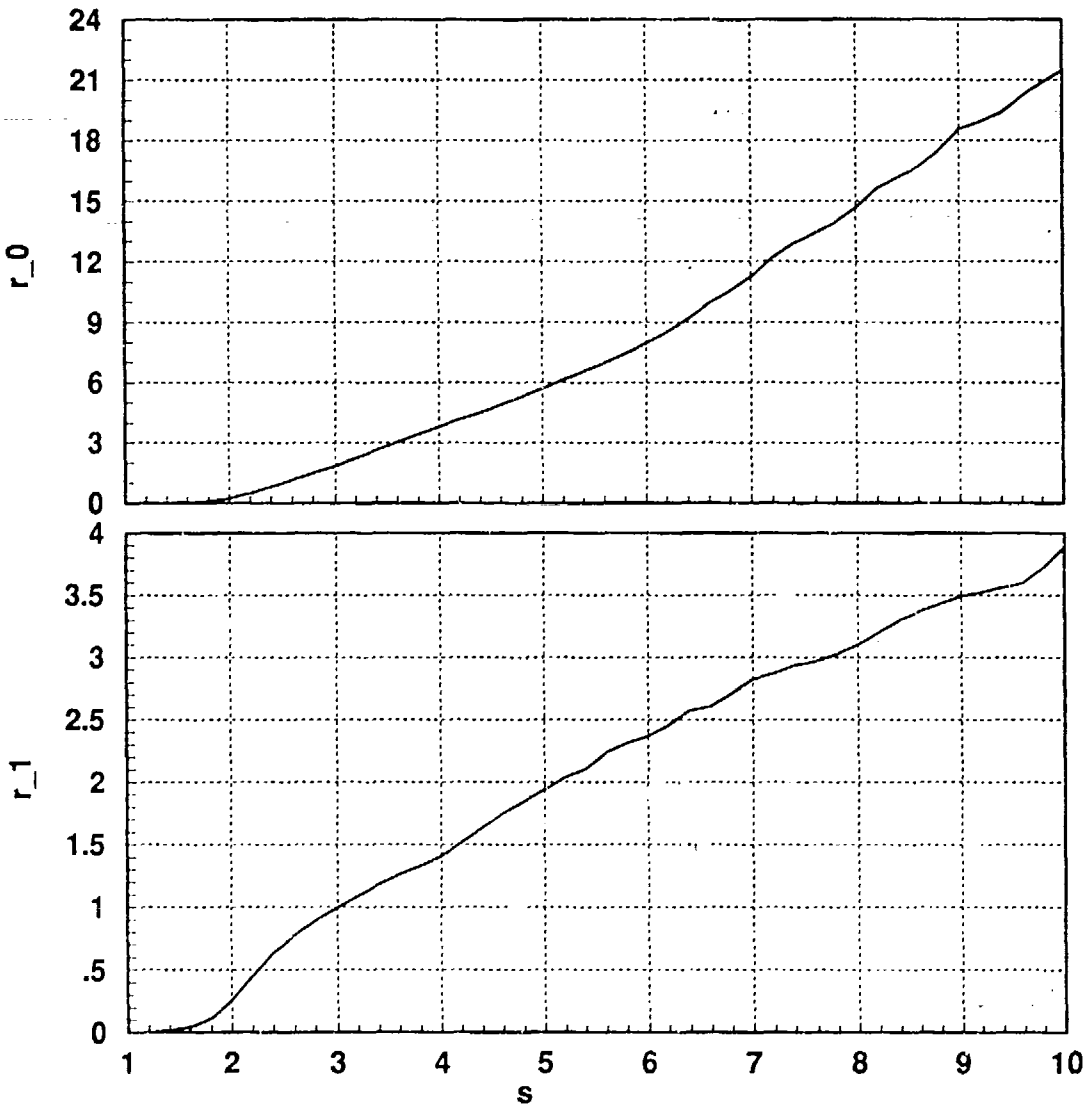

Figure 3: e_1- and e_2-maximum-performance curves

Note that, P can be considered as a perturbation of the double-integrator model $\hat{P}$. The e_1-time-optimal-performance curve of P is given by

$$up_0(T) := (\frac{T}{2})^2 \quad . \tag{23}$$

Recall that the optimal bang-bang input waveform (for $\hat{P}$) is

$$u(t) = \begin{cases} +1 & t \in [0, T/2) \\ -1 & t \in [T/2, T] \\ 0 & t > T \end{cases} \quad .$$

The curve up_0 is an upper bound on the performance of P . In order to rate the achieved performance, consider

$$low_0(T) := (\frac{0.9T}{2})^2 \quad . \tag{24}$$

If the e_1-maximum-performance curve lies above low_0 we can conclude that P achieves the performance of $\hat{P}$ within a 10% relative error in time. In other words, if $\hat{P}$ can $\hat{T}$-track r_0 , then P can T-track r_0 where $T \in [\hat{T}, 1.1\hat{T}]$. The three curves: e_1-maximum-performance curve , up_0 and low_0 are shown in Figure 4 .

Note that after 3 s , the e_1-maximum-performance curve lies in between up_0 and low_0 . In other words, for $T \in [3, 10]$ s , the 20-parameter linear program approximation generates inputs for which P achieves the performance of the rigid-body approximation $\hat{P}$ within 10% relative error in time.

Before proceeding with the rest of the results, we would like to draw the attention to the region $T \in [1, 3]$ s in Figure 4 . This region is shown again in Figure 5 .

We sought an explanation for the deviation over this region shown in Figure 5 from the rigid-body performance. To be specific, we focused on the rigid-body performance at 1 s , which is achieved by the approximation after 2 s . Note that due to the time-quantization, current result will achieve $r_0 = 0.25$ exactly in 2.2 s. In order to see the improvements in the linear program approximations versus the parameter N , we derived the e_1-maximum-performance at $T = 2$ s. The results are listed in Table 1 . Even for 100-pulse approximation, the performance improved by only 4% .

N	$\Psi(2, e_1)$
20	0.2384
30	0.2451
40	0.2460
100	0.2486

Table 1: e_1-maximum-performance at 2 s .

As another approach, we fixed $N = 20$ and decreased the time-quantization; r_0 was achieved in 2.013 s . In other words, the 20-parameter approximation generates inputs so that the plant P can 2.013-track the 0.25-step. This translates into a 102% relative error in time.

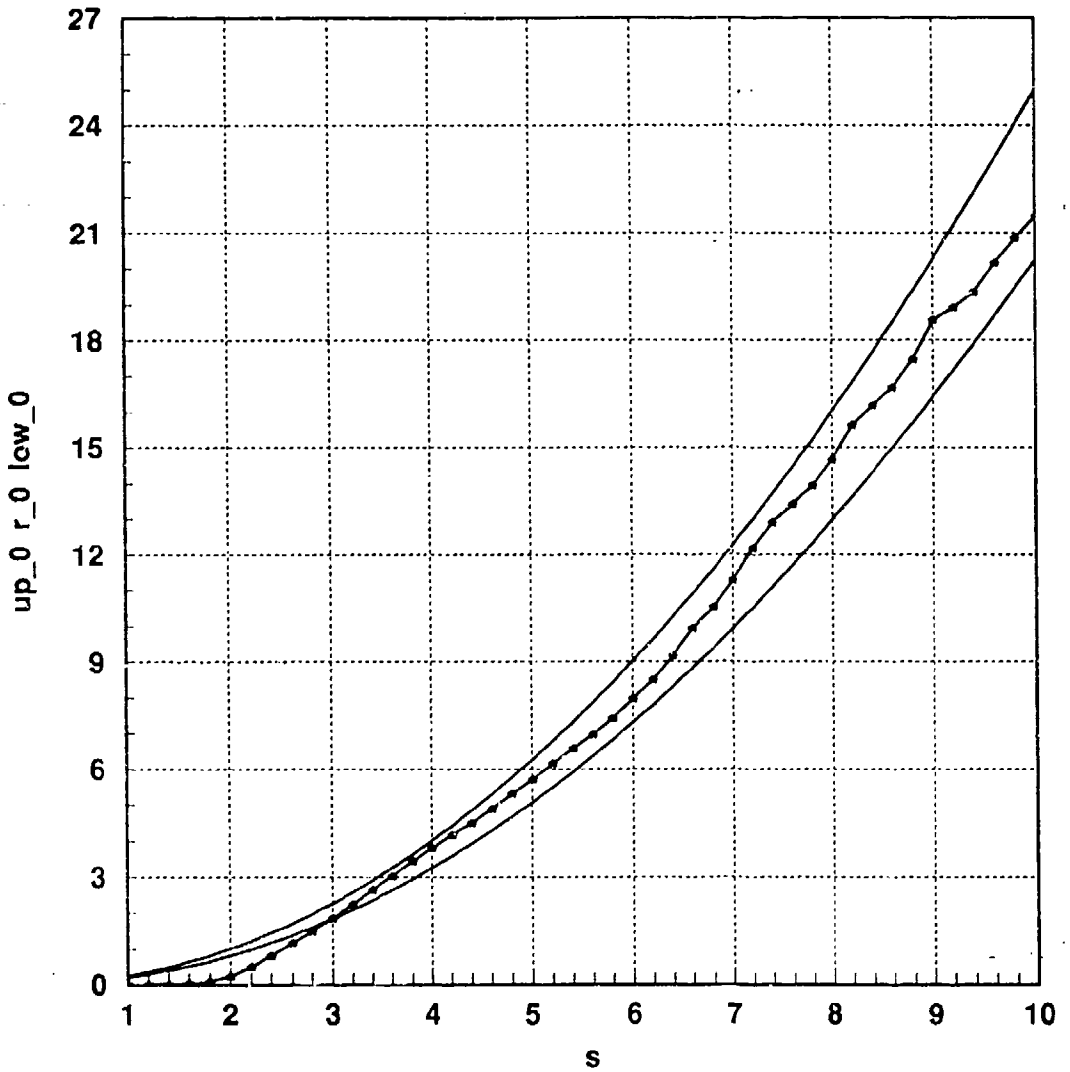

Figure 4: e_1-maximum-performance curve (*) , up_0 (23) and low_0 (24)

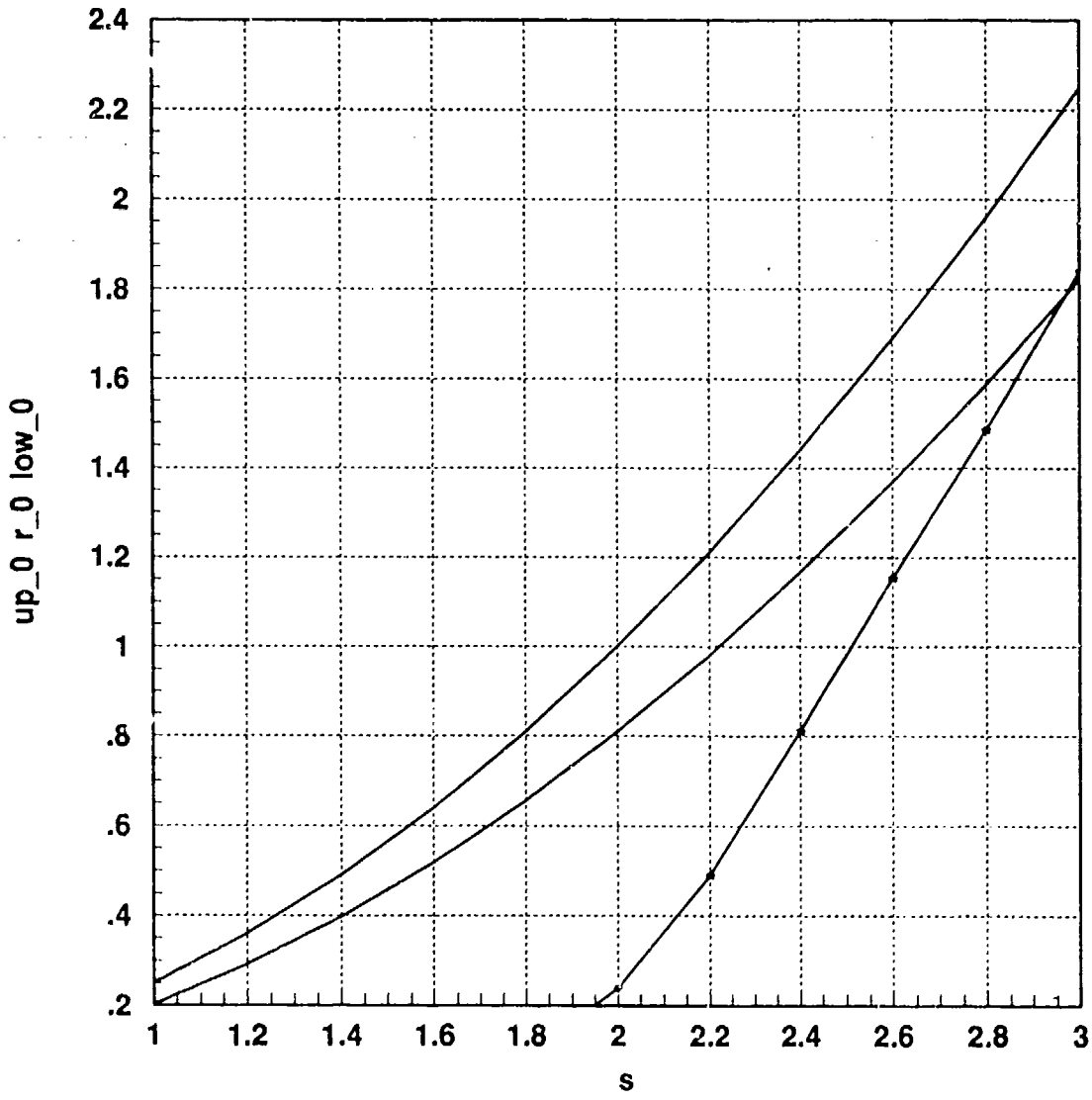

Figure 5: Figure 4 redrawn for $T \in [1, 3]$ s .

In order to account for this 102% relative error in time , the intrinsic limitation of the 1 s maneuver was revealed using the minimum energy solution as explained in Section 3.3.6 .

Consider a state-space description of the plant P in (14) , where the position is the first state. The goal is to get from $x_0 = 0 \in \mathbb{R}^8$ to $x_T = [(\frac{T}{2})^2\ 0\ \ldots\ 0]^T$, which denotes the rigid-body performance in T seconds. Let $W_C(0, T(1+\varepsilon))$ denote the controllability gramian at $T(1+\varepsilon)$. Clearly, if there exists an input $u \in \mathcal{U}_{T(1+\varepsilon)}$ such that $\|u\|_\infty \leq 1$ and u steers x_0 to x_T , necessarily,

$$[W_C^{-1}(0, T(1+\varepsilon))]_{11} \leq \frac{16}{T^3}(1+\varepsilon) \quad , \tag{25}$$

where $[\cdot]_{11}$ denotes the $(1,1)$-entry and ε denotes the relative error needed to satisfy the necessary condition. At $T = 1$ s , we obtain the results in Table 2 .

ε	$[W_C^{-1}(0,(1+\varepsilon))]_{11}/16/(1+\varepsilon)$
0	$1.2278 * 10^5$
50%	78.8319
75%	3.7966
80%	2.1550
85%	1.2437
90%	0.7323
95%	0.4421

Table 2: Necessary condition (25) at $T = 1$ s .

From Table 2 , (which are evaluations of analytically derived necessary conditions), we conclude that there exits a $u \in \mathcal{U}_T$ that steers x_0 to x_T only if $T \geq \hat{T} \in [1.85, 1.90]$ s . Recall that we are also interested in an input $\|u\|_\infty \leq 1$; even for $T = \hat{T}$ there may not be such a bounded input. Regardless, even if there is a bounded (by one) signal that achieves the performance within 1.9 s , this translates into a 90% relative error in time which is an intrinsic limitation. Compared with the 111% relative error obtained by 20-parameter linear program approximation, we conclude that the approximation error is bounded by 12% . Intuitively, 0.5 Hz mode implies that a 2 s slew will be a critical slew. Any slew time slower than 2 s will affect the frequency band above 0.5 Hz , namely the modes of the plant.

3.5.4 e_2-Maximum-Performance Curves

These results bring an approximate solution to the fast T-tracking of a moving target. Note that in the e_1 case, namely the rest-to-rest slew, the goal was to get from an initial state of the form $[r_0\ 0\ 0\ \ldots\ 0]^T$ to $[r_0 + \delta r_0\ 0\ 0\ \ldots\ 0]^T$. In other words, the target set is fixed. In the e_2-case, however, the goal is to reach from $[r_0\ 0\ 0\ \ldots\ 0]^T$ to the moving target $[r_0 + r_1 T\ r_1\ 0\ \ldots\ 0]^T$ as fast as possible.

Recall that the e_2-time-optimal-performance of the double-integrator $\hat{P}$ (namely, T-tracking $y(t) = r_1 t$ from zero steady-state) is given by

$$up_1(T) \ := \ \frac{T}{(1+\sqrt{2})} \ = \ r_1 \quad . \tag{26}$$

Note that the time-optimal bang-bang input waveform (for $\hat{P}$) is

$$u(t) \;=\; \begin{cases} +1 & t \in [0, T_1) \\ -1 & t \in [T_1, T] \\ 0 & t > T \end{cases} \quad ,$$

where

$$T_1 \;:=\; r_1 \frac{(2+\sqrt{2})}{2} \quad .$$

The curve up_1 is an upper bound on the e_2-performance of P . In order to rate the achieved performance, consider

$$low_1(T) \;:=\; (\frac{0.8T}{2})^2 \quad . \tag{27}$$

If the e_2-maximum-performance curve lies above low_1 , we can conclude that P achieves the performance of $\hat{P}$ within a 20% relative error in time. In other words, if $\hat{P}$ can $\hat{T}$-track $r_1 t$, then P can T-track $r_1 t$ where $T \in [\hat{T}, 1.2\hat{T}]$. The three curves: e_2-maximum-performance curve , up_1 and low_1 are shown in Figure 6 .

Note that after 3 s , the e_2-maximum-performance curve lies in between up_1 and low_1 . In other words, for $T \in [3, 10]$ s , the 20-parameter linear program approximation generates inputs for which P achieves the performance of the rigid-body approximation $\hat{P}$ within 20% relative error in time.

Similar intrinsic limitations could be worked out for this performance plot in Figure 6 . Note that for [4.5, 10] s , the 20-parameter approximation has at most 10% relative error.

3.5.5 $\bar{\mathcal{S}}_T$

Recall the T-polytope $\bar{\mathcal{S}}_T$ in the positive orthant of the residue-space (see (12)) . For the purpose of illustration, consider the projection of $\bar{\mathcal{S}}_T$ onto the first two coordinates of the residue-space. In the rest of this section we will refer to $\bar{\mathcal{S}}_T$ and the T-polytope $\mathcal{S}_T$ (see (10)) as the projections:

$$\begin{aligned} \bar{\mathcal{S}}_T &\leftarrow \bar{\mathcal{S}}_T \cap \{ x \in \mathbb{R}^n \mid x_3 = x_4 = \cdots = x_n = 0 \} \quad , \\ \mathcal{S}_T &\leftarrow \mathcal{S}_T \cap \{ x \in \mathbb{R}^n \mid x_3 = x_4 = \cdots = x_n = 0 \} \quad . \end{aligned} \tag{28}$$

We now comment on the approximation $\bar{\mathcal{S}}_T$ of $\mathcal{S}_T$ for the specific example.

Consider Figure 7 , showing two sets of boundaries representing the 5-isochrone and 10-isochrone, respectively.

5- and 10-Isochrones :

Using the simple N_T-linear program approximations along e_1 and e_2 , respectively, one obtains N_T isochrones . For the purpose of illustration, we focus on the 5- and 10-isochrones shown in Figure 7 . Following (28) and (12) , the polytope $\mathcal{S}_5$ is determined by the boundary $0 \quad A \quad D \quad 0$. The polytope $\mathcal{S}_{10}$ is determined by the boundary $0 \quad E \quad H \quad 0$. In order to rate the effectiveness of the approximation ($\bar{\mathcal{S}}_T$ approximating $\mathcal{S}_T$) , we solved two sets of linear programs along two more directions other than e_1 and e_2 ; specifically,

$$\Phi(T, [1\ 1\ 0\ 0\ \ldots\ 0]^T)$$

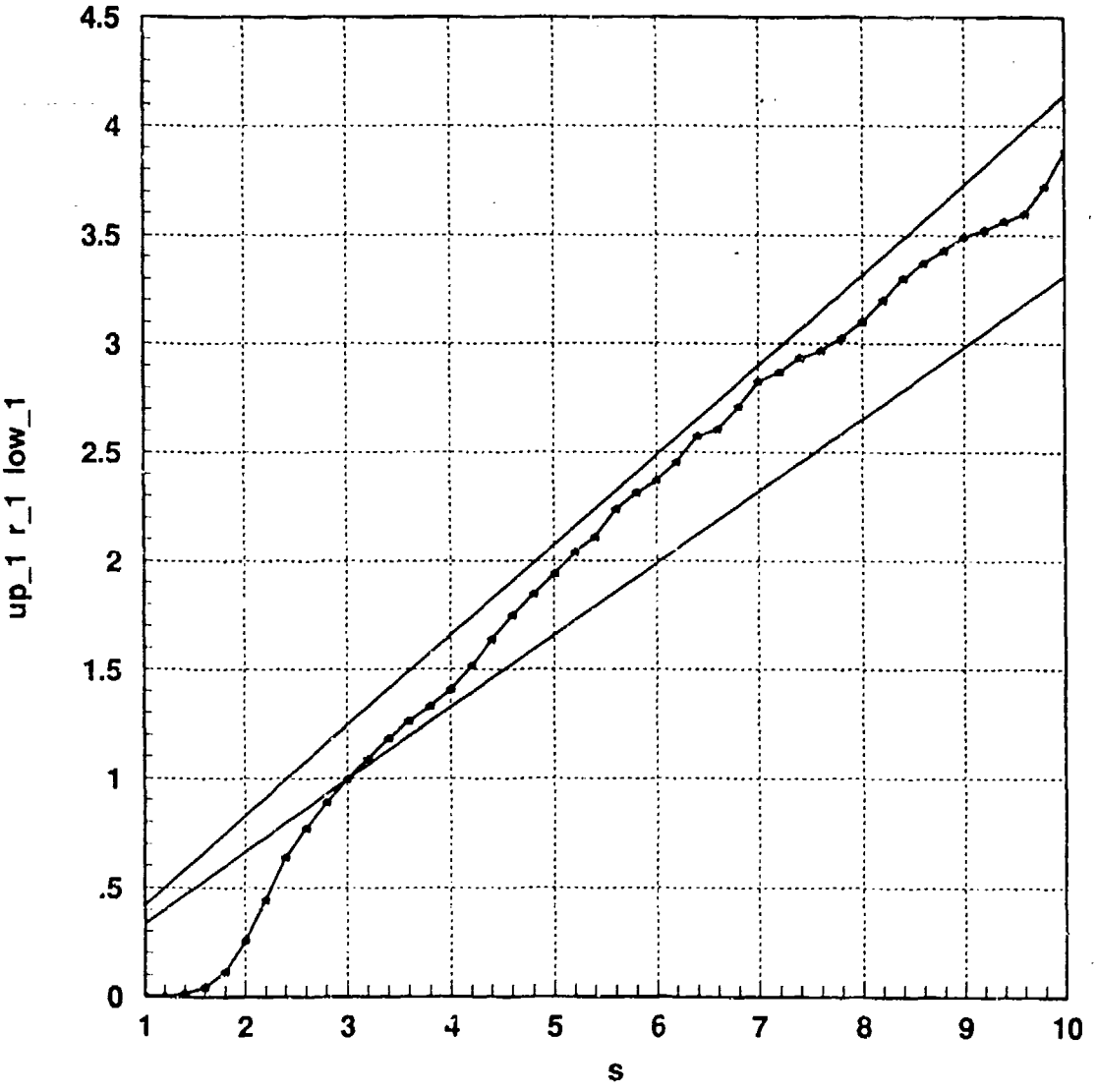

Figure 6: c_2-maximum-performance curve (*) , up_1 (26) and low_1 (27)

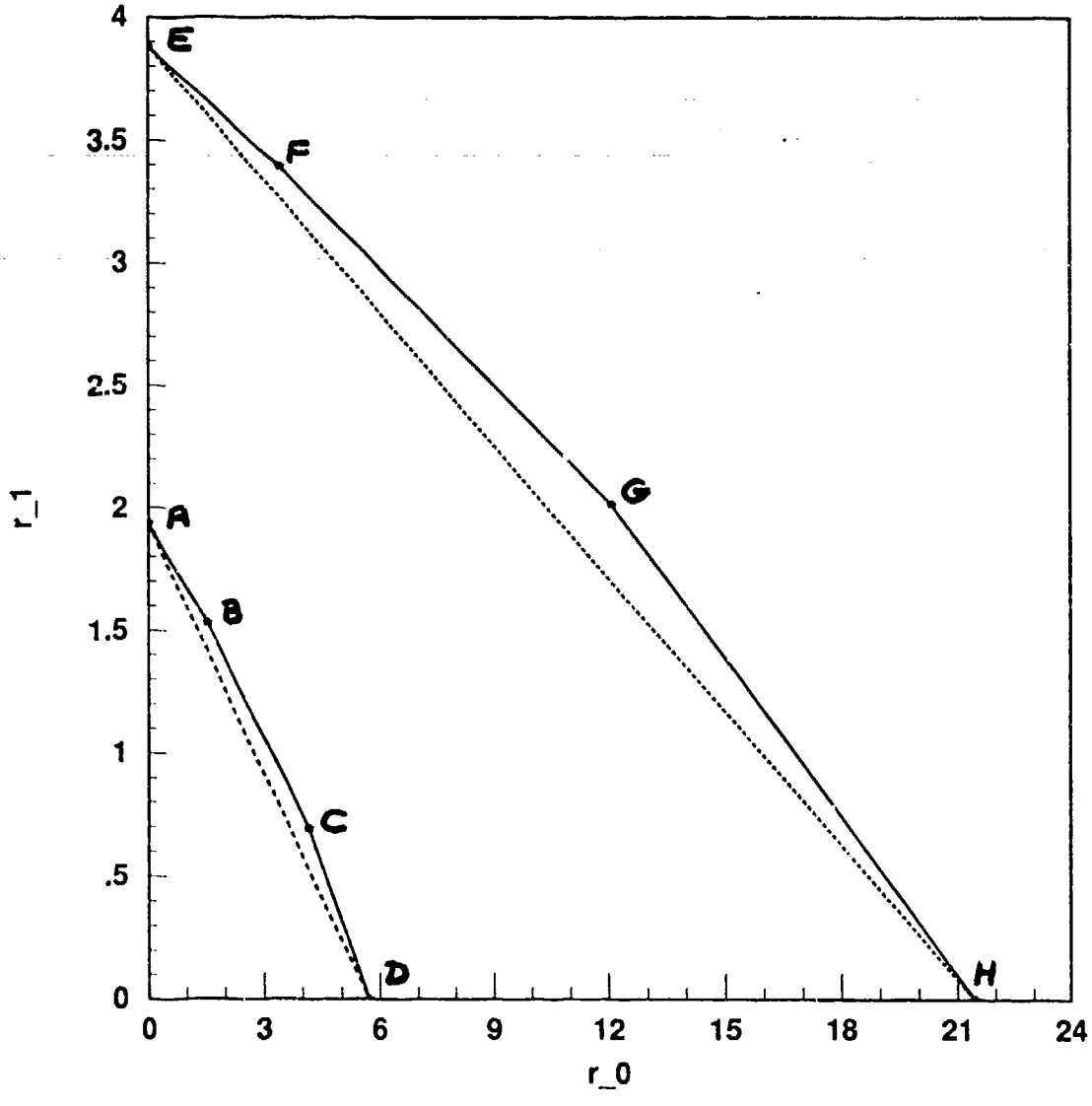

Figure 7: $\bullet\bar{\mathcal{S}}_5 \ : \ 0-A-D-0 \ \bullet\bar{\mathcal{S}}_{10} \ : \ 0-E-H-0 \ \bullet$ An approximation to $\mathcal{S}_5 \ : \ 0-A-B-C-D-0 \ \bullet$ An approximation to $\mathcal{S}_{10} \ : \ 0-E-F-G-H-0$

and

$$\Phi(T, [6\ 1\ 0\ 0\ \ldots\ 0]^T) \quad .$$

In other words, we obtained the maximum-peformance curves along the rays

$$(0 - \overrightarrow{B} - F) \text{ and } (0 - \overrightarrow{C} - G) \quad ,$$

respectively (see Figure 7) . Using the associated four-breakpoints, we obtain $0 - A - B - C - D - 0$ as an approximation to $\mathcal{S}_5$ and $0 - E - F - G - H - 0$ as an approximation to $\mathcal{S}_{10}$ (see Figure 7) . Note the amount of improvement in each case. For the 10-second case, comparison of the enclosed areas ($0 - E - H - 0$ versus $0 - E - F - G - H - 0$) reveals an 8.64% improvement.

Clearly, by introducing more directions, one can obtain successively better approximations to $\mathcal{S}_T$. Our goal was to generate a map from the residue-space into the input space. In the process, given a point in the residue-space, we seek a pair of succsessive T-isochrones for which the point is outside one but inside the next. We then use the data associated with the breakpoints of the isochrones to determine the required input. Clearly, the one-hyperplane approximation $\bar{\mathcal{S}}_T$ is the simplest. Introducing more hyperplanes increase the accuracy of the T-polytope approximation, however it complicates the generation of inputs. A multi-hyperplane approximation may eventually require another linear program solution to determine the "cooordinates" of the point in the residue-space in terms of the "corners" of the associated T-polytope.

3.5.6 A Fast T-Tracking Example

In this section we illustrate Steps 6–8 in Section 3.4.7 . Assume that the plant P in (14) is initially at rest. Let the reference trajectory r be as shown in Figure 8 .

The breakpoints and slopes in Figure 8 reveal that the sequence of inputs should satisfy the following increments in the residue-space denoted by the ordered pairs (r_0, r_1) :

$$\begin{array}{lll} \text{at } T = 0 & , & (+2,\ 0) \\ \text{at } T = 5 & , & (-2, -1) \\ \text{at } T = 12 & , & (+7, +1) \quad . \end{array}$$

Using the one-hyperplane approximations to the N_T T-polytopes, the fastest tracking times for the sequence of residue increments are 3.2 , 4.6 and 7 s , respectively. Figure 9 shows the input and the associated output of P in (14) .

3.6 Robustness Considerations

Consider a plant P of the form

$$P \ = \ \hat{P} \ + \ \frac{\widetilde{K}}{(s - \tilde{s})} \quad , \tag{29}$$

where

$$\begin{array}{l} \tilde{s} \ = \ s_0 + re^{j\theta} \quad , \quad 0 \leq r \leq 1 \quad , \quad 0 \leq \theta \leq 2\pi \quad , \\ \widetilde{K} \in \mathbb{R}^{n_o \times n_i} \quad , \quad \widetilde{K} = (I + \Delta)\widetilde{K_0} \quad , \quad \|\Delta\|_2 \leq \delta \quad . \end{array}$$

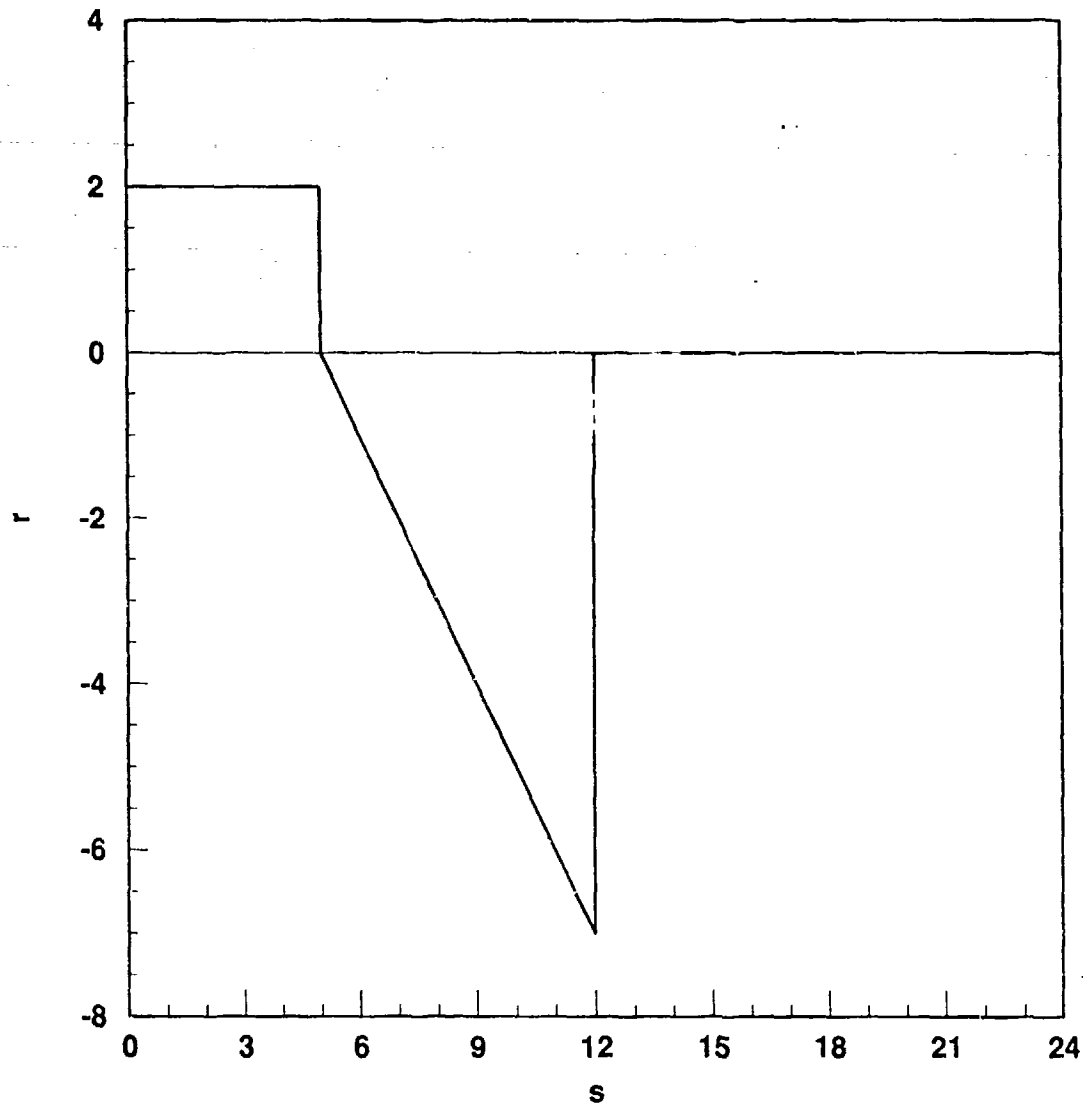

Figure 8: Reference trajectory to be fast T-tracked

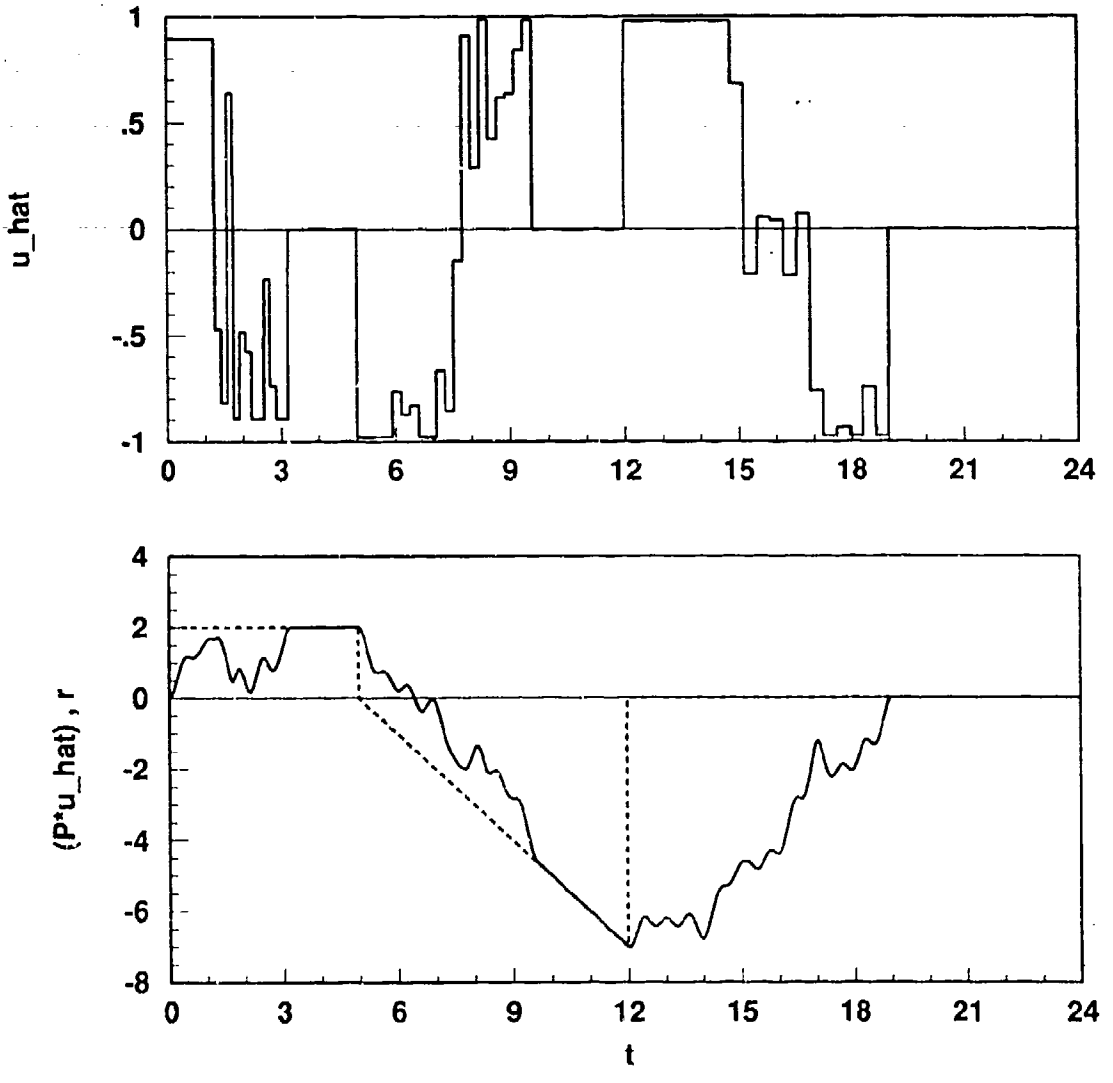

Figure 9: An input signal $\hat{u}$ such that $P * \hat{u}$ fast T-tracks r

In other words, the plant model P is "exact" up to $\hat{P}$ with an uncertainty description about the pole at s_0 . We assume that the location of this pole is uncertain, i.e., the multiplicity of the pole remains the same in the region of uncertainty. As we will see later on, the multiplicity of the pole (as long as it remains the same) and/or the region of uncertainty about the pole can be more general (i.e., multiplicity can be greater than one; the region can be any closed bounded simply connected region about the pole) .

As we have seen before, in order for P to T-track the reference signals of interest, $\hat{P}$ is assumed to have all the necessary poles. Our concern is the residual vibration due to the (possibly uncertain) poles which do not coincide with the poles of the reference signal. For example, for the plant model in (14) , steps and ramps would be the set of reference signals and $\hat{P}$ would have at least two poles at $s = 0$; the uncertainty due to, say, one of the flexible modes could be incorporated as in (29) ; note that for such a case, there would be another residue term due to $\bar{s_0}$.

The crucial point is, since the Laplace transforms of signals in $\mathcal{U}_T$ are entire, we can use the property of harmonic functions to bring an upper bound on the residual vibration due to the uncertainties. Clearly, for any signal $u \in \mathcal{U}_T$ with $\|u\|_\infty \leq 1$,

$$\|U^{(k)}(s)\| \leq T^k \frac{n_i}{\sigma}[1 - e^{-\sigma T}] \quad , \quad k \geq 0 \quad , \quad \text{for all } s \text{ such that Real}(s) \geq \sigma \quad .$$

Such a bound is too conservative, since typically we will be dealing with a weighted sum of a specific set of input signals.

Let $U_p(s)$ denote the Laplace-transform of a family of signals in $\mathcal{U}_T$ which is parametrized by $p \in \mathbb{R}^N$.

One approach would be to introduce more constraints on p , in terms of derivatives of $U_p(s)$. Using the Taylor-series expansion about s_0 , imposing the constraints

$$\widetilde{K}_0 U_p^{(j)}(s_0) = 0 \quad , \quad j = 0, \ldots, (\widetilde{N} - 1) \quad ,$$

for some $\widetilde{N} \geq 1$, guarantees that the residual term $R_{\widetilde{N}}$ is

$$R_{\widetilde{N}} \;=\; \sum_{k=\widetilde{N}}^{\infty} \frac{r^k e^{j\theta k}}{k!} U_p^{(k)}(s_0) \quad .$$

In other words, for any $\tilde{s}$, the norm of the residue of the output at $\tilde{s}$, cannot exceed

$$\|(I + \Delta)\widetilde{K}_0 R_{\widetilde{N}}\| \quad .$$

Note that, since $U_p(s)$ is entire, it cannot vanish for all $\hat{s}$ unless it is identically zero for all s . Such an approach would increase the number of constraints on p ; however, the resulting problem is still a linear program, hence the previously proposed methods still apply.

Another approach gives up the linear program setting and ends up with a convex minimization problem by minimizing the worst-case residue. Since $U_p(s)$ is harmonic, for a closed bounded simply-connected region Ω about s_0 , we have

$$\sup_{s \in \Omega} \|U_p(s)\| \;=\; \sup_{\partial\Omega} \|U_p(s)\| \quad ,$$

where $\partial\Omega$ denotes the boundary of the region $\Omega \ni s_0$. Discretize the boundary so that

$$\partial\Omega \approx \Omega_M := \{ s_i \mid i = 1, \ldots, M \} \quad .$$

For the specified direction γ in the residue-space, obtain the maximum-performance for the nominal plant

$$\hat{P} + \frac{\widetilde{K}_0}{(s - s_0)} \quad ,$$

as explained in the previous sections. In other words, solve for

$$\begin{aligned} \hat{\lambda} &= \Psi(T, \gamma) \\ \hat{p} &= \Phi(T, \gamma) \quad . \end{aligned}$$

The linear contraints on p take into account

$$\widetilde{K}_0 U_p(s_0) = 0 \quad .$$

For this $\hat{\lambda}$ the norm of the change in the residue over Ω is bounded above by

$$\kappa := \|(I + \Delta)\widetilde{K}_0\| \max_{s \in \Omega_M} \|U_{\hat{p}}(s)\| \quad .$$

Provided that κ is not desirable, choose $\lambda < \hat{\lambda}$ (i.e., give up from the performance; in addition, one may also increase N) and solve the following convex minimization problem:

$$\begin{array}{ll} \min\limits_{p \in \mathbb{R}^N} & \max\limits_{s \in \Omega_M} \|U_p(s)\| \quad . \\ \Gamma(T)p = \lambda\gamma & \\ -1 \leq p \leq 1 & \end{array}$$

Using the global minimum values (for different λ's) , one could then see how much the original performance $\hat{\lambda}$ has to be degraded in order to have a desired residual performance.

3.7 Closing the Loop

In the previous sections, we proposed a method of generating an input signal $u \in \mathcal{U}_T$, that achieves fast T-tracking of the desired γ subject to the actuator saturation constraints. By solving a sequence of linear programs, a look-up table is generated over a region in the residue-space. This look-up table is incorporated in a "signal generator" which is used to drive a unity-feedback system. We now describe the procedure.

3.7.1 Signal Generator

Consider the interconnection in Figure 10 showing the proposed "signal generator" .

The desired reference signal is represented in the residue-space by γ_r . Recall that for a given plant model, the set of admissible reference signals that can be T-tracked can be characterized by a partial-fraction expansion at the plant poles. The coefficients of this

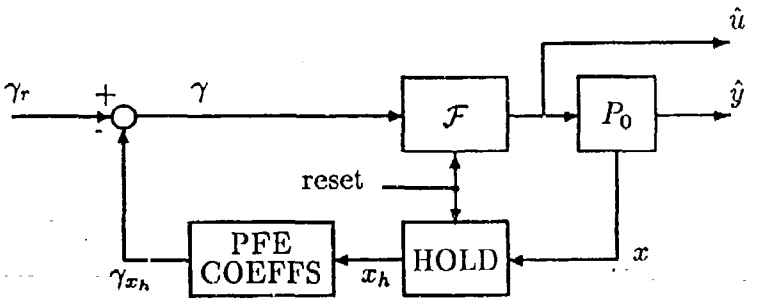

ure 10: Signal Generator

expansion are the entries of γ_r . In order to represent a series of reference signals, from now on, γ in the residue space will be identified with a waveform $\gamma : \mathbb{R}_+ \rightarrow \mathbb{R}^n$. Note that all three versions (of γ) in Figure 10 will be piecewise-constant waveforms.

Whenever there is a jump-discontinuity in γ_r , the "reset" command initializes the clock in $\mathcal{F}$ and trigg rs the "HOLD" block to hold the value of the plant's state x at the time of "reset" . Once the state x is held at x_h , the contribution of x_h in the residue-space is computed by multiplying x_h with the suitable Partial-Fraction Expansion Coefficients (denoted by the block "PFE COEFFS") . The difference between γ_r and γ_{x_h} determines the command γ .

The block denoted by $\mathcal{F}$ implements the proposed scheme in Section 3.4.7 . For a given command γ , the fastest T-tracking input $\hat{u}$ is generated from the condensed data in the look-up tables. The "reset" input synchronizes the clock in $\mathcal{F}$ in order to generate the input waveform $\hat{u}$ from a data point in $\mathbb{R}^N$. The look-up tables in $\mathcal{F}$ corresponds to the nominal plant model P_0 . As explained before, specific uncertainty descriptions about the nominal plant model P_0 can be incorporated during the pre-computations to generate the look-up tables.

One of the many drawbacks of an open-loop implementation is sensitivity to disturbances. Consider the model in Figure 11 ; the SAT_α [6] block accounts for the saturation in the actuators.

Clearly, when the input disturbance d_{in} is zero, the signal generator configuration can be used to determine the desired $\hat{u}$ for the desired $\hat{y}$. For a bounded disturbance $d_{in} \neq 0$, the nonzero tracking error may even be unbounded when P is unstable.

3.7.2 Unity-Feedback System

Once the desired $\hat{u}$ and $\hat{y}$ are determined, these signals are used in the unity-feedback configuration in Figure 12 . We now describe a conservative design procedure for determining a compensator C . Some of the steps are illustrated with a sample design where P is taken

---

[6] For a given $\alpha > 0$, $\text{SAT}_\alpha(\cdot) : \mathbb{R}^{n_i} \rightarrow \mathbb{R}^{n_i}$, $e_k^T SAT_\alpha(u) := \begin{cases} -\alpha & , \ e_k^T u \leq -\alpha \\ e_k^T u & , \ |e_k^T u| \leq \alpha \\ \alpha & , \ e_k^T u \geq \alpha \end{cases} \quad k = 1, \ldots, n_i$.

Note that $\text{SAT}_\alpha(u) = \alpha \text{SAT}_1(\frac{1}{\alpha} u)$.

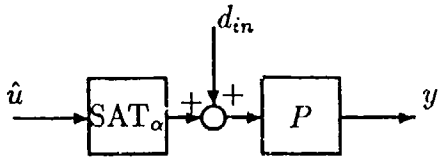

Figure 11: Plant model

as the model in (14) .

Typically the model P in Figure 11 is not the same as P_0 in the signal generator. Our goal is to design a C such that certain disturbance rejection and/or robustness characteristics are achieved by the closed-loop. The tracking specifications are totally ignored during this design procedure since the fast T-tracking is achieved by the $(\hat{u}, \hat{y})$ pair.

In the rest of the section, we assume that the nominal plant model P_0 in the signal generator and the plant model P in the unity-feedback are the same; moreover, the initial conditions are identical. The disturbance d_{in} comes in after the saturation block (see Figure 12) .

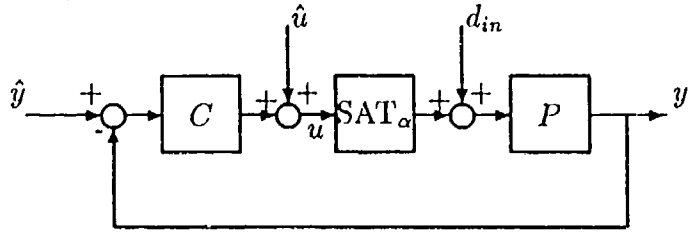

Figure 12: Closed-loop implementation

Note that the signal generator in Figure 10 does not have a SAT_α block pre-cascaded since the output of $\mathcal{F}$ is always within the bounds (by construction).

For the closed-loop system in Figure 12 , over the operation region for which $\|u\|_\infty \leq \alpha$, the closed-loop map from $(\hat{u}, \hat{y}, d_{in})$ to u is given by

$$u \;=\; (I + CP)^{-1}\hat{u} \;+\; C(I + PC)^{-1}\hat{y} \;-\; CP(I + CP)^{-1}d_{in} \quad .$$

Provided that $\hat{y} = P\hat{u}$, we obtain

$$u = \hat{u} \;-\; CP(I + CP)^{-1}d_{in} \quad .$$

Clearly, when $d_{in} = 0$, we have $u = \hat{u}$; hence the nominal closed-loop performance achieves T-tracking. Note that this is true for any stabilizing C with $\|u\|_\infty \leq \alpha$. This brings up a trade-off issue: smaller the contribution of d_{in} at u means faster T-tracking and greater sensitivity to d_{in} at the plant output y .

Let the input disturbances be such that

$$\|d_{in}\|_\infty \;\leq\; 0.25 \quad . \tag{30}$$

Suppose that $\alpha = 2$ and 50% of the actuation authority is to be used for disturbance rejection. This specification requires that a stabilizing C satisfies

$$\|CP(I + CP)^{-1}\|_1 \leq 4 \quad , \tag{31}$$

where $\|\cdot\|_1$ denotes the $\mathcal{L}_\infty$-gain. By generating the look-up tables so that $\|\hat{u}\|_\infty \leq 1$, using (30) and (31) , we obtain

$$\|u\|_\infty \leq 2 \quad .$$

Hence we have a conservative design since the SAT_2 block acts as the identity map over the operation region. Note that the T-tracking portion (i.e., the linear program solutions and determining the signal generator) is a totally separate procedure from the compensator design once the actuation authorities are allocated for fast T-tracking and disturbance rejection, respectively.

A stabilizing compensator C is designed for which (31) holds. We now use the $(\hat{u}, \hat{y})$ pair in Figure 9 to illustrate the obvious advantage of a closed-loop design. A disturbance signal satisfying (30) is shown in Figure 13 ; d_{in} has a DC component, the signal after 10 s is a sum of four sinusoids at 0.1 , 0.5 , 1 and 1.5 Hz , the last three at the modal frequencies of P . Figure 13 also shows the open-loop implementation; $P * (\hat{u} + d_{in})$ introduces a considerable tracking error.

Figure 14 shows the closed-loop signals u in y (see Figure 12 ; $\hat{u}$, $\hat{y}$ and d_{in} are as mentioned above) . The tracking error $(y - \hat{y})$ is shown in Figure 15 .

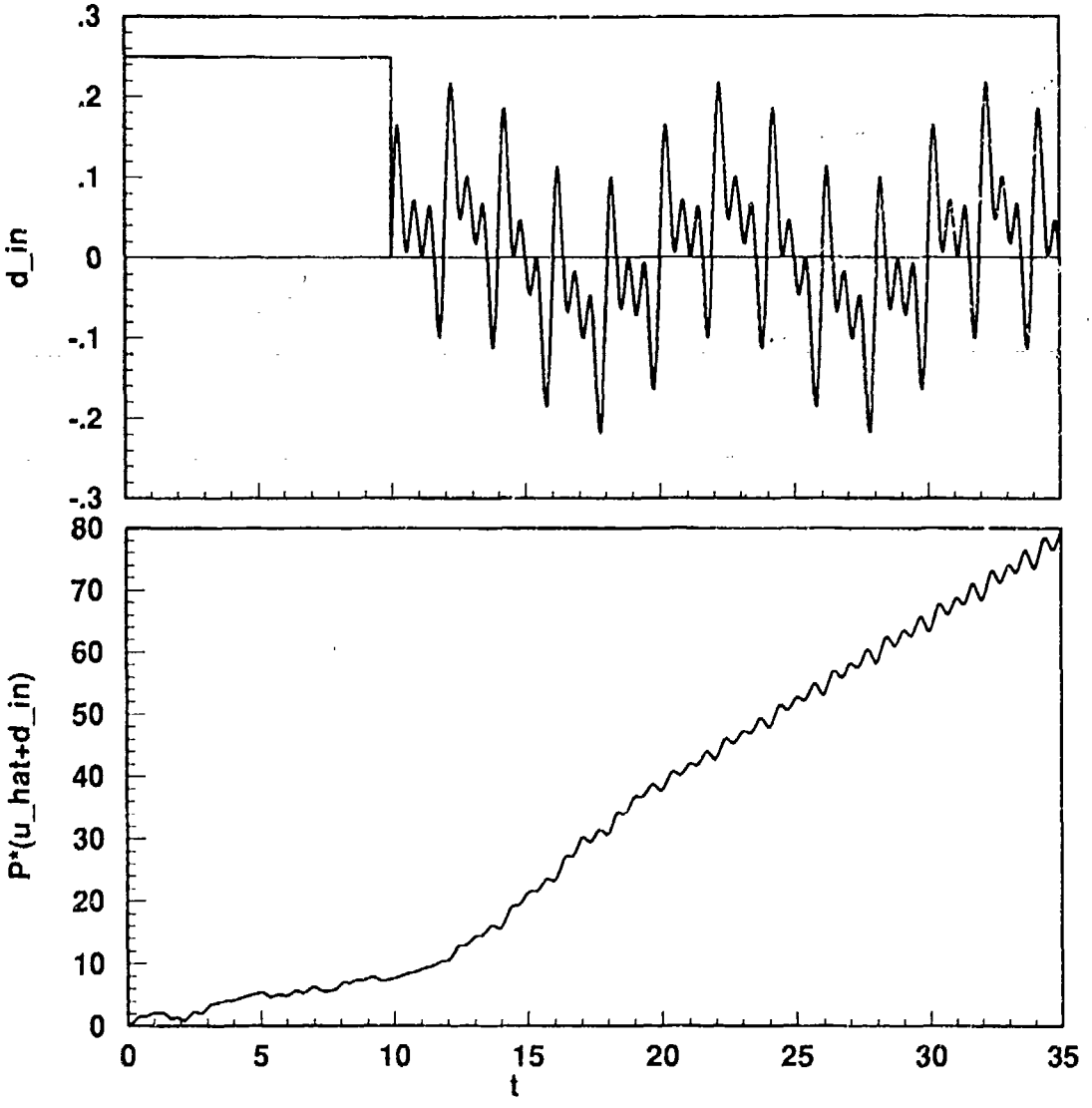

Figure 13: d_{in} and $P * (\hat{u} + d_{in})$ ($\hat{u}$ in Figure 9 ; P in (14))

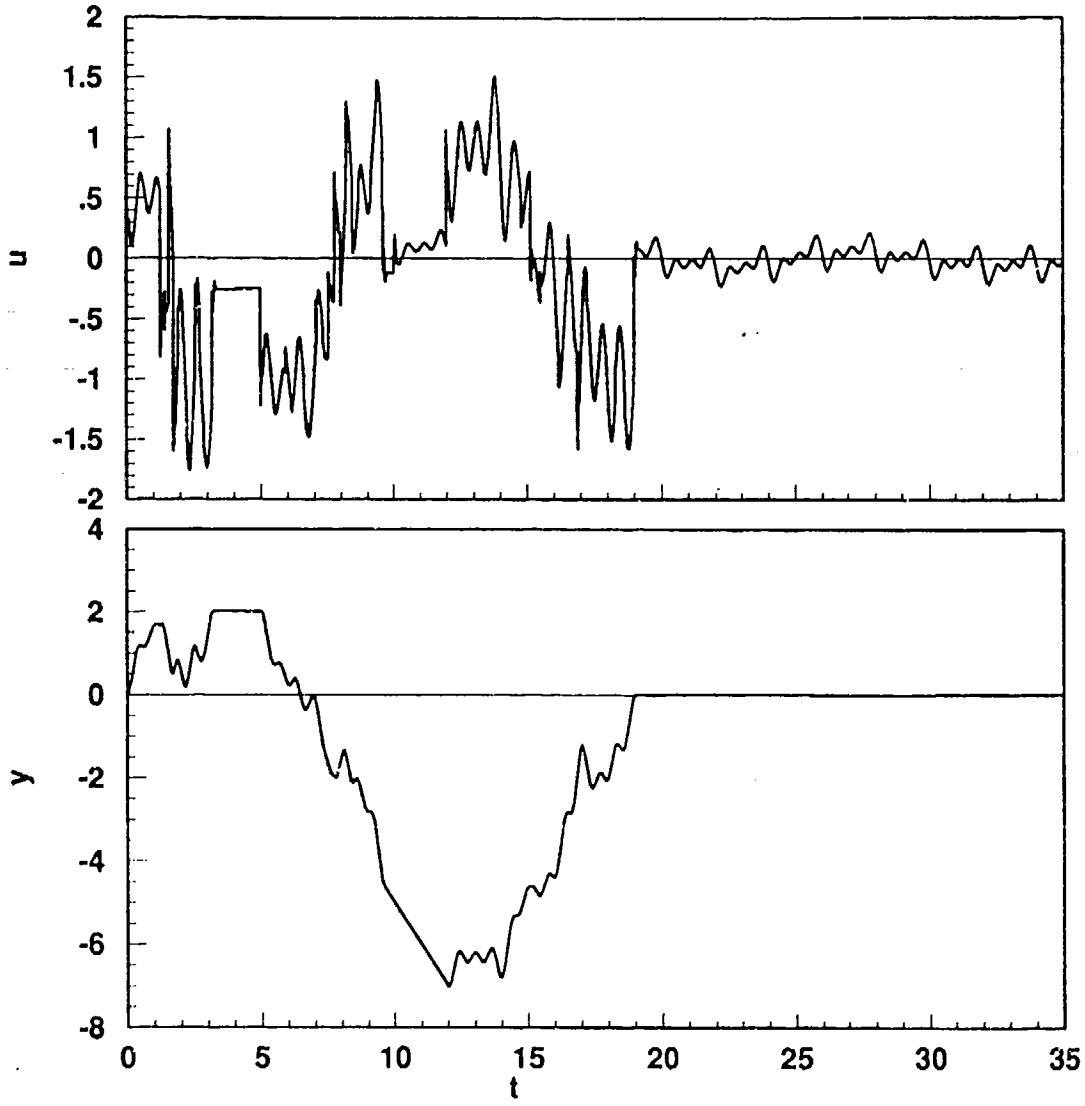

Figure 14: u and y in Figure 12 (C stabilizing for $\|u\|_\infty \leq 2$; C satisfies (31) ; $(d_{in}, \hat{u})$ and P as in Figure 13 ; $\hat{y} = P\hat{u}$)

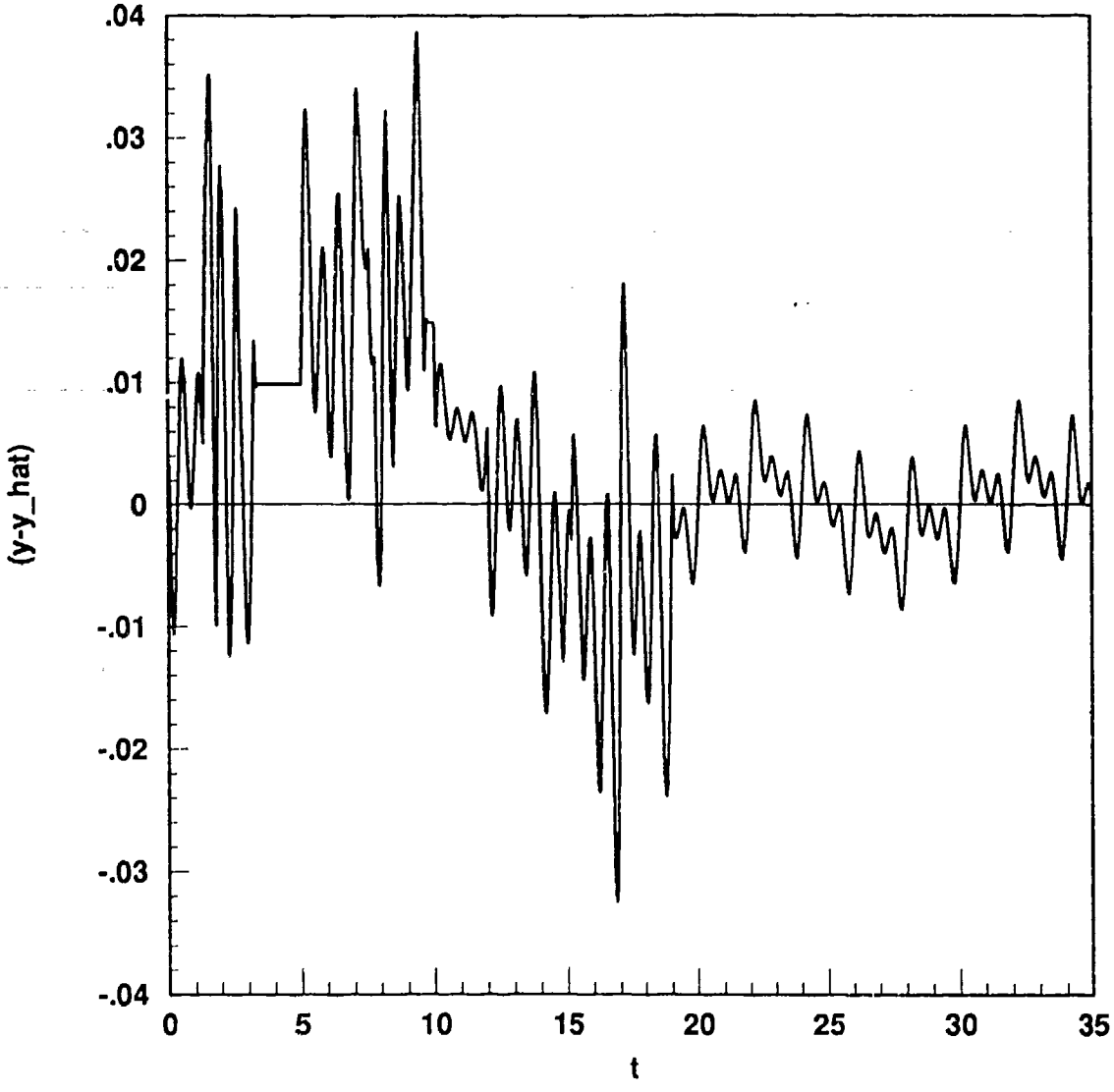

Figure 15: Tracking error $(y - \hat{y})$ (y and $\hat{y}$ as in Figure 14)

References

[Ath1] M. Athans and P. L. Falb, *Optimal Control: An Introduction to the Theory and Its Applications,* McGraw-Hill, 1966.

[Ben1] J. Ben-Asher, J. A. Burns and E. M. Cliff, "Time-Optimal Slewing of Flexible Spacecraft," *Proceedings of the IEEE Conference on Decision and Control*, pp. 524-528, Los Angeles, California, December 1987.

[Bha1] S. P. Bhat and D. K. Miu, "Precise Point-to-Point Positioning Control of Flexible Structures," *Transactions of the ASME, Journal of Dynamic Systems, Measurement and Control,* vol. 112, no. 4, pp. 667-674, December 1990.

[Sch1] S. F. Schmidt, *The Analysis and Design of Continuous and Sampled-Data Feedback Control Systems with a Saturation Type Nonlinearity,* Ph.D. Dissertation, Stanford University, June 1959.

[Sin1] G. Singh, P. T. Kabamba and N. H. McClamroch, "Time-Optimal Slewing of a Rigid Body with Flexible Appendages," *Proceedings of the IEEE Conference on Decision and Control*, pp. 1441-1442, Los Angeles, California, December 1987.

[Wor1] M. L. Workman, *Adaptive Proximate Time-Optimal Servomechanisms,* Ph.D. Dissertation, Stanford University, March 1987.

[Wor2] M. L. Workman, R. L. Kosut and G. F. Franklin, "Adaptive Proximate Time-Optimal Control: Continuous-Time Case," *Proceedings of the American Control Conference,* pp. 589-594, Minneapolis, Minnesota, June 1987.

[Wor3] M. L. Workman, R. L. Kosut and G. F. Franklin, "Adaptive Proximate Time-Optimal Control: Discrete-Time Case," *Proceedings of the IEEE Conference on Decision and Control*, pp. 1548-1553, Los Angeles, California, December 1987.

Appendix A

Published in the *Proceedings of the American Control Conference*, Minneapolis, Minnesota, June 1987.

Adaptive Proximate Time-Optimal Servomechanisms: Continuous Time Case

M. L. WORKMAN[1], R. L. KOSUT[2, 3], G. F. FRANKLIN[3]

Information Systems Laboratory
Stanford University, Stanford, CA 94305

Abstract— **A Proximate Time-Optimal Servo (PTOS) is developed, along with conditions for its stability. An algorithm is proposed for adapting the PTOS (APTOS) to improve performance in the face of uncertain plant parameters. Under ideal conditions APTOS is shown to be uniformly asymptotically stable. Simulation results demonstrate the predicted performance.**

1. INTRODUCTION

In many automatic control systems, it is desirable to effect a minimum-time response to set point changes. The *time-optimal* control is a non-linear function of the plant states and requires precise knowledge of the plant model [1]. An excellent compilation of related work is contained in Oldenburger [2]. When the plant is not precisely known, the time-optimal control law can be adapted to changes in the plant. In this paper we will describe an adaptive proximate time-optimal controller which aside from being adaptive, is more practical than the ideal time-optimal controller.

In the following section a non-linear controller is proposed which is more practical than the time-optimal controller, and as will be shown in a later section, can be very close to time-optimal. In the third section, a theorem is given which guarantees stability of the practical time-optimal controller under reasonable constraints. A specific controller is then shown to meet the stability constraints, and is also shown to be close to the time-optimal solution under reasonable assumptions. Adaptation of this proposed controller is the topic of the following section, including a theorem which has been proved showing the uniform asymptotic stability of the adaptive non-linear controller. Finally, the last section illustrates via simulation the improved performance afforded by the adaptive non-linear controller over the fixed parameter non-linear controller.

2. CONTROL DESIGN: KNOWN PARAMETERS

Consider the plant shown in Figure 2.1, a double integrator driven by a limiter or saturation block. The equations describing this system are

$$\dot{v} = a\,\mathrm{sat}(\bar{u}) \tag{2.1}$$

$$\dot{y} = v \tag{2.2}$$

where the "sat" function is defined as

$$\mathrm{sat}(z) \triangleq \begin{cases} +1\,, & z > 1 \\ z\,, & |z| \leq 1 \\ -1\,, & z < -1 \end{cases} \tag{2.3}$$

The system state x is defined as

$$x^T \triangleq [y \;\; v] \tag{2.4}$$

For time-optimal control, the objective is to minimize the time required to transfer the system from an initial state $[y_0 \;\; v_0]$ to a final state $[r \;\; 0]$, where r is a constant output reference or set point. The time-optimal control [1] for the system given by (2.1)

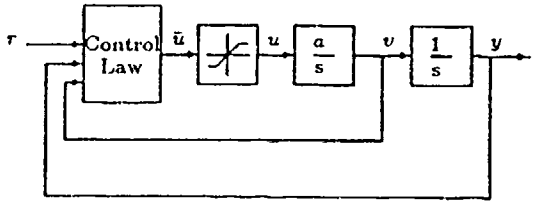

Figure 2.1: Double integrator plant with bounded control.

and (2.2) is

$$u = \mathrm{sgn}(f_{to}(y_e) - v) \tag{2.5}$$

$$f_{to}(y_e) = \mathrm{sgn}(y_e)(2a\,|y_e|)^{1/2} \tag{2.6}$$

$$y_e \triangleq r - y \tag{2.7}$$

and the signum function is defined as

$$\mathrm{sgn}(z) = \begin{cases} +1\,, & z > 1 \\ 0\,, & z = 0 \\ -1\,, & z < 1 \end{cases} \tag{2.8}$$

The sat function of the plant is imposed by some physical constraint such as power supply voltage. Combining the control law given by (2.5) and (2.7) yields the following description of the time-optimal control system

$$\dot{y} = v \tag{2.9}$$

$$\dot{v} = a\,\mathrm{sgn}(f_{to}(y_e) - v) \tag{2.10}$$

$$f_{to}(y_e) = \mathrm{sgn}(y_e)(2a\,|y_e|)^{1/2} \tag{2.11}$$

---

[1]Stanford University, on Educational (Resident Study) leave from International Business Machines Corp., San Jose, CA.

[2]Integrated Systems Inc., Palo Alto, CA. and Stanford University, Stanford, CA.

[3]Research support for both Dr. Kosut and Dr. Franklin from NASA Grant NAG-2-359.

The control law given by (2.5)- (2.7) and shown in Figure 2.2, although optimal, is not practical in many cases. Even the smallest system process or measurement noise will cause the control to "chatter" between the maximum and minimum values [3]. Removing the infinite gain operators from the time-optimal controller gives the system a finite bandwidth, and hence is much more practical.

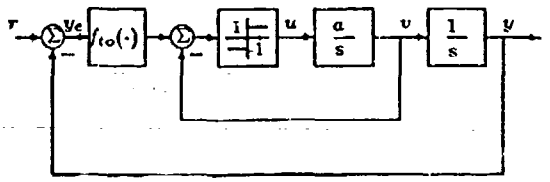

Figure 2.2: Time-optimal controller for double integrator plant.

A proximate time-optimal servomechanism (PTOS) is shown in Figure 2.3. The function $f(\cdot)$ is a finite slope[2] approximation to the switching function $f_{to}(\cdot)$ given by (2.11). The signum function of (2.10) has been replaced by the "sat" function which, together with the gain factor k_2, can be thought of as a finite slope approximation to the signum function. The equations which define this "practical" version of (2.9)-(2.11) are

$$\dot{y} = v \tag{2.12}$$

$$\dot{v} = a\ \mathrm{sat}(k_2[f(y_e) - v]) \tag{2.13}$$

where the function $f(\cdot)$ is as yet unspecified.

Without affecting the stability analysis (for step responses), we will drop r from the equations and analyze the system

$$\dot{y} = v \tag{2.14}$$

$$\dot{v} = a\ \mathrm{sat}(k_2[f(-y) - v]) \tag{2.15}$$

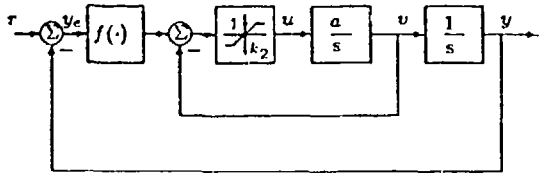

Figure 2.3: Proximate Time-Optimal controller. Linear region of the saturation function has gain k_2.

3. PTOS Stability

In this section we establish restrictions on the function $f(\cdot)$ and the gain k_2 which will guarantee stability of the system (2.14) - (2.15) depicted in Figure 2.3 for step inputs.

Theorem 1 (*Step Inputs*). *The zero solution of (2.14) and (2.15) is globally asymptotically stable if the following conditions hold:*

A1) $ak_2 > 0$.

A2) $f(0) = 0$.

A3) $f(z)z > 0\ ,\ \forall\ z \neq 0$.

A4) $\lim_{z\to\infty} \int_0^z f(\delta)\, d\delta = \infty$.

A5) $f'(y) \triangleq df(y)/dy$ *exists*, $\forall\ y$.

A6) $-a + \frac{1}{k_2} f'(-y) < f'(-y)f(-y) < a - \frac{1}{k_2} f'(-y)\ ,\ \forall\ y$.

Proof. Details of the proof are contained in [4,5] and will not be repeated here. Instead, an outline of the approach taken in the proof will be given. The proof consists of three parts. Referring to Figure 3.4, it is first shown that all trajectories originating outside the region $\mathbf{U} \subset \mathbf{R}^2$ will enter $\mathbf{U}$ in a finite time. Second, it is shown that subject to *A1* through *A6* trajectories in $\mathbf{U}$ remain inside $\mathbf{U}$. Third, it is shown that there exists a Lyapunov function for the system when $x \in \mathbf{U}$. The regions in state space correspond to the condition of the control, *unsaturated* ($\mathbf{U}$), *saturated positive* ($\mathbf{S}_+$), and *saturated negative* ($\mathbf{S}_-$), and are defined as follows:

$$\mathbf{U} \triangleq \left\{(y,v) \in \mathbf{R}^2 : f(-y) - \frac{1}{k_2} \leq v \leq f(-y) + \frac{1}{k_2}\right\} \tag{3.16}$$

$$\mathbf{S}_+ \triangleq \left\{(y,v) \in \mathbf{R}^2 : k_2(f(-y) - v) > 1\right\} \tag{3.17}$$

$$\mathbf{S}_- \triangleq \left\{(y,v) \in \mathbf{R}^2 : k_2(f(-y) - v) < -1\right\} \tag{3.18}$$

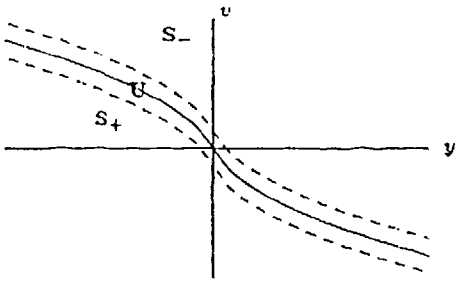

Figure 3.4: Regions $\mathbf{U}$, $\mathbf{S}_+$, and $\mathbf{S}_-$ of the phase plane. The solid curve represents the points (y, v) such that $v = f(-y)$.

3.1 An Interesting $f(\cdot)$

In this section we propose a function $f(\cdot)$ which meets the conditions of Theorem 1 and still produces nearly time-optimal response to changes in the position reference input r. The following choice for $f(\cdot)$ is easy to motivate: build a function f near to f_{to} such that the resulting system trajectory requires less than the maximum acceleration capability of the system, a.

$$f(y_e) = \begin{cases} \frac{k_1}{k_2}(y_e) & \text{for } |y_e| \leq y_l \\ \mathrm{sgn}(y_e)[(2a\alpha\,|y_e|)^{1/2} - \frac{1}{k_2}] & \text{for } |y_e| > y_l \end{cases} \tag{3.19}$$

The linear portion of $f(\cdot)$ connects the two disjoint halves of the non-linear portion. To connect the non-linear regions of $f(\cdot)$ such that $f(\cdot)$ remains continuous, we have a constraint on the gains k_1 and k_2,

$$k_1 \leq \frac{\alpha a k_2^2}{2} \tag{3.20}$$

[2]The derivative of f_{to} is infinite at $y = 0$.

and a constraint on the size of the linear region

$$\frac{1}{2\alpha a}\left(\frac{1}{k_2}\right)^2 < y_l \leq \left(\frac{k_2}{k_1}\right)^2 \frac{\alpha a}{2} \tag{3.21}$$

We can choose k_1 as a function of k_2 so that $f'(\cdot)$ is continuous. If f' is continuous, then the linear portion of $f(\cdot)$ is tangent to the non-linear square root portion at the point $y = y_l$ and smooth control results. Thus for continuous $f(\cdot)$ and $f'(\cdot)$, we have

$$k_2 = \left(\frac{2k_1}{\alpha a}\right)^{1/2} \tag{3.22}$$

and the linear region is just

$$y_l = \frac{1}{k_1} \tag{3.23}$$

Whatever the choices for k_1, k_2, and y_l in (3.19) (subject to (3.20) and (3.21)), we must verify that the conditions of Theorem 1 are met. It is clear by inspection that the first five conditions are met by (3.19), and we will check condition $A6$. The derivative $df(y_e)/dy_e$ is

$$f'(y_e) = \begin{cases} \frac{k_1}{k_2}, & 0 \leq y_e \leq y_l \\ \frac{\alpha a}{(2\alpha a y_e)^{1/2}}, & y_e > y_l \end{cases} \tag{3.24}$$

Calculating ff' yields

$$f(y_e)f'(y_e) = \begin{cases} \left(\frac{k_1}{k_2}\right)^2 y_e, & 0 \leq y_e \leq y_l \\ \alpha a - \frac{1}{k_2} f'(y_e), & y_e > y_l \end{cases} \tag{3.25}$$

Given ff', it is easy to show that (3.19) meets the conditions of Theorem 1 if $0 < \alpha < 1$.

The question which now arises is, how close to time-optimal is the proposed system ($f(\cdot)$ is as given by (3.19))? Consider the limiting case: let $k_2 \to \infty$ and α get arbitrarily close to 1. If we consider time to the target as approximated by time to the point y_l, and an upper bound on the size of r, then the time to the target of our practical system will approach from above that of the time-optimal system. This means that for unrestricted values of k_2, we can get arbitrarily close to the time-optimal system. For the system to remain practical there are restrictions to the size of k_2, and these restrictions will be addressed in Section 3.3.

In the following analysis, it is helpful to define the distance L which a repositioning from r_0 to r covers:

$$L \triangleq |r - r_0| \tag{3.26}$$

For the time-optimal system let t_{opt} denote the time it takes to move a distance L to the new target position. For a plant initially at rest we have,

$$t_{opt}(L) = \frac{2}{\sqrt{a}}\sqrt{L} \tag{3.27}$$

For PTOS, extremely small moves (changes in set point) will leave the system state in U , and the time to a given distance (allowable error tolerence) from the set point can be found from a linear analysis. For large set point changes, values of $L \gg 1/k_1$, the linear part of the response will be neglected. Although the PTOS accelerates as fast as the time-optimal one, the deceleration is slower. The time elapsed in moving from point $y = a$ to point $y = b$ at a velocity which can be written as a function of position is

$$\text{time from } a \text{ to } b = \int_a^b \frac{1}{v(y)} dy \tag{3.28}$$

The velocity of the PTOS is approximated by

$$v(y_e) \approx (2\alpha a\,|\,y_e\,|)^{1/2}\,\mathrm{sgn}(y_e) \tag{3.29}$$

during deceleration. Defining t_{ptos} as the practical controller move time, we obtain the following approximation for the move time for the practical system:

$$t_{ptos} = \frac{1}{\sqrt{a}}\sqrt{L} + \frac{1}{\sqrt{\alpha a}}\sqrt{L} \tag{3.30}$$

We can define P as the percentage increase in move time of the practical controller as

$$P \triangleq 100\%\left(\frac{t_{ptos} - t_{opt}}{t_{opt}}\right) \tag{3.31}$$

Substituting (3.27) and (3.30) into (3.31) gives,

$$P = 100\%\left[\frac{1}{2}\left(\frac{1}{\sqrt{\alpha}} - 1\right)\right] \tag{3.32}$$

This is an exciting result, in that the move time percentage increase is not a function of L, the move length. Although reasonable values of α are usually such that $\alpha \in [.9\ \ .99]$, P is plotted for a wide range of α in Figure 3.5.

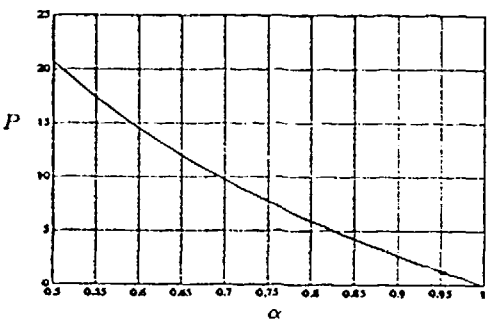

Figure 3.5: Percentage increase P in move time versus α. The point marked on the curve represents $P = 1.3$ % for $\alpha = .95$.

3.2 Designing the Linear Controller

Using a pole placement method [6,7], we can pick the control gains to effect a desired closed-loop transfer function. When a is known, choosing k_1 and k_2 as

$$k_1 = \omega_d^2/a \tag{3.33}$$

$$k_2 = 2\zeta_d\omega_d/a \tag{3.34}$$

will yield the following closed-loop transfer function

$$\frac{Y(s)}{R(s)} = \frac{\omega_d^2}{s^2 + 2\zeta_d\omega_d s + \omega_d^2} \tag{3.35}$$

Of course the k_1 and k_2 must meet the constraints (3.20) and (3.21) when using (3.19) as $f(\cdot)$ in the practical time-optimal controller. Substituting (3.33) and (3.34) into (3.20) gives a lower bound on the damping ratio ζ_d as a function of α:

$$\zeta_d \geq \frac{1}{\sqrt{2\alpha}} \tag{3.36}$$

The choice of $\omega_d = \sqrt{k_1 a}$ is both performance related and of practical concern: higher bandwidth gives faster decay of position errors, but high bandwidth necessitates that the model of our plant be accurate well above ω_d. Model uncertainty will be covered in Section 3.3.

3.3 Unmodeled Dynamics

The stability analysis of Section 3 provides us with a set of design rules for the double integrator system. However, it is well known that all systems have additional dynamics which are usually either neglected or unknown.

Initially, we will not constrain the unmodeled part of the plant to be linear or time invariant. Stability of the open loop unmodeled system will be the only constraint. The complete controller block diagram including unmodeled dynamics and an input disturbance d is shown in Figure 3.6. From Figure 3.6 we have:

$$\dot{v} = a\Delta\{\,\mathrm{sat}(\bar{u}) + d\} \tag{3.37}$$

$$\dot{y} = v \tag{3.38}$$

Since we are trying to examine the effects of the unmodeled dynamics and disturbances on the control law designed in Section 2, we have the same control law (taking Δ into account when designing the control law makes Δ *modeled* , and this is considered in [4]):

$$\bar{u} \triangleq k_2[f(-y) - v] \tag{3.39}$$

The block diagram of the complete system represented by (3.37) through (3.39) is shown in Figure 3.6.

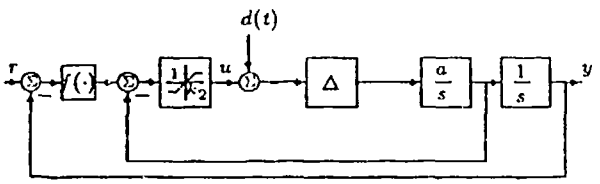

Figure 3.6: Complete servo system block diagram with unmodeled dynamics and disturbance input d.

In the following theorem, we will need to define an operator γ_∞ which gives the maximum magnitude of a function over all possible bounded inputs:

$$\gamma_\infty(\Delta\{\sigma\}) \triangleq \sup_{|\sigma| \le \|\sigma\|_\infty} |\Delta\{\sigma\}| \tag{3.40}$$

It is convenient to define

$$\Delta_1 \triangleq \Delta - 1 \tag{3.41}$$

As will be discussed later, using this operator (γ_∞) for determining peak amplitudes is correct, but yields *extremely conservative* conditions for stability. The following theorem places limits on both the unmodeled dynamics and the disturbance inputs which are *sufficient* to guarantee stability of the following system (see Figure 3.6):

Theorem 2 (*Step Inputs*). *The zero solution of (3.37) and (3.38) with control (3.39) is globally stable if the following conditions hold:*

A1) -A5) of Theorem 1, and

A6) $|f'(-y)f(-y)| < a[1 - \gamma_\infty(\Delta_1\{\,sat(u) + d\}) - \|d\|_\infty] - \frac{1}{k_2}f'(-y)$, $\forall y$

Proof. The proof follows the same attack taken in proving Theorem 1 and is contained in [4,5].

Interpretation. Theorem 2 differs from Theorem 1 in that it allows for bounded disturbances and unmodeled dynamics to perturb the double integrator model. To account for the unmodeled deviations, condition $A6$ discounts the available acceleration by a conservative amount: the absolute worst case contribution of the operator Δ_1 and the disturbance d. The factor α in (3.19) is precisely the discount factor which can be adjusted when $\gamma_\infty(\Delta_1)$ and $\|d\|_\infty$ are specified. Thus we can set:

$$\alpha = 1 - \gamma_\infty(\Delta_1\{\,\mathrm{sat}(\bar{u}) + d\}) - \|d\|_\infty \tag{3.42}$$

Thus condition $A6$ can be stated as:

$$|f'(-y)f(-y)| < a\alpha - \frac{1}{k_2}f'(-y) \tag{3.43}$$

To have moves which are close to time-optimal, the unmodeled dynamics and disturbances must be small enough such that α is nearly one, say $\alpha \in [.9, .99]$. In terms of the disturbances, the condition given by Theorem 2 is very reasonable, as the disturbances forces should be much smaller than the available force to the actuator.

The problem with condition $A6$ is that it is too conservative: it does not even allow, for example, Δ to be a real-pole of *any* bandwidth or time constant. In fact the types of unmodeled dynamics which yield reasonable α's are very limited. If we consider the system *after* the receipt of a step input, and a linear time-invariant set of unmodeled dynamics, we can expand the range of unmodeled dynamics for which stability can still be proved (using present techniques). This is best summarized in the following Corollary to Theorem 2:

Corollary 2.1 *(Step input at $t = t_0$). The system given by Equations 3.37-3.39 is globally stable if it meets the following conditions:*

A1) -A5) of Theorem 1,

A6) Δ is a stable, linear time invariant operator.

A7) $\Delta_1(s = 0) = 0$, Δ_1 has no dc gain. This is a formulation constraint. Deviations in expected gain are considered as variations in the plant gain a.

A8) $(1 + ak_2\Delta/s)^{-1}$ is a stable operator

A9) $|f'(-y)f(-y)| < a[1 - \gamma_\infty(k_2[\Delta_1/s])]\|\dot{u} + \dot{d}\|_\infty - \|\dot{d}\|_\infty] - \frac{1}{k_2}f'(-y)$, $\forall y$, $\forall t > t_0$

Proof. The proof is along the lines of Theorem 2, and is also given in [4,5]. To apply this corollary to the real-pole case ($\Delta = 1/(\tau s + 1)$), we need the peak gain of Δ_1/s:

$$\gamma_\infty(\Delta_1/s) = \gamma_\infty\left(\frac{-\tau}{\tau s + 1}\right) = \tau \tag{3.44}$$

Note that the peak gain drops toward zero as the time constant approaches zero. Setting $d = 0$ and calculating $\|\dot{u}\|_\infty$ condition $A9$ yields

$$\alpha < 1 - ak_2\tau \tag{3.45}$$

which has the qualitative characteristics we need: as the bandwidth of the real pole grows, the limit on α diminishes. Thus for $\tau = 0$, α must be less than one as in Theorem 1. Hence we can analyze the effects of practical unmodeled dynamics on the performance of the system, modulo the impulse reponse of the unmodeled dynamics term. In the case of the real pole, the performance will not be adversely affected beyond that calculable from (3.45). When very underdamped unmodeled dynamics are included however, the performance of the system must be evaluated via simulation.

4. APTOS

In this section we will derive an algorithm for adjusting the non-linear control law of Section 3.1 to uncertainty about, or slow changes in, the plant parameter a. Figure 4.7 depicts the structure of the system with adaptation of the non-linear control function using information identified from input/output data of the plant.

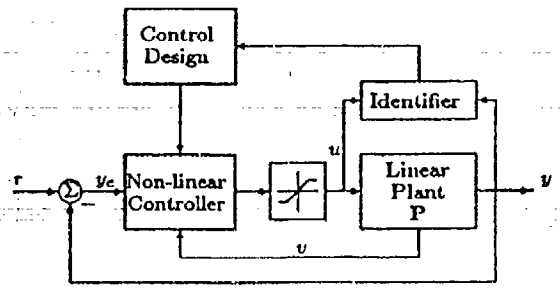

Figure 4.7: Structure of the Adaptive non-linear Controller

4.1 The Identifier

The identification scheme will be based on the following parametric model of the plant:

$$\tilde{y} = a\,\mathrm{sat}(\bar{u}) \tag{4.46}$$

where a is an unknown constant. We also assume that a is known to be in the interval $\mathcal{A} = [a_{min}, a_{max}]$.

$$a \in [a_{min}, a_{max}] \tag{4.47}$$

The measured data is $\{u\}$, and $\{y\}$. Denoting the estimate of a as $\hat{a}$, the *filtered equation error* is defined as

$$\epsilon = z - \hat{a}\phi \tag{4.48}$$

where z and ϕ are defined by

$$z \triangleq \left(\frac{s}{\tau_r s + 1}\right)^2 y \tag{4.49}$$

$$\phi \triangleq \left(\frac{1}{\tau_r s + 1}\right)^2 \mathrm{sat}(\bar{u}) \tag{4.50}$$

where s represents the Laplace transform variable. The time constant τ_r affects the bandwidth of information used by the identifier, and should be chosen much smaller than the time constant defined by the maximum "learning" rate for $\hat{a}$.

To illustrate the ideas we propose the following simple identification scheme (LMS):

$$\dot{\hat{a}} = g\phi\epsilon \tag{4.51}$$

$$\epsilon = z - \hat{a}\phi \tag{4.52}$$

where g is a positive constant chosen to give a reasonable learning rate, depending on the magnitude of system noise, and intended closed loop system bandwidth. The initial estimate for a is in $[a_{min}, a_{max}]$. It is possible to show [4] that under the condition of persistant excitation this single parameter identifier is exponentially convergent to the correct value ($\{u\}$ and $\{y\}$ are in the model set).

Parameter	Value
a	1.0
α	0.95
g	.15
τ_r	0.02
ω_d	10.
L	1 or 2

Table 1: Parameter values for simulations.

4.2 The Adaptive Controller

Using the structure of the control law (3.19) with a continuous $f'(\cdot)$ ((3.22), (3.23)), an adaptive version of the PTOS control is

$$u = \mathrm{sat}(\hat{k}_2(f(y_e, \hat{\rho}) - v)) \tag{4.53}$$

with $\hat{a}$ generated from (4.51),(4.52) and where

$$\hat{k}_1 = \omega_d^2/\hat{\rho} \tag{4.54}$$

$$\hat{k}_2 = 2\zeta_d\omega_d/\hat{\rho} \tag{4.55}$$

$$\hat{y}_l = \frac{1}{\hat{k}_1} \tag{4.56}$$

$$f(y_e, \hat{\rho}) = \begin{cases} \frac{k_1}{k_2}(y_e) & \text{for } |y_e| \le \hat{y}_l \\ \mathrm{sgn}(y_e)[(2\hat{\rho}\alpha\,|y_e|)^{1/2} - 1/\hat{k}_2] & \text{for } |y_e| > \hat{y}_l \end{cases} \tag{4.57}$$

and $\hat{\rho}$ is the projection of $\hat{a}$ into a known region:

$$\hat{\rho} = \arg_{\rho\in\mathcal{A}} \min\ |\hat{a} - \rho| \tag{4.58}$$

Hence, if the estimate $\hat{a}$ is in $\mathcal{A}$, then $\hat{\rho} = \hat{a}$. Otherwise we take the nearest value in $\mathcal{A}$. The following theorem gives sufficient conditions for stability of APTOS.

Theorem 3 *(Parameter Convergence). Suppose that*

$$\frac{1}{T}\int_{\sigma}^{\sigma+T} \phi^2(\delta)d\delta \ge \beta\ ,\ \forall\sigma \in [0, t_f] \tag{4.59}$$

where T and β are positive constants independent of t_f. Then for $t > t_f$:

$$r(t) = r_0\ ,\ \forall t \ge t_f \Rightarrow (y(t), v(t), u(t)) \to (r_0, 0, 0) \tag{4.60}$$

The proof of Theorem 3 is contained in[4].

5. Simulation Examples

In this section we will examine the performance of the PTOS and APTOS via some simulation examples. Table 1 contains the fixed parameters for all of the simulations. Responses of the ideal time-optimal controller and PTOS to two set point changes, $L = 1$, and $L = 2$ are overlayed in Figure 5.1. No noise was added to the simulation of the time-optimal controller to illustrate the behavior of the so-called *ideal* system. The unsaturated PTOS control during deceleration ($\alpha = 0.95$) affirms that $x(t_0) \in \mathbf{U} \Rightarrow x(t) \in \mathbf{U}\ ,\ \forall\, t \ge t_0$. Figure 5.2 shows PTOS responses when the plant gain a is not known, motivating the desire for an adaptive PTOS. Note the time response becomes slower with any deviation from the true value. *Adaptation* of the practical controller to a value of $a = 1$ from an initial estimate of $\hat{a}(0) = 1.5$ is shown in Figure 5.3. The initial estimate of $\hat{a}$ is too large, causing control saturation during deceleration. Although the system appears stable, as the magnitude of the set point change grows, the oscillatory behavior of the response grows. As $\hat{a}$ approaches a, the control does not saturate during deceleration, and the closed-loop behavior of the system approaches that of the ideal PTOS.

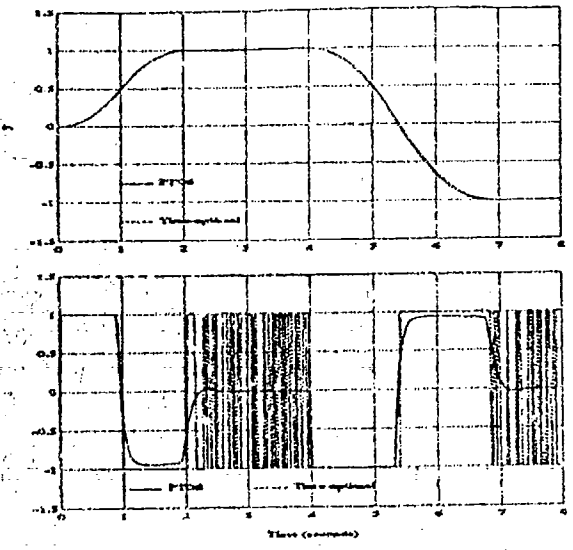

Figure 5.1: Overlay of y and u for time-optimal control and PTOS.

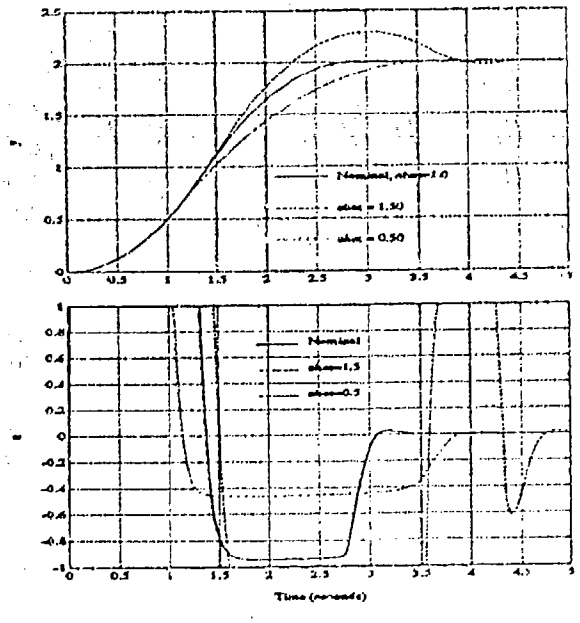

Figure 5.2: Response to a set point change before and after adjustment to the correct value of $a = 1$ from an initial estimate $\hat{a} = 0.5$ (undershoot) and $\hat{a} = 1.5$ (overshoot).

6. Conclusions

This paper contains the development of an adaptive proximate time-optimal control algorithm. Because the algorithm centers on the types of plants normally found in Servomechanisms, namely double integrator, this control structure is refered to as APTOS, or Adaptive Proximate Time Optimal Servomechanism.

APTOS was shown to be robust to errors in the plant gain estimate, plant dynamics model, and disturbance inputs. For a given set of bounds on plant model uncertainty, disturbance amplitude, and estimated plant gain error, a maximum response time degradation was derived. It was shown that for ideal conditions, the APTOS response time would approach the ideal time-optimal response. For the case of limited input authority and desirability of fast response, APTOS far out-performs standard Self-Tuning Control algorithms.

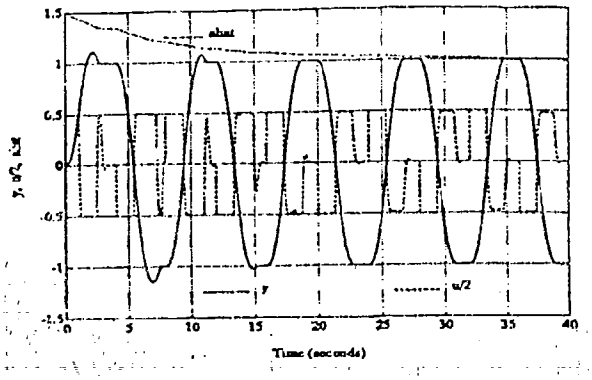

Figure 5.3: APTOS transient response when initial estimate of a is too high, under ideal conditions. Note changing control signal as $f(\cdot, \hat{a})$ is adjusted.

Because implementation of the adaptive non-linear control law is extremely complex and costly for second-order cases other than the double integrator, a discrete time version of APTOS has been developed[4,8], which facilitates implementation.

7. Acknowledgements

The authors would like to thank Danny Abramovitch, Steve Phillips, Fred Hansen, and Professor Stephen Boyd for helpful discussions and suggestions.

References

[1] Bryson and Ho, *Applied Optimal Control*, Halsted Press, 1010 Vermont Ave., N. W., Washington, D.C. 20005, 1975.

[2] Rufus Oldenburger, editor, *Optimal and self-optimizing control*, The M.I.T. Press, Cambridge Mass., 02142, 1966.

[3] M.L. Workman, *Applications of Magnetic Recording*, chapter 2: The Head Positioning Servomechanism, edited by D. Mee and E. Daniels, Mc Graw Hill, 1987, To be published second-half of 1987.

[4] Michael L. Workman, *Adaptive Proximate Time-Optimal Servomechanisms*, PhD thesis, Stanford University, 1987.

[5] M. L. Workman, R. L. Kosut, and G. F. Franklin, Adaptive proximate time-optimal control: continuous time case, *Transactions on Automatic Control*, submitted in March of 1987.

[6] Franklin and Powell, *Digital Control of Dynamic Systems*, Addison-Wesley, Menlo Park, California, 1980.

[7] Goodwin and Sin, *Adaptive Filtering Prediction and Control*, Prentice-Hall, Englewood Cliffs, N.J. 07632, 1984.

[8] M. L. Workman, R. L. Kosut, and G. F. Franklin, Adaptive proximate time-optimal control: discrete time case, *Transactions on Automatic Control*, submitted in March of 1987.

Appendix B

Published in the *Proceedings of the IEEE Conference on Decision and Control*, Los Angeles, California, December 1987.

Adaptive Proximate Time-Optimal Servomechanisms: Discrete Time Case

M. L. WORKMAN[1], R. L. KOSUT[2, 3], G. F. FRANKLIN[3]

Information Systems Laboratory
Stanford University, Stanford, CA 94305

Abstract— **After a brief review of the continuous time proximate time-optimal servomechanism (PTOS), a discrete time PTOS is developed, along with conditions for its stability. An algorithm is proposed for adapting PTOS when the plant parameters are not known yielding APTOS (adaptive PTOS). Under ideal conditions APTOS is shown to be uniformally asymptotically stable. Simulation results demonstrate the predicted performance, and experimental results validate the practicality of APTOS.**

1. INTRODUCTION

In this paper, we will develop a proximate time-optimal servomechanism (PTOS) for discrete time control of a continuous time double integrator plant. After establishing stability, the PTOS system will be extended to be adaptive (APTOS). The topic of this paper is an extension of continuous time results presented at the 1987 Automatic Control Conference, and hence a brief review of the continuous time proximate time-optimal servomechanism is presented before addressing the discrete time problem. Both the continuous and discrete time cases are covered in Workman's dissertation [1]. In the dissertation, the time-optimal trajectory was calculated for a plant modeled by a real pole followed by an integrator. The complexity of the resulting time-optimal trajectory, along with the fact that it is a transcendental function in velocity for position, motivates the transition to a discrete time implementation of the controller. Although the discrete time system is at least as complex as the continuous time system, the implementation with microprocessor technology is *much* simpler and less costly than the analog circuits required for the continuous time case.

2. REVIEW: CONTINUOUS TIME PTOS

Consider the time-optimal control system shown in Figure 2.1. The plant consists of a double integrator driven by a limiter or saturation block. The equations describing this system are[2]

$$\dot{y} = v \tag{2.1}$$

$$\dot{v} = a\,\mathrm{sgn}(f_{to}(y_e) - v) \tag{2.2}$$

$$f_{to}(y_e) = \mathrm{sgn}(y_e)(2a\,|y_e|)^{1/2} \tag{2.3}$$

where

$$y_e \triangleq r - y \tag{2.4}$$

In this form, it is helpful to define the move length L as the position error at the reciept of a new reference (step) input:

$$L \triangleq r(t_0) - y(t_0) = y_e(t_0) \tag{2.5}$$

The control law given by (2.2)- (2.3) and shown in Figure 2.1, although time-optimal, is not practical in many cases. Even the smallest system process or measurement noise will cause the control to "chatter" between the maximum and minimum values [3] Removing the infinite gain operators from the time-optimal controller gives the system a finite bandwidth, and hence is much more practical.

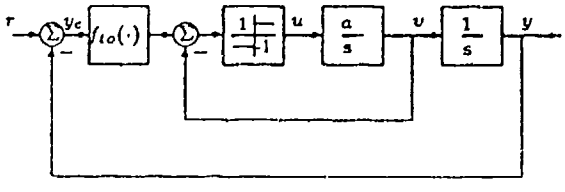

Figure 2.1: Time-optimal controller for double integrator plant.

A proximate time-optimal servomechanism (PTOS) is shown in Figure 2.2. The function $f(\cdot)$ is a finite slope[2] approximation to the switching function $f_{to}(\cdot)$ given by (2.3). The signum function of (2.2) has been replaced by the "sat" function which, together with the gain factor k_2, can be thought of as a finite slope approximation to the signum function. The equations which define this "practical" version of (2.1)-(2.3) are

$$\dot{y} = v \tag{2.6}$$

$$\dot{v} = a\,\mathrm{sat}(k_2[f(y_e) - v]) \tag{2.7}$$

where the function $f(\cdot)$ is as yet unspecified.

The following theorem gives the restrictions on the function $f(\cdot)$ and the gain k_2 which will guarantee stability of the system (2.6)- (2.7) depicted in Figure 2.2 for step inputs.

---

[1]Stanford University, on Educational (Resident Study) leave from International Business Machines Corp., San Jose, CA.

[2]Integrated Systems Inc., ~~Palo Alto~~ Santa Clara, CA. and Stanford University, Stanford, CA.

[3]Research support for both Dr. Kosut and Dr. Franklin from NASA Grant NAG-2-359. and NSF Grant ECS-8605646

[2]The derivative of f_{to} is infinite at $y = 0$.

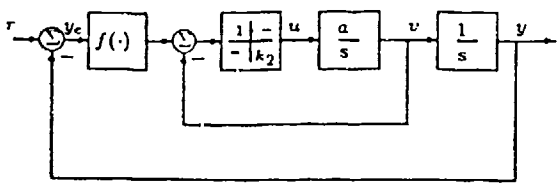

Figure 2.2: Proximate Time-Optimal controller. Linear region of the saturation function has gain k_2.

Theorem 1 (*Step Inputs*). *The zero solution of (2.6) and (2.7) is globally asymptotically stable if the following conditions hold:*

A1) $ak_2 > 0$.

A2) $f(0) = 0$.

A3) $f(z)z > 0\,,\ \forall\, z \neq 0$.

A4) $\lim_{x\to\infty} \int_0^x f(\delta)\, d\delta = \infty$.

A5) $f'(y) \triangleq df(y)/dy$ *exists*, $\forall\, y$.

A6) $-a + \frac{1}{k_2} f'(-y) < -f'(-y)f(-y) < a - \frac{1}{k_2} f'(-y)\,,\ \forall\, y$.

The proof of this theorem is rather long and is contained in [1].

A function $f(\cdot)$ which meets the conditions of Theorem 1 is given by (2.8).

$$f(y_e) = \begin{cases} \frac{k_1}{k_2}(y_e) & \text{for } |y_e| \leq y_l \\ \mathrm{sgn}(y_e)[(2a\alpha\,|y_e|)^{1/2} - \frac{1}{k_2}] & \text{for } |y_e| > y_l \end{cases} \tag{2.8}$$

The positive factor α is referred to as the acceleration discount factor, and is less than one ($0 < \alpha < 1$). Equation (2.8) is composed of a linear region ($|\, y_e \,| \leq y_l$) and a nonlinear region which is a fairly close approximation to the time-optimal switching function f_{to}. The linear portion of the curve connects the two disjoint halves of the non-linear portion. To connect the nonlinear regions of $f(\cdot)$ such that $f(\cdot)$ and $f'(\cdot)$ remain continuous, we have a constraint on the gains k_1, k_2, and the size of the linear region y_l:

$$k_2 = \left(\frac{2k_1}{\alpha a}\right)^{1/2} \tag{2.9}$$

and the linear region is just

$$y_l = \frac{1}{k_1} \tag{2.10}$$

By approximating the positioning time as the time it takes the position error to be within the linear region, we can define a percentage *increase* P in response time of a PTOS system over that of a minimum time control of the same plant.

$$\mathrm{P} \triangleq 100\% \left[\frac{1}{2}\left(\frac{1}{\sqrt{\alpha}} - 1\right)\right] \tag{2.11}$$

Note that the value of P is independent of the size of the step input (move length L). Although reasonable values of α are usually such that $\alpha \in [.9\ \ .99]$, P is plotted for a wide range of α in Figure 2.3.

A simulation of both the minimum-time controller and the PTOS system when the plant gain a is known is shown in Figure 2.4. For the case shown, the PTOS system is 1.3% slower, but has much improved control behavior during regulation mode. In addition to the linear regulation, it has also been shown [1] that PTOS has far better robustness properties to small changes in a, unmodeled dynamics, and disturbances acting on the plant.

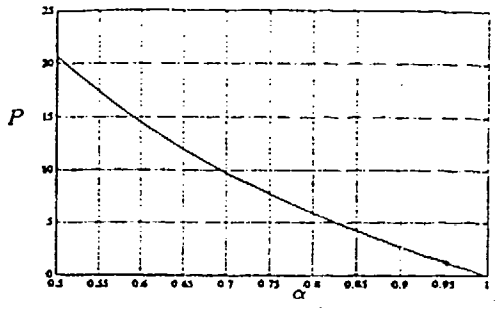

Figure 2.3: Percentage increase in move time P versus α. The point marked on the curve represents $P = 1.3$ % for $\alpha = .95$.

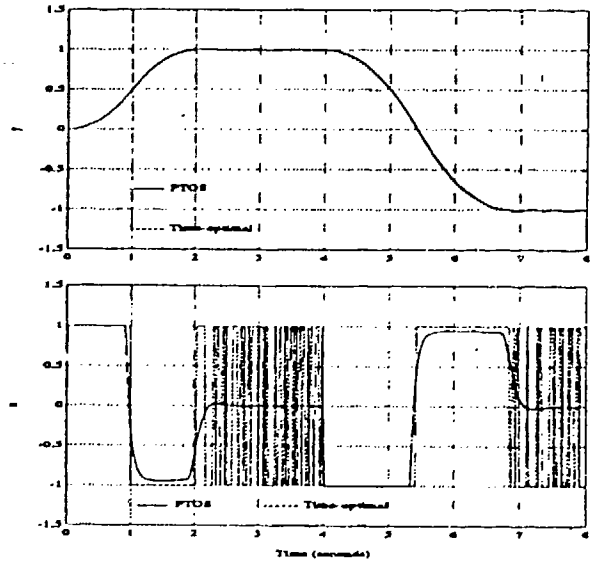

Figure 2.4: Overlay of y and u for time-optimal control and PTOS.

Although PTOS is robust to deviations in the model, performance improvements can be achieved by *adapting* PTOS (APTOS) to changes in the plant [1,4]. The continuous time APTOS, applied to the double integrator plant, performed very well. However, although it is possible to extend APTOS to other plants such as a real-pole followed by an integrator, the resulting velocity trajectory $f(\cdot)$ becomes unwieldy to adaptively adjust. This implementation difficulty can be overcome by implementation of a discrete time version of APTOS, as the microcode for the equations or look-up table entries for $f(\cdot)$ can be modified very easily in a microprocessor or signal processor based system. All we need is the theory to proceed.

3. Discrete Time Plant Model

Consider a double integrator plant driven by a zero-order hold. As in the continuous time case the states are defined as position and velocity. With an insignificant calculation delay we have the following discrete time state space description of the plant:

$$x \triangleq \begin{pmatrix} y & v \end{pmatrix}^T \tag{3.12}$$

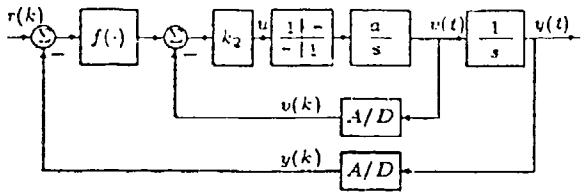

Figure 4.5: Discrete time proximate time-optimal servo (PTOS).

$$x(k+1) = \begin{bmatrix} 1 & aT_s \\ 0 & 1 \end{bmatrix} x(k) + \begin{bmatrix} aT_s^2/2 \\ aT_s \end{bmatrix} u(k) \qquad (3.13)$$

3.1 Key Approximation

The ideal time-optimal control of a discrete time system is in general very complicated. A valuable fact however, permits us to extend the strategy used in continuous PTOS [4] to discrete time systems: as the sampling rate increases, the discrete control tends to look identical to a sampled continuous time control. This does not mean that the sampling rate must be necessarily higher than would otherwise be selected to make the approximation valid. By adjusting the acceleration discount factor α, PTOS will leave enough unsaturated control margin while trajectory following that differences between continuous time and discrete time optimal control strategies can be absorbed.

4. Control Design: Known Parameters

The proposed control structure is a discrete time mapping of the same proximate time-optimal control law as used in continuous time PTOS in Section 2 with some slightly different conditions on the function $f(\cdot)$ which will be discussed later. The mapped control law is then:

$$u(k) = \text{sat}(k_2[f(y_c(k)) - v(k)]) \qquad (4.14)$$

Note that the definition of y_c is the same as in the continuous time case. Dropping the sample or time index, we have:

$$u = \text{sat}(k_2[f(y_c) - v]) \qquad (4.15)$$

To simplify the block diagrams, we will utilize the transfer characteristic of the D/A converter in place of the saturation function, as it is equivalent to the two transfer characteristics in series as long as the smallest saturation value is used. Quantization in the D/A and A/D converters will be assumed negligible. A block diagram of this system is shown in Figure 4.5.

5. PTOS Stability

In terms of the continuous time units, a map of the continuous time controller into the discrete time system yields:

$$y(k+1) = y(k) + T_s v(k) + a(T_s^2/2)u(k) \qquad (5.16)$$

$$v(k+1) = v(k) + aT_s u(k) \qquad (5.17)$$

$$u(k) = \text{sat}(k_2[f(r - y(k)) - v(k)]) \qquad (5.18)$$

For what values of k_2, and T_s is the system given by (5.16) through (5.18) stable? Unfortunately the answer to this question is more complex than it is in the continuous time case. The increased complexity is due to the lack of continuous trajectories in the state space, and to the analytical complexity of discrete time Lyapunov functions.

In the continuous case, if all trajectories point into a region of the phase plane from the boundries of the region, it is fairly clear that any trajectory originating inside the region must be trapped inside the region. The argument hinges on the continuity of the trajectories: any trajectory originating on the inside of a region must pass through a point on the boundry to leave the region, and since all trajectories originating on points of the boundaries go to the interior of the region.

Such is not the case for discrete time systems. All we have are *points*, not continuous trajectories. Thus the argument used in the continous time case fails: we do not have to have a point on the boundry to exit a region. Notwithstanding the difficulties, it is still possible to prove stability of our discrete time practical time-optimal controller. The difficulty will come when we try to check the conditions for stability. But we're getting ahead of ourselves, first let us state a theorem for stability.

Theorem 2 (*Step Inputs*). *The zero solution of the system given by (5.16) through (5.18) is globally asymptotically uniformly stable if the following conditions hold:*

A1) $0 < ak_2T_s < 2$. *Note the upper limit in contrast to the continuous time case.*

A2) -A5) of Theorem 1

A6) $-\frac{1}{k_2} < f(-[y + \Delta y]) - (v + \Delta v) < \frac{1}{k_2}$, $\forall\,(y, v) \in \mathrm{U}$. U *corresponds to the region in state space where the control is unsaturated.*

A7) $|f'(y)| < \frac{1}{2T_s}$, $\forall y$,

where Δy *and* Δv *are defined as follows:*

$$\Delta y = T_s v + \frac{aT_s^2}{2}\, sat(k_2[f(-y) - v]) \qquad (5.19)$$

$$\Delta v = aT_s\, sat(k_2[f(-y) - v]) \qquad (5.20)$$

Proof. The proof of this theorem is along the lines of the proof of the continuous time proof of Theorem 1 and the details are also contained in [4]. The approach to the proof is useful in understanding the origin of the constraints of Theorem 2. Referring to Figure 5.6:

1. Show that the system state will always enter a region U in state space where the control is unsaturated (conditions *A1*, *A7*), and then

2. Show that once the system state is in U , it will remain in U (conditions *A6*, *A7*),

3. Finally, show that there is a Lyapunov function for the system in the region U (conditions *A1*, *A2*, *A3*, *A4*, *A5*, *A7*).

Remarks. Condition *A1* differs from the continuous case in that it puts an *upper limit* on the value of ak_2T_s. This limit effectively puts a lower limit on the ratio of sampling frequency to desired velocity loop bandwidth. If k_2 is chosen such that the function $f(\cdot)$ is continuous, then

$$k_2 = \left(\frac{2k_1}{a\alpha}\right)^{1/2}$$

and upon substituting this into condition *A1* we obtain

$$k_1 T_s^2 < 1$$

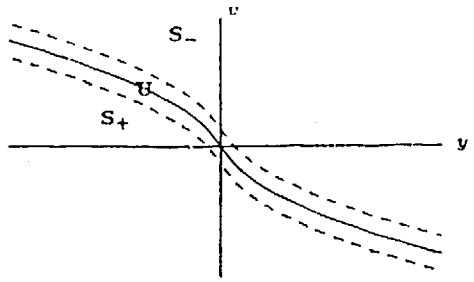

Figure 5.6: Regions U , S_+ , and S_- of the phase plane. The solid curve represents the points (y, v) such that $v = f(-y)$.

But this is less restrictive than the constraint imposed on $k_1 T_s^2$ by condition $A7$ as we shall see later in Section 7.

Condition $A6$ is the most difficult to analyze. It simply states that at no point in U can the next control be of magnitude greater than or equal to one. It is difficult to determine what this means directly in terms of restrictions on the function $f(\cdot)$. It would help if we knew whether condition $A6$ approached the similar condition for the continuous time case as the sampling time approached zero.

6. Stability in the Limit

We would expect that condition $A6$ Theorem 2 would approach that of Theorem 1 in the limit as $T_s \to 0$. To verify this expectation, we will substitute the plant equations for Δy and Δv into condition $A6$ of Theorem 2 and find the limits.

To begin, we will assume that we can examine the condition $A6$ on the boundaries of U . For high enough sampling rates there will be points in the neighborhood of the boundaries, and by continuity of $f(\cdot)$ we know that conditions of positiveness and negativeness of the control will apply in those neighborhoods.

Condition $A6$ of Theorem 2 is:

$$-\frac{1}{k_2} < f(-(y+\Delta y)-(v+\Delta v) < \frac{1}{k_2} \tag{6.21}$$

with Δy and Δv given by (5.19) and (5.20). On the positive boundary of U $(u = 1)$

Substituting Δy and Δv on the positive boundary of U $(u = 1)$ into (6.21) and taking the limit of all three terms as $T_s \to 0$ yields the following:

$$-\infty < [-f(-y) + \frac{1}{k_2}]f'(-y) < a \tag{6.22}$$

and thus

$$-\infty < -f(-y)f'(-y) < a - \frac{1}{k_2}f'(-y) \tag{6.23}$$

Checking the boundary where $u = -1$ yields the following inequality:

$$-a + \frac{1}{k_2}f'(-y) < f(-y)f'(-y) < \infty \tag{6.24}$$

These two inequalities together yield condition $A6$ of Theorem 1, namely:

$$-a + \frac{1}{k_2}f'(-y) < -f(-y)f'(-y) < a - \frac{1}{k_2}f'(-y) \tag{6.25}$$

Thus the constraint $A6$ of Theorem 2 approaches the similar constraint for the continuous time system as $T_s \to 0$. This is a pleasing result, especially in light of the complexity of the discrete time analysis. Besides providing a validation of the condition in discrete time, the preceeding analysis also leads to the conclusion that for high enough sampling rates, the function $f(\cdot)$ chosen for the continuous time system should meet the conditions necessary for stability set forth in Theorem 2.

Thus the velocity trajectory function $f(\cdot)$ used in the continuous time PTOS (2.8) will be used in the discrete time PTOS as well, along with the conditions for a continuous magnitude and slope (2.9)-(2.10).

6.1 Evaluation of condition $A6$

Choosing $f(\cdot)$ and $f'(\cdot)$ to be continuous functions, of the form (2.8), has a benefit in that it allows us to check condition $A6$ on the boundaries of U ($u_k = 1$ and $u_k = -1$)[1] as shown in Figure ??. This is easier than evaluating $A6$ for all points in U . Evaluating $A6$ on the boundary $u_k = +1$ yields:

$$-1 < k_2[-f(y - T_s f(y) - T_s/k_2 + aT_s^2) + f(y) + \frac{1}{k_2} - aT_s] < 1 \ , \ \forall y \tag{6.26}$$

Checking the remaining boundary $(u = -1)$, yields:

$$-1 < k_2[-f(y - T_s f(y) + T_s/k_2 - aT_s^2) + f(y) - \frac{1}{k_2} + aT_s] < 1 \ , \ \forall y \tag{6.27}$$

Note that if the function $f(\cdot)$ is symmetric the conditions need only be checked for non-negative values of y.

The conditions given by (6.26) and (6.27) are difficult to analyze directly (substituting (2.8) in for $f(\cdot)$). Instead, a numerical analysis will be used to shed some light on exactly what the tradeoffs are in choosing ω_d, T_s, and α given a.

Before a numerical analysis of the above conditions can be performed, a design rule must be chosen for the free parameters in the control law, namely the gain k_1 and the deceleration discount factor α.

7. Linear Control Law

Designing the linear controller for the discrete time system is again more complicated than the continuous time case. Let's define the ratio of sampling frequency to desired bandwidth as N

$$N \triangleq \frac{\omega_s}{\omega_d} = \frac{f_s}{f_d} \tag{7.28}$$

For most discrete time servomechanisms, the value of N is greater than five. Astrōm and Wittenmark [5] claim a good rule of thumb is to have

$$N \approx 20\sqrt{1-\zeta^2}$$

which for $\zeta = .707$ means $N \approx 14$. For values of N as large as these, one would expect that the discrete time system gain k_1 should be close to that of the continuous time case for the same desired closed loop bandwidth. Unfortunately, although the damping ratio's are very close, the bandwidths of the two systems are significantly different when N is as large as 10 as seen in Figure 7.7.

Condition $A7$ of Theorem 2 put a restriction on the slope of the function $f(\cdot)$. Let

$$c = \frac{1}{2}\sup_y |f'(y)| = \frac{1}{2}\frac{k_1}{k_2} \tag{7.29}$$

Since condition $A7$ is that $c < 1/4$, it follows that,

$$\frac{k_1}{k_2} < \frac{1}{2} \tag{7.30}$$

Substituting for k_2 yields:

$$k_1 T_s^2 < \frac{2}{a} \tag{7.31}$$

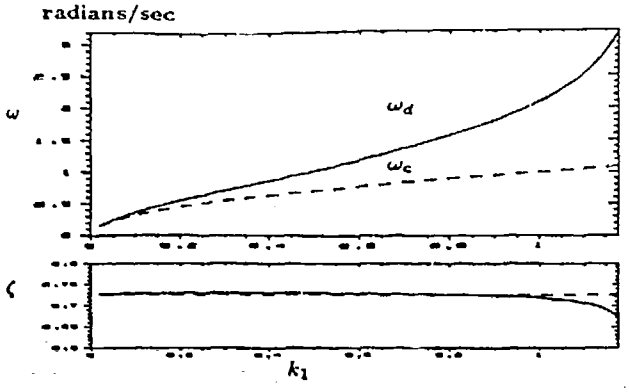

Figure 7.7: Closed loop bandwidth and damping as a function of the gain k_1, for a sampling interval of 1 second. The bandwidth and damping of a continuous system is shown by the dashed line for comparison.

which is larger than the result given by condition *A*1.

A much more difficult task is that of checking condition *A*6. Since substituting the expression given by (2.8) for $f(\cdot)$ leaves us with something which appears to be analytically intractable, we will resort to checking the condition numerically. A program written in PASCAL searched for the *largest* sampling interval T_s which would allow condition *A*6 to remain true, as a function of a range of given k_1's. From k_1 and k_2, the closed loop (-3 dB) bandwidth of the system was calculated as follows. Given k_1, calculate

$$k_2 = \left(\frac{2k_1}{a\alpha}\right)^{1/2} \tag{7.32}$$

$$p_1 = \frac{ak_1T_s^2}{2} + ak_2T_s - 2 \tag{7.33}$$

$$p_2 = \frac{ak_1T_s^2}{2} - ak_2T_s + 1 \tag{7.34}$$

$$r = \sqrt{p_2} \tag{7.35}$$

the closed loop bandwidth can be found from (given the system has complex poles):

$$\omega_d = \frac{1}{T_s}\left[\left(\arccos\left(\frac{p_1}{-2r}\right)\right)^2 + \left(\frac{\ln(p_2)}{2}\right)^2\right]^2 \tag{7.36}$$

A plot of the *minimum* N and *maximum* $k_1T_s^2$ versus α is shown in Figure 7.8. The

In summary, the desired bandwidth of the closed loop controller is not significantly restricted by condition *A*7 of Theorem 2, but is restricted by condition *A*6. In other words, the Lyapunov function is not placing an active constraint on N, but the condition of remaining in the region U once in it, or avoiding jumping over U entirely, does place an active constraint on the sampling rate versus desired bandwidth. This is evident in Figure 7.9. The constraint on N could be avoided by changing the function $f(\cdot)$ to account for sample time, but only at the cost of loss of performance (increase in response time).

8. Unmodeled Dynamics

Taking unmodeled dynamics into account in Theorem 2 is, within the present analytical framework, impossible. Since analyzing condition *A*6 of Theorem 2 explicitly is not possible, it is

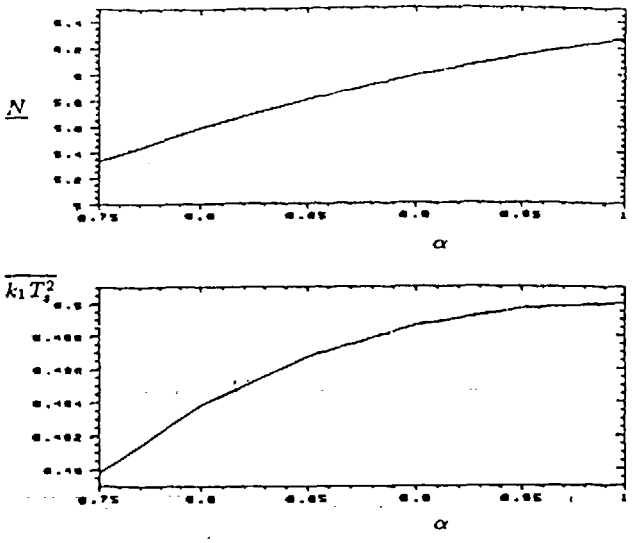

Figure 7.8: The maximum value of $k_1T_s^2$ and minimum value of N versus α. As design guides, these two curves could be considered constants: $N > 6.2$, and $k_1T_s^2 < .49$.

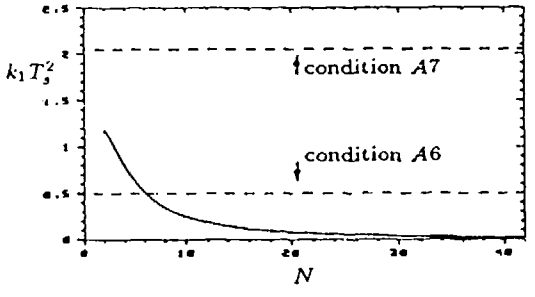

Figure 7.9: The value of $k_1T_s^2$ as a function of N, for $\alpha = .95$ and the upper limits imposed by conditions *A*6 and *A*7.

hard to imagine that throwing in more complexity will help in the analysis. Thus, unfortunately we will have to fall back on Section 6 and make the assumption that for fast enough sampling rates, the unmodeled dynamics analysis for the continuous time case should apply[1]. While this is not particularly satisfying, when coupled with system simulations, it is a practical approach.

The design procedure for discrete time is thus to apply continuous time measures of unmodeled dynamics to the system, chose an appropriate acceleration discount factor α, and verify this choice by simulation of system performance.

9. Adaptive PTOS

The same structure as used in the continuous time APTOS will be used for the discrete time APTOS, with appropriate changes in the identification algorithms: replace the plant gain a by the estimated plant gain $\hat{a}$ in (2.8), and adjust the control gains k_1 and k_2 by $\hat{a}$ as well.

9.1 IDENTIFIER

To fix ideas, we will propose and analyze a simple one parameter identifier in the APTOS structure. In terms of polynomials in the unit delay operator q^{-1}, the input-output relationship of the double integrator plant is

$$(q^{-1} + q^{-2})u = \left(\frac{2}{a_{nom}T_s^2}\right)(1-q^{-1})^2 y \qquad (9.37)$$

where a_{nom} represents the nominal or expected value of the plant gain a. If the measured data is $\{ u, y, t = 0, T_s, 2T_s, \cdots \}$ then we can form an equation error as follows:

$$e \triangleq z - \phi \qquad (9.38)$$

where,

$$z = \left(\frac{2}{a_{nom}T_s^2}\right)(1-q^{-1})^2 y \qquad (9.39)$$

$$\phi = (q^{-1} + q^{-2})u \qquad (9.40)$$

Consider the LMS identifier for the *normalized* plant gain $\hat{a}$:

$$e \triangleq z - \hat{a}\phi \qquad (9.41)$$

$$\hat{a}_{k+1} = \hat{a}_k + g\phi e \qquad (9.42)$$

where g is a positive constant. Define the parameter error as

$$\tilde{a} = \hat{a}a_{nom} - a \qquad (9.43)$$

The following Theorem gives conditions for convergence of this single parameter identifier.

Theorem 3 *(Parameter Convergence). If*

1. $g\phi_k^2 \in (0,2)$
2. $\exists T > 0, \beta > \alpha > 0$ *such that for all* k:

$$\beta \geq \sum_{l=0}^{l=T-1} \phi_{k+l}^2 \geq \alpha$$

then the parameter error $\tilde{a} \to 0$ *as* $k \to \infty$ *exponentially fast.*

Proof. The proof is contained in [1].

Thus as long as condition 2 of Theorem 3 holds, adaptive control based on $\hat{a}$ works. This is because exponential convergence of $\hat{a}$ gaurantees that at some point the function $f(y_c, \hat{a})$ will meet the conditions of Theorem 2 are met ($\alpha < 1$). To gaurantee condition 2 of Theorem 3 holds, there must be enough changes in the input reference command r. In implementation, the parameter estimate is *not* updated when the system is in regulation mode, which prevents parameter drift due to lack of persistant excitation. Hence, after a countable number of input command changes, the system is tuned.

10. SIMULATION AND EXPERIMENT

A simulation of the adaptive behavior of the discrete time APTOS system is shown in Figure 10.10. An experimental setup using a torque motor and an inertial load was used to test the APTOS system. The adaptive behavior of the experimental system matched simulation very well. Once tuned, the simulation and measured responses were extremily close, as can be seen in Figure 10.

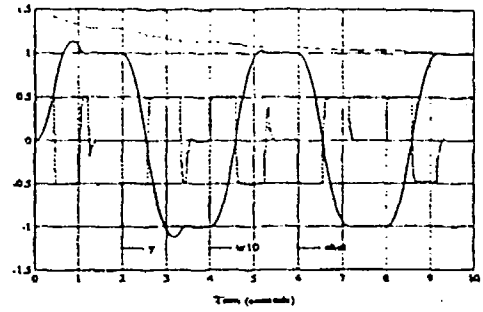

Figure 10.10: APTOS behavior to an initial error in parameter estimate of 50%.

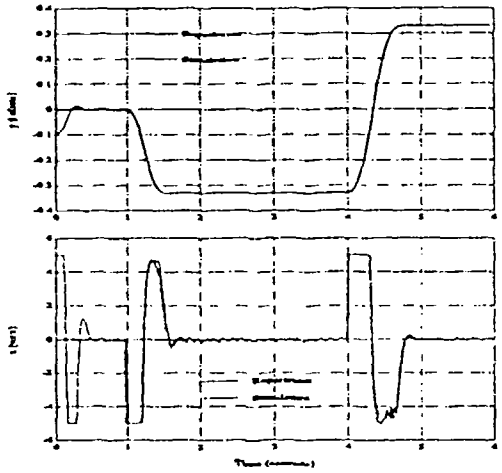

Figure 10.11: Experiment versus simulation.

REFERENCES

[1] Michael L. Workman, *Adaptive Proximate Time-Optimal Servomechanisms*, PhD thesis, Stanford University, 1987.

[2] Bryson and Ho, *Applied Optimal Control*, Halsted Press, 1010 Vermont Ave., N. W., Washington, D.C. 20005, 1975.

[3] M.L. Workman, *Applications of Magnetic Recording*, chapter 2: The Head Positioning Servomechanism, edited by D. Mee and E. Daniels, Mc Graw Hill, 1987, To be published second-half of 1987.

[4] M. L. Workman, R. L. Kosut, and G. F. Franklin, Adaptive proximate time-optimal control: continuous time case, In *Proceedings of the Automatic Control Conference*, page pp. ???, June 1987.

[5] K. J. Åström and B. Wittenmark, *Computer Controlled Systems, Theory and Design*. Prentice Hall, Englewood Cliffs, N.J. 07632, 1984.

Appendix C

Published in the *Proceedings of the SPIE Conference*, Los Angeles, California, January 1988.

Minimum-Time Control of Large Space Structures

Robert L. Kosut* , Antonio M. Pascoal* , Michael L. Workman† , and Gene F. Franklin‡

*Integrated Systems Inc., 2500 Mission College Blvd. Santa Clara, CA 95054
†IBM Corporation, 5600 Cottle Road, San Jose, CA 95193
‡Information Systems Laboratory, Stanford University, Stanford, CA 94305

Abstract

An Extended Proximate Time-Optimal Servomechanism (XPTOS) is developed for the control of a flexible structure with a single structural mode. The resulting control system is closed-loop , and embodies in its structure the characteristics of a time-optimal control law and the fine tracking properties of a properly tuned linear regulator. Simulation results demonstrate the performance of the XPTOS, and its robustness in the face of uncertain plant parameters.

1 Introduction

One of the challenging tasks facing control engineers and theorists is the design of control systems to achieve rapid slewing and precision pointing of large space structures (LSS). With increasing demands being placed on the design and construction of lightweight LSS optical tracking systems, the need has arisen for sophisticated control algorithms that make optimal use of the maximum torque available for rapid slew, and achieve high tracking accuracy after the tracking error signals have become sufficiently small.

The "ideal" solution to this problem is obtained by computing the optimal open-loop "switching" actuation sequence that steers the structure from initial to final (target) position in minimum time [5,6]. In practice, such a solution is very difficult to obtain, and a proximate time-optimal control law is usually derived by considering the rigid body motion only. The resulting input actuation sequence may result in significant excitation of the structural modes, and therefore it must be modified so that its power spectrum has significantly lower harmonic content. One approach is the sine-versine torque shaping technique, which attempts to achieve a good tradeoff between slewing time and structural mode excitation [1]. The resulting control law, however, is open- loop and therefore the control system becomes very sensitive to modeling errors and exogenous disturbances. In order to overcome these difficulties, a number of techniques have been proposed which combine feedforward sine-versine torque excitation with linear feedback information to provide for active damping of the structural modes [2,3].

In this paper, we consider the design of a practical "proximate" time-optimal feedback controller for a flexible structure with a single structural mode. The controller blends the time-optimal characteristics of a nonlinear (switching) control law, and the fine tracking properties of a properly tuned linear regulator. Furthermore, it exhibits good robustness properties against plant parameter variations. The approach pursued here follows from some previous work reported in [8,9,10] on a proximate time-optimal servomechanism (PTOS) for a rigid structure with high frequency unmodeled dynamics that are outside of the performance bandwidth. We extend these techniques by taking directly into account the existence of a lightly damped mode, which may possibly be within the desired performance bandwidth. The resulting control law, referred to as the extended proximate time-optimal servomechanism (XPTOS), retains the simplicity of the basic structure introduced in the PTOS and offers attractive advantages when compared with the approaches conventionally used for time-optimal control of large space structures.

The organization of the paper is as follows. Section 2 contains a brief description of a proximate time-optimal servomechanism (PTOS) introduced in [8,9]. Section 3 is devoted to the extended proximate time-optimal servo (XPTOS). Section 4 contains a detailed example that illustrates the performance of the control algorithm introduced in Section 3. Finally, Section 5 contains the conclusions and suggestions for further research.

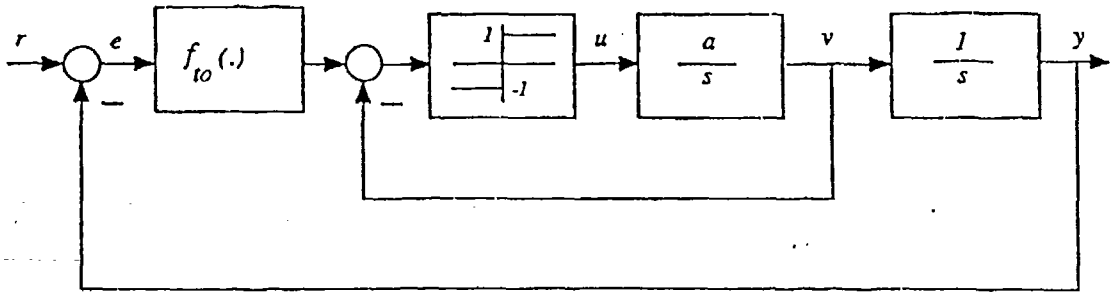

Figure 1: Time-Optimal Controller for Double Integrator Plant

2 The Proximate Time-Optimal Servo (PTOS): A Review

This section contains a brief review of a proximate time-optimal servomechanism (PTOS) described in Workman, Kosut, and Franklin [9] for a double integrator plant.

2.1 The PTOS algorithm

Let the plant P be described by the system of equations

$$\begin{aligned} \dot{y} &= v\,, \\ \dot{v} &= au\,, \end{aligned}$$

where u and y denote the plant input and output respectively, a is the maximum acceleration available, and $|u(t)| \leq 1$. Let the plant state x be defined by

$$x^T = [y\, v].$$

Given an initial state $x_0^T = [y_0\, v_0]$ at time $t = 0$, suppose it is required to steer x_0^T to a target state $x_t^T = [r\, 0]$ in minimum time. The resulting time-optimal control, depicted in Figure 1, is given by [5]

$$u = \mathrm{sgn}\left(f_{to}(e) - v\right)\,, \tag{1}$$

$$f_{to}(e) = \mathrm{sgn}(e)(2a|e|)^{\frac{1}{2}}\,, \tag{2}$$

$$e = r - y\,, \tag{3}$$

where

$$\mathrm{sgn}(z) = \begin{cases} +1\,, & z > 1 \\ 0\,, & z = 0. \\ -1\,, & z < 1 \end{cases} \tag{4}$$

The control law given by (1)–(4), although optimal, is not practical. In fact, any process or measurement noise will make the control signal u "chatter" between its maximum and minimum values, thus exciting unmodeled dynamics that are always present in a more accurate model of a real plant. Even in the absence of exogenous signals, the time-optimal controller lacks robustness with respect to neglected dynamics, since a lightly damped mode will induce a limit cycle (Workman, [8]). To circumvent this difficulty, a more practical implementation of a time- optimal controller was introduced in [8]. The resulting control system, referred to as a proximate time-optimal servomechanism (PTOS), is diagrammed in Figure 2.

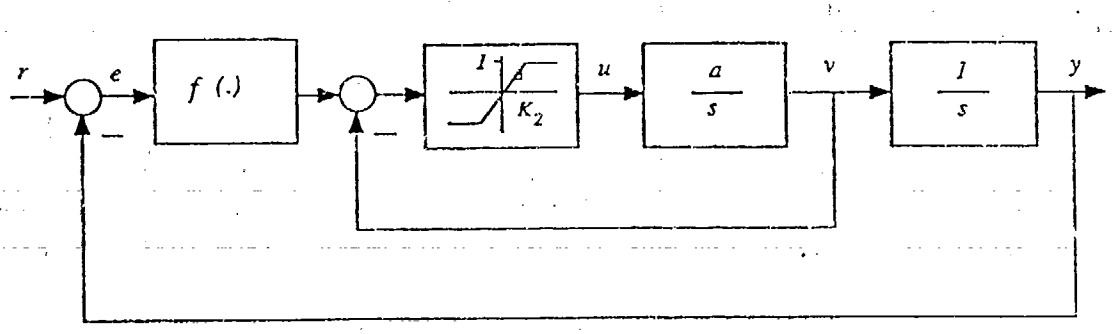

Figure 2: Proximate Time-Optimal Servomechanism (PTOS)

The equations that describe this "practical" version of the optimal control law are

$$\dot{y} = v, \tag{5}$$

$$\dot{v} = a\,\mathrm{sat}\left(k_2[f(e) - v]\right)\ ;\ k_2 > 0\ , \tag{6}$$

where

$$\mathrm{sat}(z) = \begin{cases} +1\ , & z > 1 \\ z\ , & |z| \le 1 \\ -1\ , & z < -1 \end{cases}\ , \tag{7}$$

and

$$f(e) = \begin{cases} \frac{k_1}{k_2}(e)\ ; & |e| \le y_l \\ \mathrm{sgn}(e)\left[(2a\alpha|e|^{1/2} - \frac{1}{k_2}\right]\ ; & |e| > y_l \end{cases} \tag{8}$$

In (8), k_1, k_2 and y_l are positive real constants, and $0 < \alpha < 1$, referred to as the *acceleration discount factor*, is a tuning parameter.

The finite-gain operator $\mathrm{sat}(\cdot)$ has replaced the infinite gain operator $\mathrm{sgn}(\cdot)$, and the switching function $f_{to}(e)$ (the derivative of which is infinite at $e = 0$) has been substituted by $f(e)$, which is linear in the range $|e| \le y_l$. To connect the nonlinear parts of $f(\cdot)$ in (8) such that $f(\cdot)$ remains continuous and has a continuous first derivative, the following additional constraints were imposed in [8,9]:

$$k_2 = \sqrt{\frac{2k_1}{a\alpha}}\ , \tag{9}$$

and

$$y_e = \frac{1}{k_1}\ . \tag{10}$$

Stability of the resulting closed-loop system (for step inputs) follows from the fact that the zero solution of

$$\dot{y} = v$$

$$\dot{v} = a\,\mathrm{sat}\left(k_2[f(-y) - v]\right)$$

is globally asymptotically stable (see [8, Theorem 3.1]). In addition, the closed-loop system is close to time-optimal in the following sense:

Let $x_0^T = [r_0, 0]$ denote the plant initial state, and suppose it is desired to steer x_0^T to $[r, 0]$ in minimum time. Using the (time-optimal) control law in (1)-(4), the minimum maneuver time t_{opt} is

$$t_{opt}(L) = \frac{2}{\sqrt{a}}\sqrt{L}\ , \tag{11}$$

where

$$L = |r - r_0| .$$

We now consider the PTOS system described in (5)–(8). For large set point changes such that $L >> \frac{1}{k_1}$, the time it takes for the closed loop system to settle in the linear region of operation can be approximated by

$$t_l(L) = \frac{1}{\sqrt{\alpha}}\sqrt{L} + \frac{1}{\sqrt{a\alpha}}L , \tag{12}$$

where, as shown in [8], $t_l(L)$ is such that $|r - y(t_l(L))| \approx \frac{1}{k_1}$. Defining P as the percentage increase in maneuver time of the practical controller, it follows from (11)-(12) that

$$P = 100\% \left[\frac{1}{2}\left(\frac{1}{\sqrt{\alpha}} - 1\right)\right] .$$

Clearly, P is independent of the move length L. Moreover, P is close to 0 for values of α close to 1. The above analysis is based on the assumption that, in the linear region of operation, the dynamics of the closed-loop system decay sufficiently fast on the time-scale of $t_l(L)$. This can be achieved by proper selection of k_1 and α, as described below.

2.2 Designing the Linear Controller

Let $H(s) = Y(s)/R(s)$ denote the transfer function of the closed-loop system of Figure 2, when operating in the linear region. With the usual notation for a second order system, and using (9), it follows that

$$H(s) = \frac{\omega_d^2}{s^2 + 2\zeta_d\omega_d s + \omega_d^2} , \tag{13}$$

where

$$\omega_d = \sqrt{\frac{k_1}{a}} , \tag{14}$$

and

$$\zeta_d = \frac{1}{\sqrt{2\alpha}} . \tag{15}$$

Thus, the overall closed-loop system bandwidth ω_d and damping factor ζ_d can be independently controlled by the parameters k_1 and α, respectively. As shown in [8,9], the PTOS algorithm can be applied to the control of a purely rigid body with high frequency unmodeleds dynamics that are outside of the performance bandwidth ω_d. However, if the structural modes are within the desired closed loop system bandwidth, then they must be treated explicitly in the initial design. This is the subject of the next section.

3 The Extended PTOS Algorithm (XPTOS)

In this section, we address the problem of designing a proximate time-optimal controller for a flexible large space structure. In this preliminary study, we restrict ourselves to the (idealized) case where the structure P to be controlled is linear and contains a single structural mode. Hence, P can be described by the transfer function

$$P(s) = \frac{a_r}{s^2} + \frac{a_f}{s^2 + 2\zeta\omega_n s + \omega_n^2} , \tag{16}$$

where ω_n and ζ denote the frequency and damping of the structural mode respectively, and a_r and a_f are real numbers. We assume that both output position and rate measurements are available for measurement. In this case, the plant admits the state-space realization

$$\begin{aligned} \dot{x} &= Ax + Bu , \\ y_m &= Cx , \end{aligned} \tag{17}$$

where

$$A = \left[\begin{array}{cc|cc} 0 & 1 & 0 & 0 \\ 0 & 0 & 0 & 0 \\ \hline 0 & 0 & 0 & 1 \\ 0 & 0 & -\omega_n^2 & -2\zeta\omega_n \end{array}\right], \quad B = \begin{bmatrix} 0 \\ a_r \\ 0 \\ a_f \end{bmatrix}, \quad C = \begin{bmatrix} 1 & 0 & 1 & 0 \\ 0 & 1 & 0 & 1 \end{bmatrix}, \tag{18}$$

$y_m = (y, \dot{y})$, and $x^T = (y_r, v_r, y_f, v_f)$ denotes the state-space vector. We shall henceforth refer to (y_r, v_r) and (y_f, v_f) as the rigid body and structural mode coordinates, respectively.

3.1 Proximate Time-Optimal Control of a Flexible Structure

Consider the autonomous linear process (17)–(18). Given an initial state x_0 at time $t = t_0$, suppose it is required to steer x_0 to a final (target) state x_f in minimum time, by using inputs u such that $|u(t)| \leq 1$. The problem of time-optimal control thus defined has been the subject of extensive research, and a vast body of literature is available on its theoretical and practical aspects (see Lee and Markus [5] and Oldenburg [6] for a rigorous exposition). Under fairly generic conditions the optimal steering controller $u_{opt}(t)$ exists and is of the relay type, i.e. it assumes the values ± 1 and switches a finite number of times. A closed-loop implementation of the optimal control law, however, requires the construction of high-order switching surfaces. For systems with state-space dimension greater than two, these surfaces become so complex as to exclude their use in the implementation of practical time-optimal control algorithms.

An interesting approach to the solution of this problem has been reported by Kalman (in Oldenburg [6]), who used linear transformations in the phase space to replace a "high-order system with a second-order system which closely approximates the former". In particular, a nearly optimally compensated third-order saturating servomechanism was described for the plant $G(s) = \frac{1}{s^2(T_1 s+1)}$ consisting of a pure inertia and a first-order lag. The resulting control law relies on a single switching curve, and is effective if the dynamics of the first-order lag are sufficiently fast. Clearly, this procedure is not directly applicable to the flexible structure described in (17)–(18), since the structural mode typically has very small damping ζ, and therefore a very long settling time.

In Schmidt[7], a technique for the design of nonlinear saturating controllers to achieve proximate time-optimal control of high order plants was described. In what follows, and motivated by the work reported in [6] and [7], we propose a (nonlinear) feedback scheme for proximate time-optimal control of (17)-(18) that preserves the basic structure of PTOS.

3.2 The structure of the XPTOS

The rationale behind the XPTOS control system can be explained as follows: the dynamic behavior of the flexible structure described in (17)–(18) can be decomposed into its rigid and structural dynamics, which are completely specified by the state-space coordinates (y_r, v_r) and (y_f, v_f) respectively. To steer the structure from an initial to a final (target) position, apply the PTOS strategy to control the rigid body motion, and blend it smoothly into a linear state-feedback control law that actively damps out the structural modes. The resulting scheme is depicted in Figure 3.

Let $\hat{x} := [\hat{y}_r, \hat{v}_r, \hat{y}_f, \hat{v}_f]$ denote the estimate of $x := [y_r, v_r, y_f, v_f]$, obtained from the state-estimator dynamics

$$\dot{\hat{x}} = A\hat{x} + Bu + K_0[y_m - C\hat{x}], \tag{19}$$

where K_0 is such that $(A - K_0 C)$ is asymptotically stable. Then, the following description of XPTOS is obtained:

$$\begin{aligned} \dot{x} &= Ax + Bsat(u), \\ y_m &= Cx, \end{aligned} \tag{20}$$

where

$$u = k_2\left[f(e) - \hat{v}_r - \frac{k_3}{k_2}\hat{y}_f - \frac{k_4}{k_2}\hat{v}_f\right], \tag{21}$$

$$e = r - \hat{y}_r, \tag{22}$$

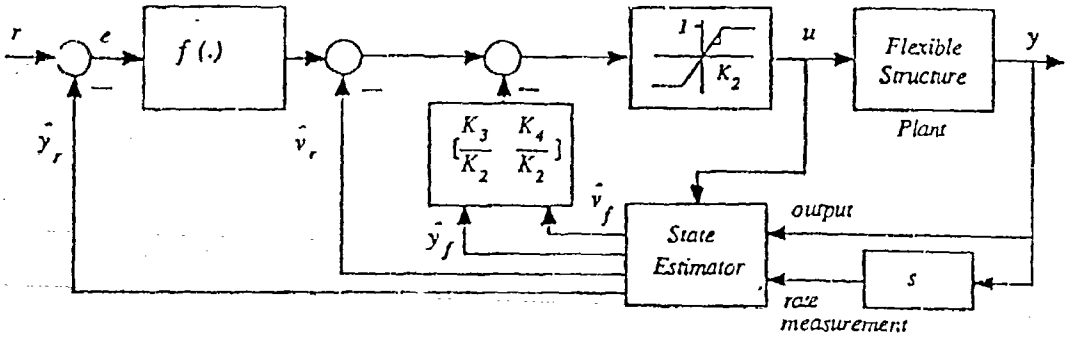

Figure 3: Extended Proximate Time-Optimal Servomechanism (XPTOS)

$f(\cdot)$ is defined in (8), and

$$K_s = [k_1\, k_2\, k_3\, k_4] \tag{23}$$

is such that $(A - BK_s)$ is asymptotically stable.

3.3 XPTOS: Design Methodology

The purpose of this section is to provide some guidelines for the design of the XPTOS system to accomplish rapid slewing of the flexible structure described in (17)-(18). In a typical retargeting maneuver, the objective is to steer rapidly the output y from 0 (at time $t = 0$) to the final target value r_0, and remain there. To accomplish this, we propose a design methodology that is based on the following control strategy: during the initial phase of the maneuver, let the nonlinear characteristics of XPTOS takeover, in an attempt to steer the rigid body dynamics (y_r, v_r) from $(0, 0)$ at $t = 0$ to $(r_0, 0)$ in minimum time; in the last phase of the maneuver, use the properties of a properly tuned linear regulator to achieve high tracking accuracy and active damping of the structural mode.

It is clear from the considerations above that the following constraints (inherited from the PTOS design methodology described in Section 2) must be observed:

$$\text{(C1)} \quad k_2 = \sqrt{\frac{2k_1}{a_r \alpha}}, \quad \text{(C2)} \quad 0 < \alpha < 1.$$

In practice, the degree of flexibility of the structure places a lower limit L_{min} on the size of the maneuver for which the "bang- bang"characteristics of XPTOS should be explored. Thus, given L_{min} select k_1 so that

$$\text{(C3)} \quad k_1 > \frac{1}{L_{min}}.$$

We now examine the constraints that arise from the performance requirements in the linear region of operation.

Consider the XPTOS system diagrammed in Figure 3, and described by equations (18)-(23). In the linear region of operation, and in the absence of any input signal r, the system can be simply viewed as the combination of a state-observer and a linear regulator. The evolution of the feedback system is then governed by the equations

$$\dot{x} = Ax - BK_s\hat{x}, \tag{24}$$

$$\dot{\hat{x}} = K_0 C x + (A - K_0 C - BK_s)\hat{x}, \tag{25}$$

where

$$K_s = [k_1\, k_2\, k_3\, k_4]. \tag{26}$$

Furthermore, the poles of the interconnected system consist of the observer poles (eigenvalues of $A - K_0C$), together with the regulator poles (eigenvalues of $A - BK_s$). The first requirement on the system (24)-(26) is that it be

asymptotically stable. In addition, K_0 and K_s must be selected so that the XPTOS exhibit good tracking properties (i.e. fast dynamics) in the linear region of operation.

3.3.1 Selection of K_s

The PTOS design methodology detailed in section 2.2 reduces to the solution of simple algebraic equations. A similar procedure may be derived for the design of XPTOS. In fact, it is straightforward to derive an expression for $d(s)$, the regulator characteristic polynomial, in terms of K_s and α. Furthermore, given α and any set $\mathcal{E}$ of desired closed-loop (complex conjugate) eigenvalues, it is possible to ascert the existence (and in the affirmative case compute) K_s so that K_s satisfies the constraints (C1)-(C3), and the roots of $d(s)$ equal $\mathcal{E}$. This method becomes rather cumbersome (and therefore not practical) if extended to plants with more than one structural mode. With this objective in sight, we describe a different design method.

Assuming the state vector x is available for measurement, we seek a linear control law of the form

$$u = -K_s x \ , \tag{27}$$

where $K_s = [k_1\ k_2\ k_3\ k_4]$ is suitably chosen to minimize the quadratic performance index

$$J = \int_0^\infty [x^T(t)Qx(t) + \rho u^2(t)]dt \ ; \tag{28}$$

$\rho > 0$ and Q symmetric, positive semidefinite

subject to

$$\dot{x} = Ax + bu \ ; \ x(0) = x_0 \tag{29}$$

In the sequel, we will refer to the problem described above as the linear quadratic regulator (LQR) problem. Let $Q = z^T z$ for some row vector z, and let the pairs (A, b) and (A, z) be stabilizable and detectable, respectively. Then, K_s is obtained from the positive definite solution of an algebraic Riccati equation, and the resulting feedback control law stabilizes the system (29)(Kwakernaak and Sivan,[4]).

We remark that for our purposes, the LQR design methodology is simply viewed as a design tool that provides a systematic way of "scanning" a large set of stabilizing feedback laws. Thus, ρ and z are tuning parameters that control the location of the regulator poles to achieve good tracking properties.

The inclusion of the constraints (C1)-(C3) into the LQR design problem is considerably difficult, and we therefore propose the following iterative algorithm for the design of XPTOS:

Step 1. Select an initial estimate for z, and let ρ vary in some interval $[\rho_{\min}, \rho_{\max}]$. For each value of ρ, solve the LQR problem (28)-(29) to obtain a stabilizing feedback gain $K_s(\rho)$.

Step 2. Plot K_1 and $\alpha = 2k_1/k_2^2 a_r$ as functions of ρ, and check that a value of $\rho = \rho^*$ exists for which (C1)-(C3) are satisfied. In case these constraints are not satisfied, modify z and/or the interval $[\rho_{\min}, \rho_{\max}]$ and go back to *Step 1.*

Step 3. Check the final location of the regulator poles. (i.e., eigenvalues of $A - BK_s$). As a design rule, require the "dominant" time-constant of the regulator system to be much smaller than $t_{opt}(J_{\min}) = 2(J_{\min}/a_r)^{1/2}$, where $t_{opt}(J_{\min})$ is the (theoretical) minimum time required for retargeting of the rigid body only (i.e., make $\min R_e[\lambda_i(A - BK_s)] >> 1/t_{opt}(J_{\min})$). If this condition is not met, modify z and/or the interval $[\rho_{\min}, \rho_{\max}]$, and go back to *Step 1.*

Remark 3.1 In the analysis above, we eschew the question of existence of a vector K_s such that (C1)-(C3) are satisfied, and K_s solves the LQR problem for some choice of ρ and z.

Remark 3.2 The choice of the quantities ρ and z is not straightforward, and requires some insight into how they affect the relative magnitude of the gains k_1, k_2, k_3 and k_4, as well as the location of the regulator poles. Considerable insight into this process is gained by examining the asymptotic behavior of the regulator poles as $\rho \to 0$ and $\rho \to \infty$ (Kwakernaak and Sivan [4]).

3.3.2 Selection of K_0

Without any constraints imposed on its elements, K_0 is simply obtained as the optimal solution to a stochastic observer problem (Kwakernaak and Sivan, [4]). In this case, the state excitation noise and the measurement noise characteristics act as tuning parameters to force the dynamics of the observer to be sufficiently fast compared with the regulator dynamics.

4 XPTOS Performance: An Illustrative Example

In this section, we examine the performance of the XPTOS via a simulation example. As a representative test case, we have selected a flexible structure for which the PTOS algorithm (designed without consideration for the structural mode) gave unsatisfactory results. The performance of the XPTOS is compared against the slew maneuvers that are obtaibned by using a sine-versine open-loop control law [1]. Furthermore, we examine the robustness of both algorithms with respect to parameter variations.

The flexible structure to be controlled has the state-space representation described in (17)-(18), with

$$a_r = 3\ ,\ a_f = 50\ ,\ \zeta = .005\ ,\ \text{and}\ \omega_n = 26.8\ \text{rad-sec}^{-1}\ .$$

The design methodology described in Section 3 gives the following values for the XPTOS parameters:

$$\begin{aligned} \alpha &= .8\ , \\ k_s &= [12.67\ 3.25\ .74\ .65]\ , \\ \text{and}\quad k_0 &= \begin{bmatrix} 29.91 & 3.92 \\ 12.50 & 9.18 \\ 11.27 & -8.52 \\ -58.53 & 101.15 \end{bmatrix}\ . \end{aligned}$$

The structure was subject to rest-to-rest maneuvers with amplitude $L = 1$. In order to compare the different control strategies, we have (arbitrarily) defined the *maneuver time* t_m as the time after which the error signal $r - y$ becomes smaller than .018. With reference to Figures 4 through 8, the graphical summaries of the state and control time histories are discussed.

Case 1. (Fig. 4) is a rest-to-rest maneuver using the XPTOS algorithm. The initial phase of the maneuver aims at rapidly steering the rigid body state $(y_r, v_r) = (0,0)$ to the neigborhood of the final target value $(1,0)$. This results in considerable excitation of the flexible mode. However, its amplitude is rapidly reduced after the initial surge in the input control profile. In fact , the maneuver time t_m equals 1.32 seconds. Compare with $t_{opt} = 2(1/3)^{1/2} = 1.1547$, the (theoretical) minimum time required to steer the rigid body only, in the absence of the flexible mode (eq. (11)).

Case 2. (Fig. 5) is presented as evidence of the "stabilizing" effect of the nonlinear switching function $f(\cdot)$ in (8). Let the function f in (21) be defined by $f(e) = (k_1/k_2)e$ for all e. The resulting control system is of the relay- type, with a single nonlinear element at the input of the flexible structure. The response is highly oscilatory throughout the maneuver, and the maneuver time t_m increases to 1.95 seconds.

Case 3. (Fig. 6) is a rest-to-rest maneuver using the (open-loop) sine-versine control law [1]

$$u(t) = \frac{1}{3}\left[\frac{4\sqrt{3}}{9}\left(\frac{\sin 2\pi t}{\Delta_T}\right)\left(1 - \cos\frac{2\pi t}{\Delta_T}\right)\right]\ ,$$

where the (theoretical) rigid body slew time is

$$\Delta_T = \sqrt{\frac{6\pi}{\sqrt{3}}} = 1.9046\ \text{seconds}\ .$$

The resulting maneuver causes less excitation of the structural mode (in comparison with Case 1), but is noticeably slower, with t_m=1.6 seconds.

Case 4. (Fig. 7) displays the robustness of the XPTOS with respect to plant parameter variations. We notice that in both cases considered, $t_m < 1.36$ seconds.

Case 5. (Fig. 8) depicts the inherent lack of robustness of the sine-versine control algorithm. Clearly, a practical control system based on this algorithm requires switching to a linear regulator at the end of the sine-versine rigid body slew time Δ_T. However, this will further increase the total maneuver time.

5 Conclusions and Suggestions for Future Research

In this paper, we have developed an Extended Proximate Time-Optimal Servo (XPTOS) for the control of a flexible structure containing a single structural mode. The performance of the closed-loop control algorithm was illustrated with a representative example, which displays the excellent slewing and tracking properties of the XPTOS. A comparison was made with typical slew maneuvers obtained by applying a sine-versine control law.

Future work will require a rigorous analysis of the stability of the XPTOS, following the methodology proposed in [8]. It is our objective to refine the design technique exposed in section 3 in order to accomodate disturbances and sensor noise, and provide some robustnesss against the presence of neglected higher-frequency structural modes.

6 Acknowledgements

We wish to thank Mr. Scot K. Morrison of Integrated Systems Inc. for many helpful discussions on this subject. The research is sponsored by SDIO/IST and managed by AFSOR.

References

[1] J.N. Aubrun, N.K. Gupta, M.G. Lyons and G. Margulies, "Large Space Structures Control: An Integrated Approach", *Proceedings of the AIAA Guidance, Navigation and Control Conference*, Boulder, CO, August 1979.

[2] M. Barrett and D. Dugajski, "Robust Control of a Large Space Antenna", *AIAA Guidance, Navigation and Control Conference*, Monterey , CA, August 1987.

[3] M.A. Floyd, "Single-Step optimal Control of Large Space Structures Model", Department of Aeronautics and Astronautics, MIT, Sc.D. Thesis, June 1984.

[4] H. Kwakernaak and R. Sivan, *Linear Optimal Control Systems*, John Wiley & Sons, Inc., 1972.

[5] E.B. Lee and L. Markus, *Foundations of Optimal Control Theory* ,

[6] R. Oldenburger, editor, *Optimal and Self-Optimizing Control*, the M.I.T. press, Cambridge, MA, 02142, 1966.

[7] S.F. Schmidt, "The Analysis and Design of Continuous and Sampled Data Feedback Control Systems with a Saturation Type Nonlinearity", Ph.D. thesis, Stanford University, 1959.

[8] M.L. Workman, "Adaptive Proximate Time-Optimal Servomechanisms", Ph.D. thesis, Stanford University, 1987.

[9] M.L. Workman, R.L. Kosut, and G.F. Franklin, "Adaptive Proximate Time-Optimal Servomechanisms: Continuous-Time Case", *Proceedings Automatic Control Conference*, Minneapolis, MN, June 1987.

[10] M.L. Workman, R.L. Kosut, and G.F. Franklin, "Adaptive Proximate Time-Optimal Servomechanisms: Discrete-Time Case", *IEEE Conference on Decision and Control*, Los Angeles, CA, December 1987.

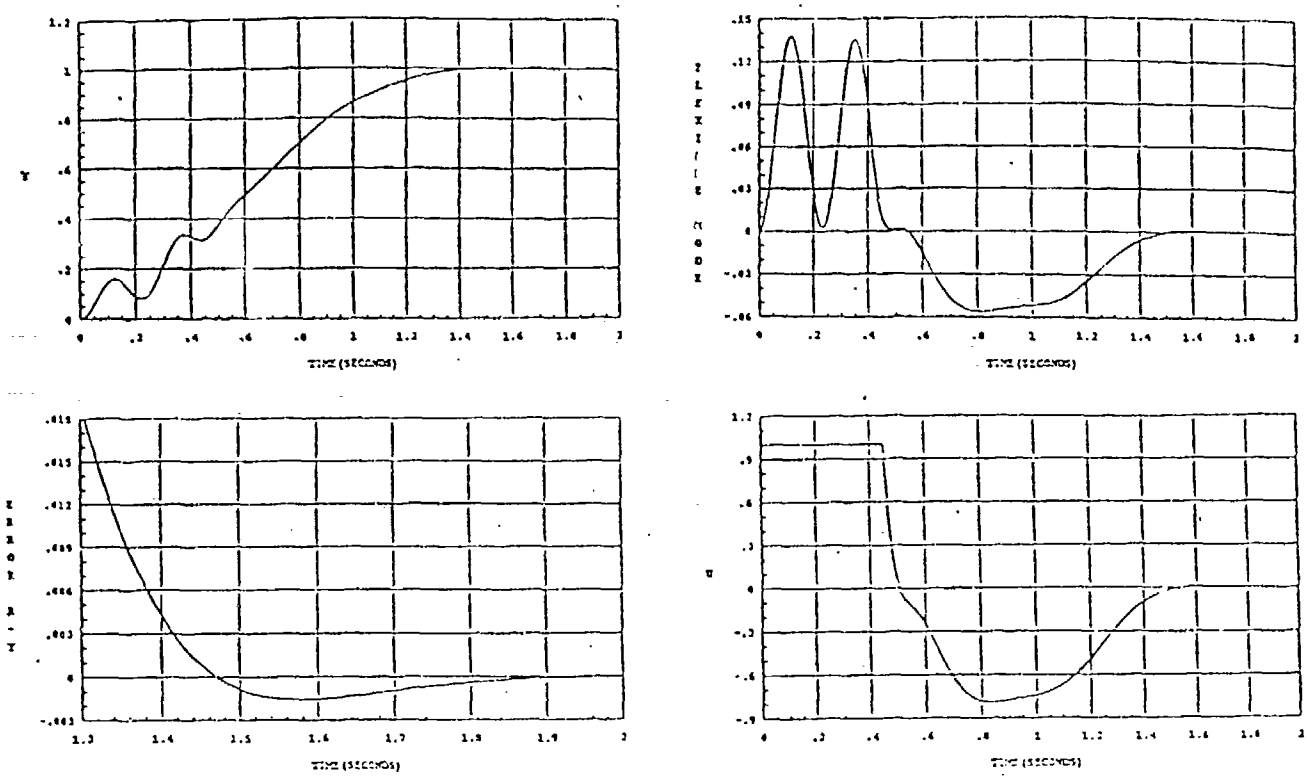

Figure 4: Case 1, Performance of the XPTOS

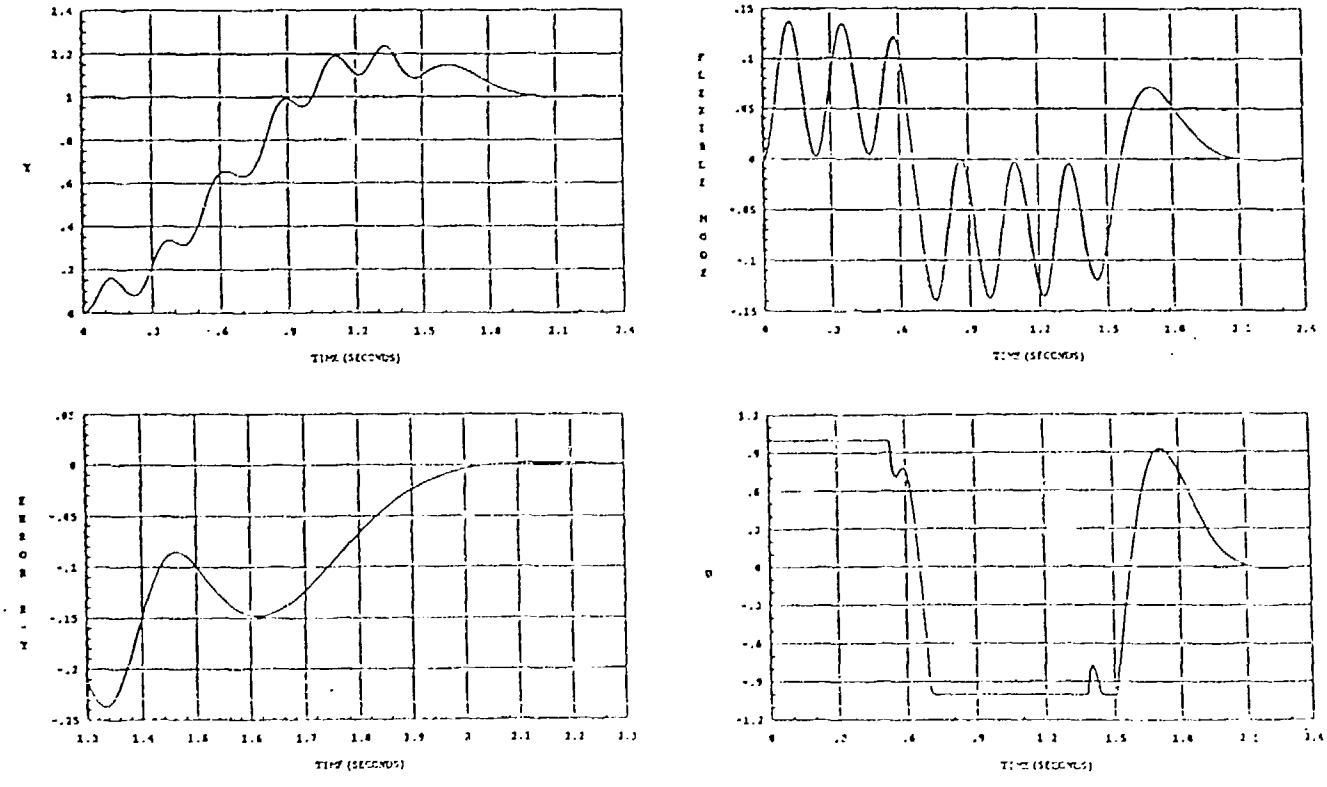

Figure 5: Case 2, Performance of the Relay Servomechanism

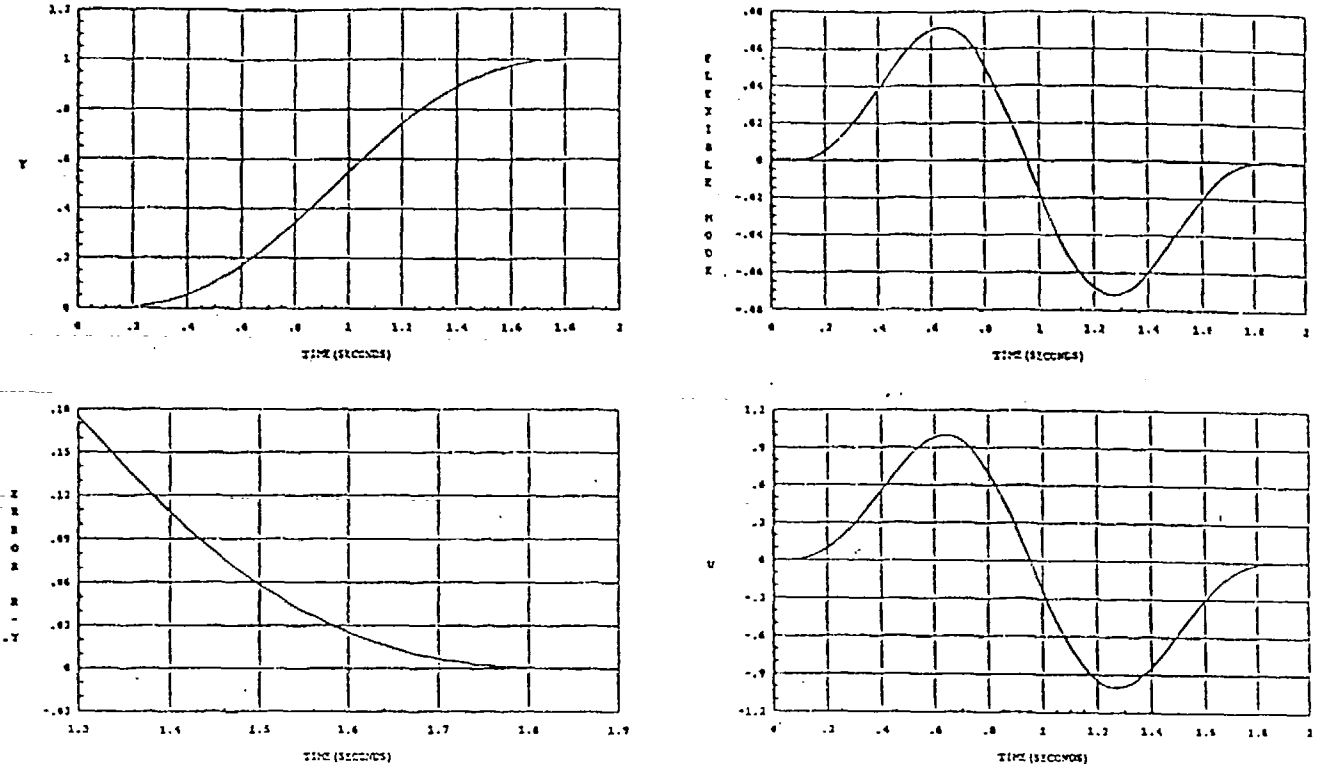

Figure 6: Case 3, Performance of the Sine-Versine Control Algorithm

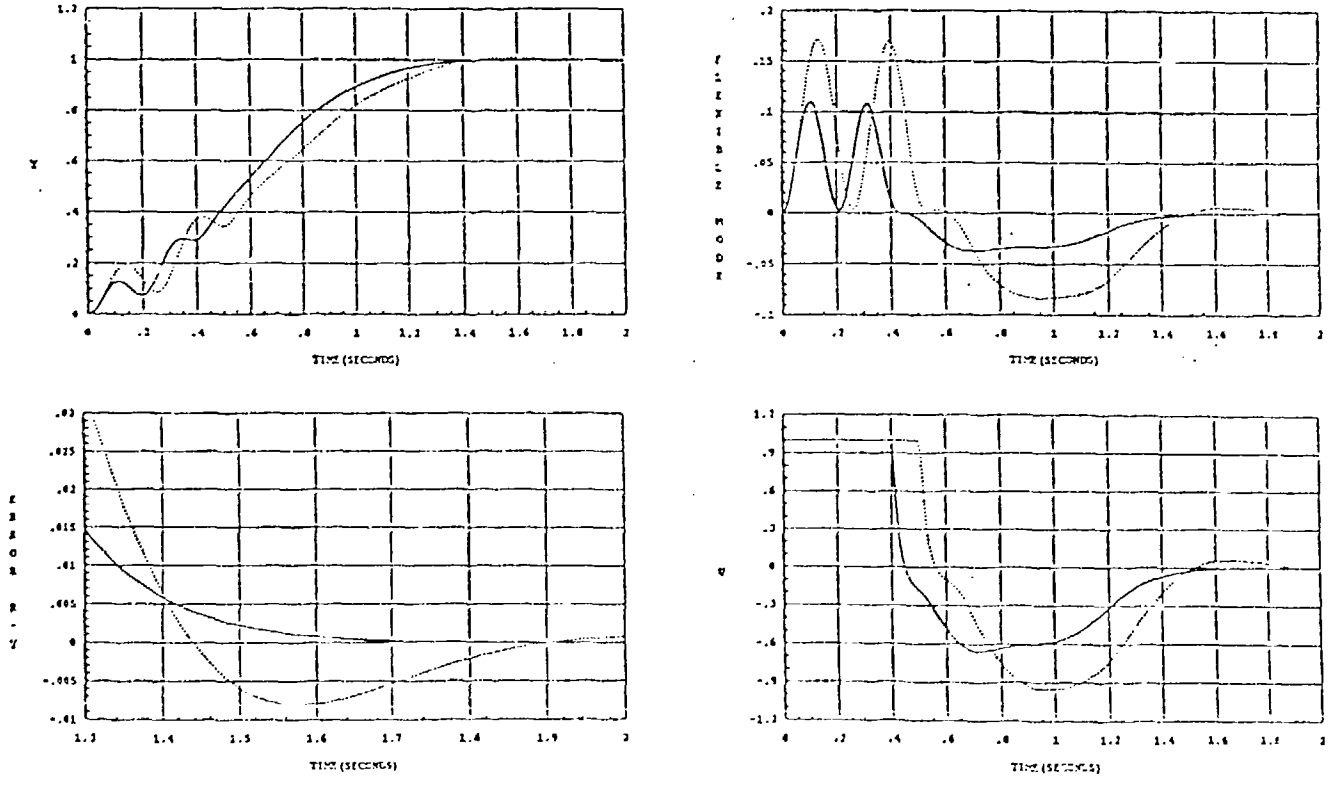

Figure 7: Case 4, Robustness of the XPTOS
—— $\omega_n = 30$ rad-sec^{-1} ; $a_r = 3.5$
- - - - $\omega_n = 24$ rad-sec^{-1} ; $a_r = 2.6$

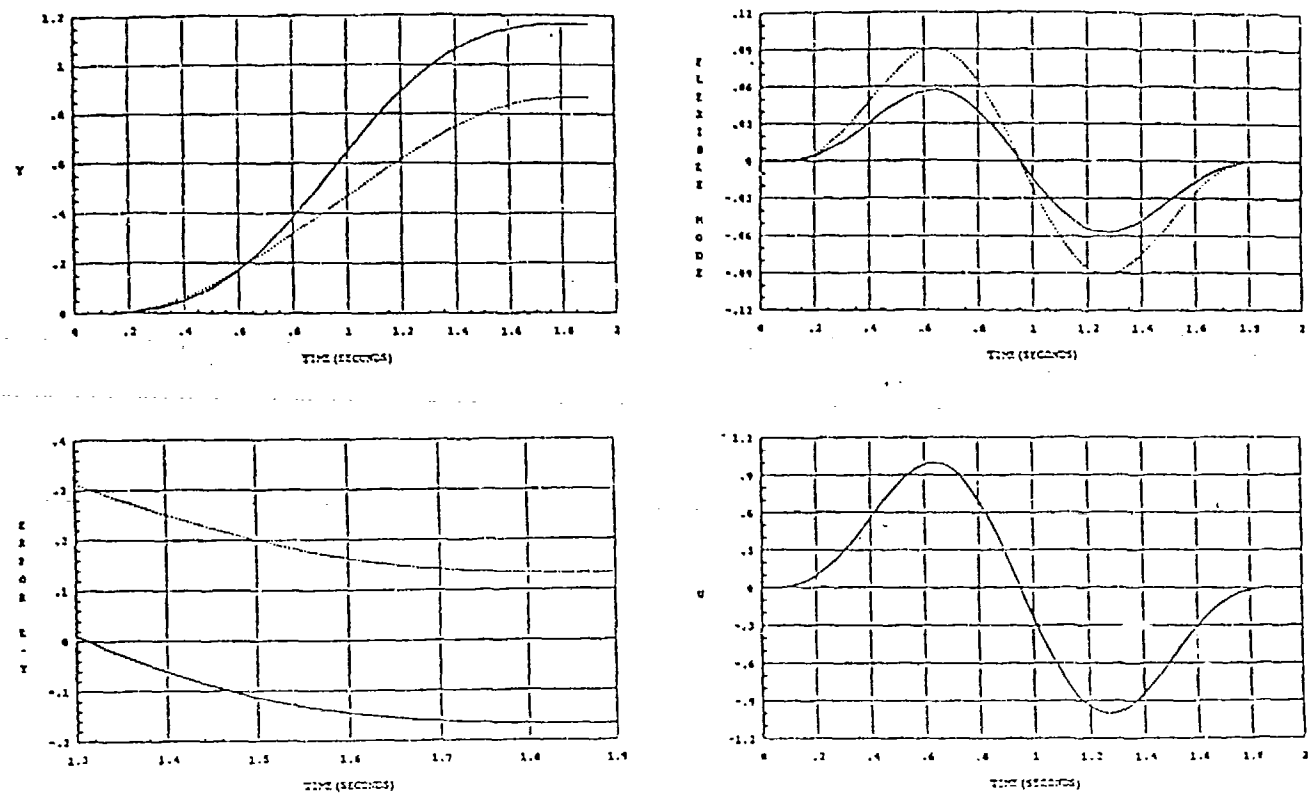

Figure 8: Case 5, Nonrobustness of the Sine-Versine Control Algorithm
—— $\omega_n = 30$ rad-sec^{-1} ; $a_r = 3.5$
. . . . $\omega_n = 24$ rad-sec^{-1} ; $a_r = 2.6$

Appendix D

Published in the *Proceedings of the American Control Conference*, Pittsburgh, Pennsylvania, June 1989.

Adaptive Time-Optimal Control of Flexible Structures

A. M. Pascoal & R. L. Kosut
Integrated Systems Inc.
2500 Mission College Blvd.
Santa Clara, CA 95054

G. F. Franklin & D. R. Meldrum
Information Systems Laboratory
Stanford University, CA 94305

M. L. Workman
IBM Corporation
5600 Cottle Road
San Jose, CA 95193

Abstract The Extended Proximate Time-Optimal Servo (XPTOS) developed in [8] is analyzed for stability using new techniques, and the performance of it compared against alternate methods such as sine-versine for the fast slewing of flexible structures. The XPTOS system operates in closed loop, and blends in its structure the characteristics of a time-optimal control law and the fine tracking properties of a properly tuned linear regulator. This study is addressed to the (idealized) case of flexible structures that contain a single or dominant structural mode. Simulation results demonstrate the performance of the XPTOS, and delineate its range of applicability.

1 Introduction

The advent of lightweight flexible structures has presented engineers and theorists with a multitude of challenging tasks in the area of control systems design (e.g., [2], [3], [6], [7]). Required are sophisticated control algorithms that make optimal use of the maximum torque available for rapid slew, and achieve high positioning or tracking accuracy after the position or tracking error has become sufficiently small.

In this paper, we develop a practical time-optimal controller for rapid slewing of flexible structures; in particular, the case where the structure model contains a *single* structural mode. A nonlinear feedback controller is obtained that blends the time-optimal characteristics of a switching control law, and the fine tracking properties of a properly tuned linear regulator. The approach pursued here is a reiteration and extension to the original work by Workman [8], [10], [9] on a proximate time-optimal servomechanism (PTOS), and on an extended adaptive form of PTOS (XAPTOS) for control of both rigid structures with high frequency unmodeled dynamics that are outside of the performance bandwidth, as well as flexible structures with resonances close to but beyond the bandwidth of the linear regulation mode of operation. The techniques exposed in [10], [9] are extended by taking directly into account the existence of a lightly damped structural mode as was done by Workman in [10], and in addition provide a technique suggested by Franklin which aids in extension of XAPTOS (or XPTOS without the adaptive feature) to the case of a flexible mode or modes which may possibly be within the performance bandwidth. Numerical simulations show that the XPTOS algorithm is robust against plant parameter variations.

The paper is organized as follows. Section 2 contains a brief description of the proximate time-optimal servomechanism (PTOS) presented in [8], [9]. Section 3 is devoted to the extended proximate time-optimal servomechanism (XPTOS) and presents some new theoretical results on stability. Section 4 illustrates the performance of the XPTOS via a parametric study. Section 5 describes the extended adaptive proximate time-optimal servomechanism (XAPTOS) which combines the XPTOS with a weighted recursive least squares (WRLS) identification of the plant parameters as developed in [8]. Finally, Section 6 contains the conclusions and suggestions for future research.

2 Time-Optimal Control of a Rigid Body

2.1 The Proximate Time-Optimal Servomechanism: A Review

Let the plant P be described by the system of equations

$$\begin{aligned} \dot{y} &= v \\ \dot{v} &= a_r \,\mathrm{sat}(u) \end{aligned} \tag{1}$$

where u and y denote the plant input and output respectively, a_r is the maximum magnitude of (rigid body) acceleration available, and $\mathrm{sat}(\cdot)$ is the normalized saturation function, *i.e.*, $\mathrm{sat}(x) = x$, $|x| \leq 1$ and $\mathrm{sat}(x) = \mathrm{sgn}(x)$, $|x| > 1$ where $\mathrm{sgn}(\cdot)$ is the "sign" function. Given an initial state (y_0, v_0) at time $t = 0$, suppose it is required to reach a desired state $(y, v) = (y_{\mathrm{des}}, 0)$ in minimum time. The well known time-optimal controller is given by [4]

$$\begin{aligned} u &= \mathrm{sgn}\left(f_{\mathrm{tos}}(e) - v\right) \\ f_{\mathrm{tos}}(e) &= \mathrm{sgn}(e)\sqrt{2a_r|e|} \\ e &= y_{\mathrm{des}} - y \end{aligned} \tag{2}$$

The time-optimal control law (2), although optimal, is not practical. In fact, the existence of process or measurement noise will make the control signal u "chatter" between its maximum and minimum values, thus exciting unmodeled dynamics that are always present in a more accurate model of a real plant. Even in the absence of exogenous signals, the time-optimal controller lacks robustness with respect to neglected dynamics, as the presence of (ignored) lightly damped modes may induce the onset of limit cycles (Workman, [8]). To circumvent these difficulties, a proximate time-optimal servomechanism (PTOS) was introduced by Workman [8] and Workman, Kosut, and Franklin [9]. The resulting control system is diagrammed in Figure 1.

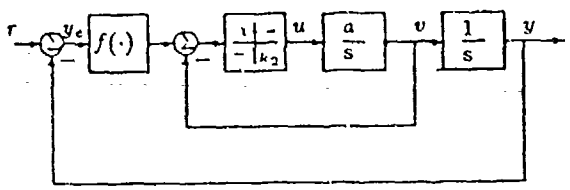

Figure 1: Proximate Time-Optimal Servomechanism

The equations describing the PTOS controller are

$$u = K_2[f_{\text{ptos}}(e) - v]$$

$$f_{\text{ptos}}(e) = \begin{cases} (K_1/K_2)e, & |e| \le e_\ell \\ \text{sgn}(e)\left[\sqrt{2a|e|} - 1/K_2\right], & |e| > e_\ell \end{cases} \quad (3)$$

where K_1, K_2, a, and e_ℓ are positive real constants and are the control design variables. Observe that whenever $|e| \le e_\ell$, the PTOS control is linear, that is

$$u = K_1 e - K_2 v, \quad \forall |e| \le e_\ell$$

Thus, e_ℓ is the size of the linear region, K_1, K_2 are the linear position and velocity control gains, respectively, and the constant a is a design acceleration.

As explained in reference [8], the linear and nonlinear portions of $f_{\text{ptos}}(\cdot)$ in (3) can be connected in such a way as to preserve the continuity of $f_{\text{ptos}}(\cdot)$ and its derivative. This requires the satisfaction of the following constraints:

$$a = \frac{2K_1}{K_2^2} \qquad e_\ell = \frac{1}{K_1} \quad (4)$$

With the above constraints, we have the following stability result from [8], [9].

Theorem 1 (Rest-to-Rest Stability) *The equilibrium state $(y, v) = (y_{\text{des}}, 0)$ of the system (1) with PTOS controller (3) is globally asymptotically stable if*

$$0 < a < a_r \quad (5)$$

The ratio a/a_r is referred to in [9] as the *acceleration discount factor*. Thus, during deceleration the PTOS controller uses less acceleration than is actually available. The acceleration a will be referred to here as the *discount acceleration*.

2.2 Designing the Linear Controller

Let $H(s) = Y(s)/R(s)$ denote the transfer function of the closed-loop system of figure 1, when operating in the linear region. With the usual notation for a second order system, and using (9), it follows that

$$H(s) = \frac{\omega_d^2}{s^2 + 2\zeta_d\omega_d s + \omega_d^2} \quad (6)$$

provided that,

$$K_1 = \omega_d^2/a_r \qquad K_2 = 2\zeta_d\omega_d/a_r \quad (7)$$

Using the constraints (4),

$$a = a_r/(2\zeta_d^2) \qquad e_\ell = a_r/\omega_d^2 \quad (8)$$

Clearly then, from the above Theorem, $a < a_r$ if $\zeta_d > 1/\sqrt{2}$, and hence, rest-to-rest stability of the PTOS system is insured.

Thus, the overall closed-loop system bandwidth ω_d and damping factor ζ_d can be independently controlled by the parameters K_1 and a, respectively. As shown in [8]–[9], the PTOS algorithm can be applied to the control of a purely rigid body with high frequency dynamics that are outside of the performance bandwidth ω_d. However, if the structural modes are within the desired closed loop system bandwidth, then they must be treated explicitly in the initial design. This is the subject of Section 3.

3 Time-Optimal Control of a Flexible Structure

The flexible structure to be controlled is described by

$$\begin{aligned} \dot{x}_r &= v_r \\ \dot{v}_r &= a_r \,\text{sat}(u) \\ \dot{x}_f &= v_f \\ \dot{v}_f &= -2\zeta_f\omega_f v_f - \omega_f^2 x_f + a_f \,\text{sat}(u) \\ y &= x_r + x_f \end{aligned} \quad (9)$$

The transfer function from $\text{sat}(u)$ to the output y is then $P(s) = P_r(s) + P_f(s)$ where

$$P_r(s) = \frac{a_r}{s^2} \qquad P_f(s) = \frac{a_f}{s^2 + 2\zeta_f\omega_f s + \omega_f^2} \quad (10)$$

The states (x_r, v_r) denote the rigid-body mode and (x_f, v_f) denotes the flexible mode at frequency ω_f with modal damping ζ_f. Without any rate damping mechanism, $\zeta_f << 1$, a typical range being $\zeta_f \in [.001, .005]$.

3.1 The structure of the XPTOS

The rationale behind the XPTOS can be explained as follows. To steer the structure from an initial rest position to a target rest position, the PTOS control strategy is first applied to control the rigid body motion, and later smoothly blended into a linear state-feedback control law that actively damps out the structural mode vibration induced by the PTOS control law. Although the idea for the XPTOS *structure* was already presented in [8], here we define an approach to the problem of flexible modes within the bandwidth of the controller by separating the rigid body motion and the flexible motion.

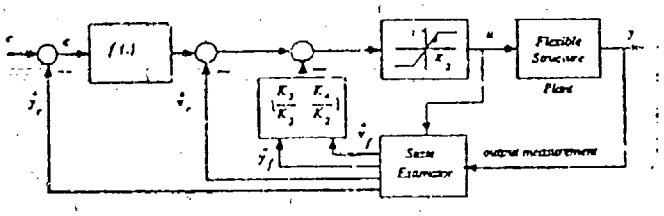

Figure 2: The Extended Proximate Time Optimal Servomechanism (XPTOS)

The resulting control scheme, depicted in Figure 2, is described as follows:

$$\begin{aligned} u &= K_2[f_{\text{ptos}}(\hat{e}_r) - v_r] - u_f \\ \hat{e}_r &= y_{\text{des}} - \hat{x}_r \\ u_f &= K_3\hat{x}_f + K_4\hat{v}_f \end{aligned} \tag{11}$$

The quantities $\hat{x}_r, \hat{v}_r, \hat{x}_f, \hat{v}_f$ are estimates (or measurements) of x_r, v_r, x_f, v_f, respectively, and $\hat{e}_r$ is an estimate of the rigid-body position error $e_r = y_{\text{des}} - x_r$. Observe that in the PTOS controller (3) the error used there is the output error $e = y_{\text{des}} - y$.

Suppose that y, u are the available measurements. Then a state observer system is of the form:

$$\begin{aligned} \dot{\hat{x}}_r &= \hat{v}_r + L_1(y - \hat{y}) \\ \dot{\hat{v}}_r &= a_r \,\text{sat}(u) + L_2(y - \hat{y}) \\ \dot{\hat{x}}_f &= \hat{v}_f + L_3(y - \hat{y}) \\ \dot{\hat{v}}_f &= -2\zeta_f\omega_f\hat{v}_f - \omega_f^2\hat{x}_f + a_f \,\text{sat}(u) + L_4(y - \hat{y}) \\ \hat{y} &= \hat{x}_r + \hat{x}_f \end{aligned} \tag{12}$$

The observer gains $L_1, \ldots, L_4$ are chosen by the usual means so that $(\hat{x}_r, \hat{v}_r, \hat{x}_f, \hat{v}_f) \to (x_r, v_r, x_f, v_f)$ as $t \to \infty$, exponentially fast. Recall that to select the observer gains in this way requires precise knowledge of the plant parameters a_r, ω_f, ζ_f, and a_f.

3.2 Stability of XPTOS: Full State Feedback

We now present a new stability result for rest-to-rest maneuvers of (9) using the XPTOS control with *full* state feedback. Due to limited space the proof is omitted and is available upon request. The control is

$$\begin{aligned} u &= K_2[f_{\text{ptos}}(e_r) - v_r] - u_f \\ e_r &= y_{\text{des}} - x_r \\ u_f &= K_3x_f + K_4v_f \end{aligned} \tag{13}$$

Before stating the stability result, we define the transfer functions $G(s)$ and $F(s)$ by

$$G(s) \stackrel{\text{def}}{=} \frac{1}{s}F(s) \stackrel{\text{def}}{=} \frac{P_r(s)}{1 + (K_2 s)P_r(s) + (K_3 + K_4 s)P_f(s)} \tag{14}$$

With $P_r(s)$ and $P_f(s)$ from (10),

$$F(s) = \frac{a_r(s^2 + 2\zeta_f\omega_f s + \omega_f^2)}{s^3 + \beta s^2 + \Upsilon s + K_2 a_r \omega_f^2} \tag{15}$$

where $\beta = K_2a_r + K_4a_f + 2\zeta_f\omega_f$ and $\Upsilon = \omega_f^2 + K_3a_f + 2\zeta_f\omega_f K_2 a_r$. Observe that $G(s)$ is the transfer function from $K_2 f_{\text{ptos}}(e)$ to x_r when the control is unsaturated, *i.e.*, $|u| \le 1$.

Theorem 2 (XPTOS: Rest-to-Rest Stability) *Referring to the system of Figure 2 as described by (9) and (11), suppose that:*

(i) *$F(s)$ in (15) is stable.*

(ii) *There exists a constant $q \ge 0$ such that for $G(s)$ in (14),*

$$\text{Re}[(1 + j\omega q)G(j\omega)] + 1/K_1 > 0, \quad \forall \omega \in \mathbb{R} \tag{16}$$

(iii) *The discount accele[illegible] $(\cdot)$ satisfies*

$$0 < a < \frac{a_r}{2} \tag{17}$$

where

$$\begin{aligned} g_f(t) &= \mathcal{L}^{-1}\{(K_3 + K_4 s)P_f(s)\} \\ h_f(t) &= \mathcal{L}^{-1}\{[-\omega_f^2 K_4 + \\ &\qquad (K_3 - 2\zeta_f\omega_f K_4)]P_f(s)\} \end{aligned} \tag{18}$$

and where $\|\cdot\|_1$ denotes the L_1-norm $\|f\|_1 = \int_0^\infty |f(t)|\,dt$.

Under these conditio[illegible] system is rest-to-rest stable, that is, [illegible] is initially at rest, then for all $y_{\text{des}} \in \mathbb{R}$, the state (x_r, v_r, x_f, v_f) asymptotically approaches $(y_{\text{des}}, 0, 0, 0)$.

Graphical Frequency Test

Condition (ii) has the following well known geometric interpretation, *e.g.*, [1]. Plot $\omega\text{Im}[G(j\omega)]$ vs. $\text{Re}[G(j\omega)]$ as ω varies in $[0, \infty)$. This plot is known as the *Popov plot of $G(s)$*. Condition (ii) states that the Popov plot must lie to the right of a straight line of positive slope $1/q$

passing through the point $-1/K_1 + j0$. Thus, condition (ii) can be checked graphically.

As an example, we show that Theorem 1 (control of a pure rigid body) is a special case of Theorem 2 with

$$a_f = K_3 = K_4 = 0$$

Thus, condition (iii) becomes

$$0 < a < a_r$$

as stated in (5). To satisfy (i) and (ii), we have

$$G(s) = \frac{1}{s}\left(\frac{a_r}{s + K_2 a_r}\right)$$

In this case $F(s)$ from (15) is stable because a_r and K_2 are both positive. Moreover,

$$\begin{aligned} \mathrm{Re}[G(j\omega)] &= -\frac{a_r}{\omega^2 + a_r^2 K_2^2} \\ \omega \mathrm{Im}[G(j\omega)] &= -\frac{a_r^2 K_2}{\omega^2 + a_r^2 K_2^2} \end{aligned}$$

Thus,

$$\omega \mathrm{Im}[G(j\omega)] = a_r K_2 \mathrm{Re}[G(j\omega)]$$

This means that the Popov plot is a straight line through the origin with a positive slope and is always to the right of the point $-1/K_1 + j0$ for any value of $K_1 > 0$, and so (iii) holds. This proves the PTOS Theorem.

4 Parametric Study of XPTOS

The study described in this section was motivated by the following question: for what values of the plant parameters $a_r, a_f, \omega_f, \zeta_f$ is the XPTOS effective in rapidly slewing the structure from an initial to a final rest position? In particular, (i) how far is the XPTOS performance from being time-optimal, and (ii) what improvement does it show when compared with the slewing maneuvers that are obtained by simply using the PTOS, with complete disregard for the structural mode? In this section we assess the domain of applicability of the XPTOS by fixing the rigid body parameter a_r, and letting a_f and ω_f vary over a certain range. For simplicity, we consider the case where $\zeta_f = 0$.

4.1 Time-Optimal Slewing

Time-optimal rest-to-rest maneuvers for flexible structures with control input saturation have been characterized in the work of Ben-Asher, Burns, and Cliff [16] and Singh, Kabamba, and McClamroch [17]. For the problem at hand, the time-optimum rest-to-rest control $u^*(t)$ exists and is unique, is bang-bang, and exhibits antisymmetric characteristics, *i.e.*,

$$u^*(t_f - \tau) = -u^*(t_f + \tau), \quad 0 \le \tau \le t_f/2$$

where t_f is the optimum slewing time (see [17]. Furthermore, $u^*(t)$ can be computed using the methods described in [17] and [16]. For the flexible structure (9), (10) with $a_r = 30$ and $\zeta_f = 0$, Figure 3 is a plot of the optimal slewing time as a function of the structural mode natural frequency ω_f, as the structure is subject to rest-to-rest maneuvers of amplitude $|y_{des}| = 1$. This represents a fundamental limitation to the performance that is achievable with bounded input control, and as such, it is a benchmark against which the performance of other algorithms can be compared. An interesting fact

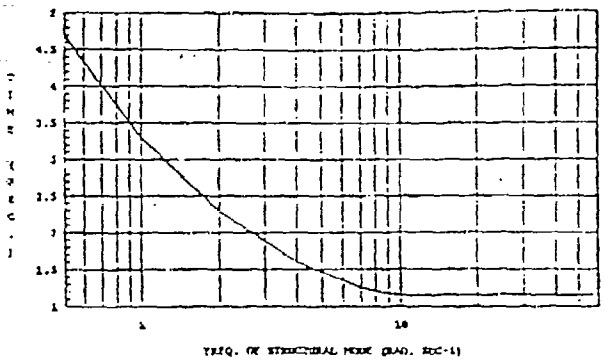

Figure 3: Time-Optimal Control of a Flexible Structure (Performance Characteristics)

is that the optimal control strategy is independent of the ratio a_f/a_r, and the optimal slewing time is very close to the rigid body optimal maneuver time for sufficiently large values of ω_f. As the natural frequency of the structural mode decreases, the optimal slewing time becomes increasingly larger (see [16] for a thorough discussion concerning the asymptotic behavior of the time-optimal solution).

4.2 Performance of PTOS and XPTOS

The PTOS and XPTOS control algorithms were tested by subjecting the flexible structure (9), (10) to rest-to-rest maneuvers with amplitude $|y_{des}| = 1$. The parameters a_r and ζ_f were fixed at 3.0 and 0.0 respectively, while a_f/a_r and ω_f were varied over the discrete sets

$$S_{a_f/a_r} = \{.25, .5, 1.0, 2.0, 3.0\} ,$$

and

$$S_{\omega_f} = \{8, 9, 10, 12, 14, 16, 18, 20, 30, 40, 50\} ,$$

respectively. Assuming that both the output position and velocity and available for measurement, the PTOS was designed taking into account the rigid body motion, only. This led to the design parameters $K_1 = 20$ and $a/a_r = .9$, irrespective of the values assumed by the parameters in the sets S_{a_f/a_r} and S_{ω_f}. Figure 4 is a plot

of slewing time versus a_f/a_r and ω_f, where the slewing time here is defined as the time after which the tracking error $y_{des} - y$ becomes smaller than .01.

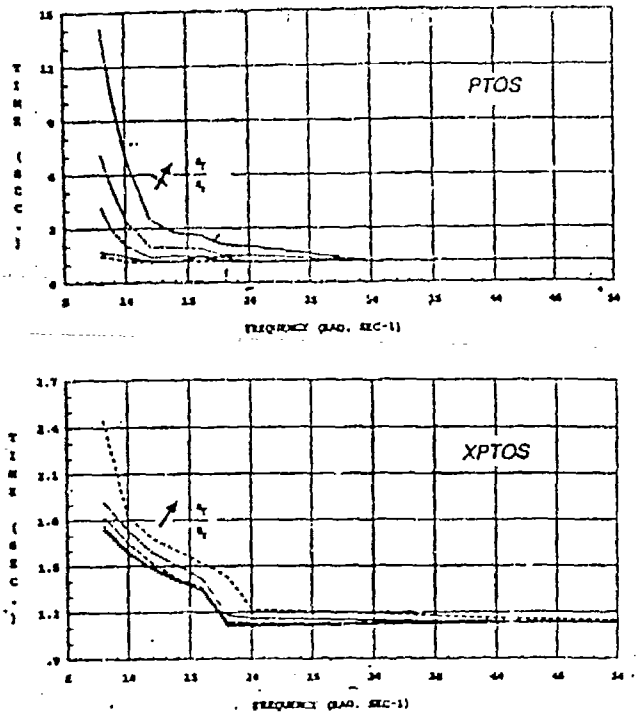

Figure 4: Performance of PTOS and XPTOS (Slewing Time Versus Frequency of Structural Mode)

For large values of ω_f and/or small values of a_f/a_r, the practical slewing time approaches the time-optimal rigid body maneuver time. As the frequency ω_f decreases or a_f/a_r increases, the PTOS maneuver time increases rapidly in comparison with the theoretical optimum value. The XPTOS maneuver time exhibits the same trend in behavior, but the performance deterioration occurs at a slower rate. In fact, over the range of frequencies [8, 20] rad sec^{-1} its performance shows a drastic improvement over the performance obtained with the XPTOS.

5 Adaptive Control

If the flexible parameters ω_f and a_f are not known or are slowly changing, the performance of the flexible structure may be improved with an adaptive XPTOS algorithm called XAPTOS. In this section the XAPTOS strategy (see [8], [9], [10]) is described and applied to the flexible structure (9), (10). The discrete-time system is more efficient to implement than the continuous-time system and hence a discrete-time version of the XPTOS control (11) is combined with a parameter identifier and a state estimator to form XAPTOS.

5.1 XAPTOS for a Flexible Structure

The main idea behind XAPTOS is to combine a general self tuning observer controller (GSTOC) [8] with the XPTOS controller. A weighted recursive least squares (WRLS) algorithm is used to identify the unknown plant parameters and a state space model of the plant is formed. The estimator and control gains are obtained via pole placement and used in the XPTOS controller.

A development of XAPTOS for the flexible structure (9), (10) is now described. The overall dynamic relationship between the input and output of the structure is described by the discrete-time transfer function $P(z^{-1}) = P_r(z^{-1}) + P_f(z^{-1})$ where

$$\begin{aligned} P_r(z^{-1}) &:= a_r \frac{T^2}{2} \frac{z^{-1}+z^{-2}}{1-2z^{-1}+z^{-2}} \\ P_f(z^{-1}) &= \frac{a_f(1-\cos\omega_f T)(z^{-1}+z^{-2})}{\omega_f^2(1-2\cos\omega_f T z^{-1}+z^{-2})} \end{aligned}$$

and T is the sampling interval. Assuming that the rigid body parameter a_r is known, the problem is to determine the flexible mode parameters a_f and ω_f from the measurement vector which forms the regressor

$$\phi^T(k) = [\eta(k-1) \;\; \mu(k-1)]$$

where

$$\begin{aligned} \eta(k) &= y(k) - 2y(k-1) + y(k-2) - \\ &\quad c_0(u(k-1) + u(k-2) \\ \mu(k) &= u(k) - u(k-1) - u(k-2) + u(k-3) \\ c_0 &= a_r \frac{T^2}{2} \\ c_1 &= 2\cos\omega_f T \\ c_2 &= \frac{a_f}{\omega_f}(1-\cos\omega_f T) \end{aligned}$$

Then the input-output behavior is described by

$$Y_f(k) = \hat{\theta}^T(k)\phi(k), \quad k = 0, 1, 2, \ldots$$

where $\hat{\theta}(k) = [c_1 \;\; c_2]^T$ and $Y_f(k) = \eta(k) + \eta(k-2)$ is a function of $y(j)$ and $u(j)$, $j = k-4, \ldots, k$. The parameter vector $\hat{\theta}(k)$ can then be determined using WRLS:

$$\hat{\theta}(k+1) = \hat{\theta}(k) + \left[\frac{P(k-1)\phi(k)}{\kappa^{-1} + \phi^T(k)P(k-1)\phi(k)}\right](y(k) - Y_f(k))$$

$$P(k) = \frac{1}{\gamma}P(k-1) - \frac{1}{\gamma}\left[\frac{P(k-1)\phi(k)\phi^T(k)P(k-1)}{\kappa^{-1} + \phi^T(k)P(k-1)\phi(k)}\right]$$

where $0 < \gamma < 1$ and $\kappa = 1 - \gamma$.

With the parameter estimates a_f and ω_f, a state-space model of the plant is formed which partitions the known double integrator plant from the identified flexible mode and has the state vector:

$$x^T(k) = [x_r \;\; v_r \;\; x_f \;\; v_f]$$

A state vector of this form is desirable since the position and velocity estimates are needed in the XPTOS control algorithm.

With the state space model, a state estimator and a controller are constructed for the plant. The desired estimator and controller characteristic polynomials, α_e and α_c, are formed by the known rigid body mode pole locations and a radial pole projection of the identified flexible mode pole locations. The estimator and control gains are determined via pole placement. A closed form expression of the estimator gains, L, and the control gains, K, are determined and used on-line in the XAPTOS algorithm:

$$L = e^T[h^T \ \Phi^T h^T \ \Phi^{2^T} h^T \ \Phi^{3^T} h^T]^{-1} \alpha_e(\Phi^T)$$

$$K = e^T[\Gamma \ \Phi\Gamma \ \Phi^2\Gamma \ \Phi^3\Gamma]^{-1} \alpha_c(\Phi)$$

5.2 Simulation Results

The XAPTOS algorithm as described above but with full-state feedback was implemented in simulations on the flexible structure (9), (10). Figure 5 presents the results of the identification of a_f and ω_f. Future results will include the case of XAPTOS with both the identifier and the state estimator.

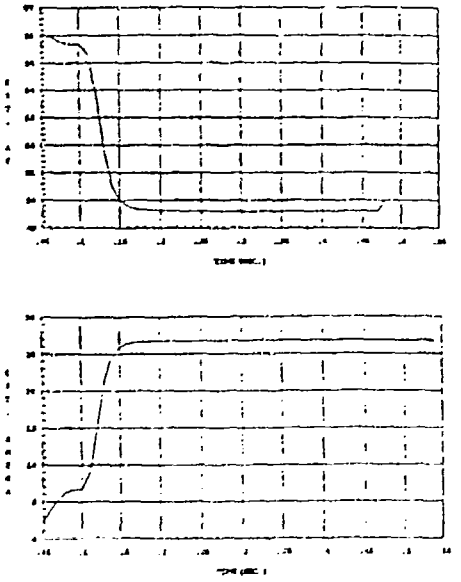

Figure 5: Identification of Plant Parameters a_f (top) and ω_f (bottom)

6 Concluding Remarks

In this paper, we have developed an Extended Proximate Time-Optimal Servo (XPTOS) for rapid slewing of flexible structure models containing a single structural mode. Some preliminary results were obtained concerning the stability of the proposed closed-loop control scheme. The performance of the control algorithm was illustrated with a representative example, which displays the fine slewing and tracking properties of the XPTOS, as well as its robustness against plant parameter variation. A detailed parametic study was conducted to assess the domain of applicability of the XPTOS. The XAPTOS algorithm was described and shown to adaptively control the flexible structure.

Future work requires a complete analysis of the stability of the XPTOS. It is also our objective to refine the design technique exposed in section 3 to accommodate disturbances and sensor noise, and provide robustness against the presence of neglected high frequency structural modes.

References

[1] M. Vidyasagar, *Nonlinear Systems Analysis*, Prentice-Hall, New Jersey, 1978.

[2] E. Schmitz and R. Cannon, Jr. " *Further Experiments on the End-Point Control of a Flexible One Link Robot*", Journal of Dynamic Systems, Measurement and Control, 1985.

[3] J.N. Aubrun, N.K. Gupta, M.G. Lyons and G. Margulies, *"Large Space Structures Control. An Integrated Approach"*, Proceedings of the AIAA Guidance and Control Conference, Boulder, CO, August 1979.

[4] E.B. Lee and L. Markus, *"Foundations of Optimal Control Theory "*, Wiley, New York, 1967.

[5] R. Oldenburger, editor *"Optimal and Self-Optimizing Control"*, the M.I.T. press, Cambridge, MA, 02142, 1966.

[6] M. Barrett and D. Dugajski, *"Robust Control of a Large Space Antenna"*, AIAA Guidance, Navigation and Control Conference, August 1987, Monterey.

[7] M. Floyd, *"Single-Step Optimal Control of Large Space Structures Model"*, Department of Aeronautics and Astronautics, MIT, Sc.D. Thesis, June 1984.

[8] M.L. Workman, *"Adaptive Proximate Time-Optimal Servomechanisms"*, Ph.D. thesis, Stanford University, 1987.

[9] M.L. Workman, R.L. Kosut and G.F. Franklin, *"Adaptive Proximate Time-Optimal Servomechanisms: Continuous-Time Case"*, Proceedings Automatic Control Conference, June 1987, Minneapolis

[10] M.L. Workman, R.L. Kosut, and G.F. Franklin, sl "Adaptive Proximate Time-Optimal Servomechanisms: Discrete-Time Case", IEEE Conference on Decision and Control, December 1987, Los Angeles.

[11] C. Johnson and W. Wonham, *"On a Problem of Letov in Optimal Control"*, Proc. 1964 JACC, Minneapolis.

[12] S.F. Schmidt, *"The Analysis and Design of Continuous and Sampled Data Feedback Control Systems with a Saturation Type Nonlinearity"*, Ph.D. Thesis, Stanford University, 1959.

[13] M. Vidyasagar, *"Nonlinear Systems Analysis"*, Prentice-Hall, 1978.

[14] J. Salle and S. Lefschetz, *"Stability by Liapunov's Direct Method"*, Academic Press, 1961.

[15] H. Kwakernaak and R. Sivan, *"Linear Optimal Control Systems"*, John Wiley & Sons, Inc., 1972.

[16] J. Ben-Asher, J. Burns, and E. Cliff, *"Time Optimal Slewing of Flexible Spacecraft"*, Proceedings of the 26th Conference on Decision and Control, December 1987, Los Angeles.

[17] G. Singh, P. Kabamba, and N. Clamroch, *"Time Optimal Slewing of a Rigid Body with Flexible Appendages"*, Proceedings of the 26th Conference on Decision and Control, December 1987, Los Angeles.

Appendix E

To appear in the *Proceedings of the IEEE Conference on Decision and Control*, Brighton, United Kingdom, December 1991.

Fast Finite-Time Tracking with Saturating Actuators

M. Güntekin Kabuli R. L. Kosut *

Integrated Systems Inc., 3260 Jay Street, Santa Clara, CA 95054-3309

Abstract

An approximation to the time-optimal tracking problem is expressed in terms of a sequence of linear programs which are set up using a transfer function approach. The results are applicable to any linear time-invariant finite-dimensional multi-input multi-output plant. An example illustrates the feasibility of the approach.

1. Introduction

Pontryagin's Maximum Principle (see e.g., [1]) brings a complete solution to the problem associated with the minimum-time tracking (of a fixed or moving target) subject to actuator saturation. In order for such an approach to be implementable, one requires a characterization of the switching surfaces in the state-space. Complete solutions for single-input single-output low order models have been derived in the literature. The bang-bang nature of the solution requires a relay in the implementation; hence, chattering subject to disturbances. One way to overcome this difficulty is to approximate the infinite-gain nonlinearity (namely, the relay) with a finite-gain nonlinearity. Hence one is bound to step back from the time-optimal result for the sake of implementation. Even if one reformulates the open-loop minimum-time problem as a fast finite-time tracking problem (for a given reference trajectory, determine an input (subject to actuator saturation) so that the tracking error remains at zero after a finite time-instant) a feasible solution method for a closed-loop design generally remains a challenge. The demand for fast tracking with saturating actuators has produced a variety of closed-loop implementations ranging from using idealized relays, finite-gain relays, adaptation methods, etc. [6,7,8] . In the meantime, openloop solution to the problem with flexible modes has been studied in detail, for specific cases with no damping. The resulting proposed nonlinear optimization problems are derived using the necessary optimality conditions posed by the Maximum Principle, for specific plant models [2,5] .

In this paper, an approximation to the time-optimal tracking problem is proposed for linear time-invariant finite-dimensional multi-input multi-output plants. The approximation relies on a transfer function approach to formulate constraints on the set of admissible finite-duration signals that achieve precise point-to-point positioning of flexible structures [3] . The results reported in this paper have already been used to design fast finite-time tracking *closed-loop* feedback systems. Due to space limitations, a portion of the open-loop results are reported. An example illustrates the feasibility of the approach.

2. Preliminaries

Let the plant, P , be strictly proper and have a minimal state-space description (A,B,C) , with n_i inputs, n_o outputs and n_s states. The state-space description can be in continuous-time or discrete-time. The results will be exclusively stated for the continuous-time strictly proper multi-input multi-output plant P . Since the approach relies on a rational transfer function description, with appropriate modifications, discrete-time setting can also be handled.

Definition ($\mathcal{U}_T$) : For a given $T \in (0,\infty)$, $\mathcal{U}_T$ denotes the set of all bounded inputs of duration T , where

$\mathcal{U}_T := \{ u : \mathbb{R}_+ \to \mathbb{R}^{n_i} \mid u(t) = 0 \text{ for } t > T \ , \ \|u\|_\infty < \infty \}$. □

Definition (T-track) : For a given $T \in (0,\infty)$, y is said to T-track r iff $y(t) = r(t)$ for all $t \geq T$. □

Fact 1 : For a given plant P with a minimal description (A,B,C) , and a reference r , there exists an input $u \in \mathcal{U}_T$ such that $(P * u)$ T-tracks r if and only if $r \in \mathcal{R}_T$, where

$$\mathcal{R}_T := \left\{ r : \mathbb{R}_+ \to \mathbb{R}^{n_o} \mid r(t) = Ce^{At}x_0, x_0 \in \mathbb{R}^{n_s}, t \geq T \right\} . \square$$

From Fact 1 , we conclude that the Laplace transform of a signal in $\mathcal{R}_T$ can only have poles at the plant poles.

Fact 2: For a given plant P with a minimal description (A,B,C) , let $r \in \mathcal{R}_T$. Then there exists a unique $r_T \in \mathcal{U}_T$ and a unique $x_r \in \mathbb{R}^{n_s}$ such that $r(t) = r_T(t) + Ce^{At}x_r$. □

3. Transfer Function Approach

Let $r \in \mathcal{R}_T$ and the plant be at an initial state x_0 at $t = 0$. Let r_T and x_r describe the unique decomposition of r as in Fact 2 . The goal is to find a $u \in \mathcal{U}_T$ such that

$$R_T(s) + C(sI - A)^{-1}x_r = C(sI - A)^{-1}(x_0 + BU(s)) .$$

Without loss of generality, we assume that x_0 is zero. If x_0 is not zero, redefine x_r as $(x_r - x_0)$.

Proposition 1 : Let P have the expansion $P(s) = \sum_{i=1}^{k} \sum_{j=1}^{m_i} \frac{K_{ij}}{(s-s_i)^j}$, where $K_{ij} \in \mathbb{R}^{n_o \times n_i}$. Let $r \in \mathcal{R}_T$. Consider the unique decomposition $r =: r_T + r_{exp}$, where $r_T \in \mathcal{U}_T$ and $r_{exp} = Ce^{At}x_r$. Under these assumptions: 1. $r_{exp} \in \mathcal{R}_T$; moreover, $R_{exp}(s) = \sum_{i=1}^{k} \sum_{j=1}^{m_i} \frac{\widehat{K}_{ij}}{(s-s_i)^j}$, where $\widehat{K}_{ij} \in \mathbb{R}^{n_o}$. 2. The set of all signals $u \in \mathcal{U}_T$ such that $(P * u)$ T-tracks r is given by

$$\left\{ u \in \mathcal{U}_T \mid \widehat{K}_{i,(m_i-j+1)} = \frac{1}{(j-1)!} \left[\frac{d^{j-1}}{ds^{j-1}} \left[(s-s_i)^{m_i} P(s) U(s) \right] \right]_{s=s_i} , \right.$$
$$\left. i = 1, \ldots, k ; j = 1, \ldots, m_i \right\} . \square$$

A Convex Approximation to the Minimum-Time Tracking Problem : Choose a basis of $\mathcal{U}_T$; for a specified N , truncate it to a finite collection $\{h_i\}_{i=1}^{N}$. Consider the subclass of signals in $\mathcal{U}_T$ whose Laplace transforms are of the form $U(s) = \sum_{i=1}^{N} p_i H_i(s)$. Clearly, all of the matching constraints in Proposition 1 translate into a *linear* equation in terms of $p \in \mathbb{R}^N$, say, $\Gamma(T)p = \gamma$. The entries of γ are solely determined by the entries of $\widehat{K}_{ij}$ corresponding to r_{exp} (see Proposition 1) . We will refer to the space γ is in as the residue-space (an abuse of notation; after all, not all entries of γ correspond to the residues in the partial fraction expansion) . By introducing the actuation saturation constraints, we end up with a convex feasibility problem:

$$\text{Find } p \in \mathbb{R}^N \text{ such that } \Gamma(T)p = \gamma \text{ and } \|p^T h\|_\infty \leq 1 \ ,$$

where $h(t) := [h_1(t) \ \ldots \ h_N(t)]^T$. For a specified T and N , the maximum performance along the desired direction γ is determined by $\max_{p \in \mathbb{R}^N, \lambda \in \mathbb{R}} \lambda$. Clearly, one can then solve a sequence

$$\Gamma(T)p = \lambda\gamma$$
$$\|p^T h\|_\infty \leq 1$$

of convex minimization problems by varying T (and N) to sweep a maximum performance curve; hence, obtaining an approximation to the minimum-time problem.

A Particular Choice for $U(s)$: A time-optimal input signal is necessarily bang-bang. While there is no upper-bound on the finite number of switchings in general, for a fixed number of switchings, say N , one can choose a sequence of N pulses (with alternating amplitudes) with varying widths as a family of functions in $\mathcal{U}_T$. One can then solve for the constraints in Proposition 1 to obtain a family of nonlinear (non-convex) algebraic equations [4] . Similar algebraic equations are obtained by applying the Pontryagin's Maximum Principle to specific cases of P, using state-space computations [2,5] .

For a fixed T , consider the weighted sum of a sequence of N pulses with uniform widths (T/N) ; i.e., $U(s) = \frac{e^{sT/N}-1}{s} \sum_{k=1}^{N} p_k e^{-ksT/N}$. Since the input signal is piecewise constant, the actuation bounds can be expressed as $-1 \leq p \leq 1$, where $p \in \mathbb{R}^N$ is to be determined.

An Approximation to the Minimum-Time Problem by a Sequence of Linear Programs: For a given plant P and N , the maximum performance function $\Psi : (0,\infty) \times \mathbb{R}^n \to \mathbb{R}_+$ is defined in terms of the linear program $\Psi(T,\gamma) := \max_{p \in \mathbb{R}^N, \lambda \in \mathbb{R}} \lambda$,

$$\Gamma(T)p = \lambda\gamma$$
$$-1 \leq p \leq 1$$

where $\Gamma(T)$ is obtained by the matching conditions in Proposition 1 . Any $p \in \mathbb{R}^N$ for which the linear program returns the value $\Psi(T,\gamma)$, is used to define the relation $\Phi : (0,\infty) \times \mathbb{R}^n \to \mathbb{R}^N$, where

*Research supported by AFOSR under contract F49620 88 C-0012

$\Phi(T,\gamma) := \hat{p}$. For a specified time-instant T , $\Psi(T,\gamma)$ determines the maximum-performance one can achieve along the specified direction γ . For a fixed direction γ , by sweeping over T , one obtains the γ-maximum-performance curve $(T, \Psi(T,\gamma))$, $T \in \mathbb{R}_+$. Instead of generating the γ-maximum-performance curve for $T \in \mathbb{R}_+$, introduce a time-resolution of ΔT and discretize the curve; i.e., for a pre-determined k_{max} , evaluate $(T, \Psi(T,\gamma))$, $T = k\Delta T$, $0 \le k \le k_{max}$.

The sub-optimal (due to the approximations) time-instant $\hat{T}$ for which the residue γ is achieved is in the interval $\hat{T} \in [T_l, T_l + \Delta T]$, where $\Psi(T_l,\gamma) \le 1$, and $\Psi(T_l + \Delta T, \gamma) \ge 1$. The T-polytope $\mathcal{S}_T$,

$$\mathcal{S}_T := \{ \lambda\gamma \mid \gamma \in \mathbb{R}^n , \|\gamma\|_2 = 1 , \lambda \in [0, \Psi(T,\gamma)] \}$$

is the set of all points in the residue-space that can be reached in T seconds. The boundary of this set, denoted by $\partial\mathcal{S}_T$, is referred to as the T-isochrone. Consider the T-polytope $\tilde{\mathcal{S}}_T$ which is a subset of $\mathcal{S}_T$; $\tilde{\mathcal{S}}_T := \{ \sum_{i=1}^n \lambda_i \Psi(T,e_i) e_i \mid \|\lambda\|_1 \le 1 \}$, where $\{e_1, \ldots, e_n\}$ is a basis in $\mathbb{R}^n$.

A Map from the Residue-Space to the Input Space : Our goal is to construct a map, possibly using look-up tables, such that given a desired reference signal and the states of the plant, an input signal is generated so that the plant output T-tracks the reference signal as fast as possible. The desired reference signal (which should be in $\mathcal{R}_T$) and the initial state determines the amount of change necessary in the residues of the output signal. For this reason, we will focus on the following subproblem: For a given γ in the residue-space determine an input signal such that the output of the plant achieves the residues specified by γ as fast as possible. From now on, we will use the standard orthonormal basis $\{e_1, \ldots, e_n\}$ in $\mathbb{R}^n$. In order to cut down on the storage space, we will identify $\tilde{\mathcal{S}}_T$ with its "positive orthant":

$$\tilde{\mathcal{S}}_T := \{ \sum_{i=1}^n \lambda_i \Psi(T,e_i) e_i \mid \|\lambda\|_1 \le 1 , \lambda \ge 0 \} .$$

Let the signum function $SGN : \mathbb{R}^n \to \mathbb{R}^n$ be defined as the entry by entry signum function over $\mathbb{R}$. Let the operator $.*$ denote element-by-element product in $\mathbb{R}^n$. Suppose that $\gamma \in \partial\tilde{\mathcal{S}}_T$. Let $\hat{\gamma}$ be defined by $\gamma =: SGN(\gamma) .* \hat{\gamma}$. Clearly, $\gamma \in \partial\tilde{\mathcal{S}}_T$ if and only if $\hat{\gamma} \in \partial\tilde{\mathcal{S}}_T$. Since $\hat{\gamma}$ can be expressed as a convex combination

$$\hat{\gamma} =: \sum_{i=1}^n \hat{\lambda}_i \Psi(T,e_i) e_i , \quad \hat{\lambda} \ge 0 , \ \|\hat{\lambda}\|_1 = 1 ,$$

we conclude that the input that achieves $\hat{\gamma}$ residue in T seconds is represented by $\hat{p} = \sum_{i=1}^n \hat{\lambda}_i \Phi(T,e_i)$. The input that achieves γ residue in T seconds is represented by $p = \sum_{i=1}^n \hat{\lambda}_i \left(e_i^T SGN(\gamma)\right) \Phi(T,e_i)$. Note that $-1 \le p \le 1$.

We now outline the procedure:

1. Fix N , ΔT and k_{max} .
2. Solve $(n \cdot k_{max})$ linear programs; i.e., for the k_{max} time points solve for and store $\Psi(T,e_i)$, $\Phi(T,e_i)$, $i = 1, \ldots, n$.
3. For a given $\hat{\gamma}$ determine the smallest T such that $\hat{\gamma} \in \tilde{\mathcal{S}}_T$. We propose the following procedure: Let $\eta \in \mathbb{R}^{k_{max}}$ be defined as

$$e_k^T \eta := 1 / \left(\sum_{i=1}^n \frac{e_i^T \hat{\gamma}}{\Psi(T_k, e_i)} \right) , \quad k = 1, \ldots, k_{max} .$$

Let the ℓth entry of η be the first entry which is less than or equal to one. Since $\hat{\gamma}$ was in $\tilde{\mathcal{S}}_{(k_{max}\Delta T)}$ to start with, such an ℓ exists. Hence, we conclude that, among the family of T-isochrones, $\hat{\gamma}$ can be achieved no faster than T_ℓ seconds.

4. Once the index ℓ and the multiplier $e_\ell^T \eta$ is determined, extract the input sequence from $p \in \mathbb{R}^N$:

$$p := \sum_{i=1}^n \frac{(e_\ell^T \eta)(e_i^T \gamma)}{\Psi(T_\ell, e_i)} \Phi(T_\ell, e_i) .$$

Example

Consider the single-input single-output plant

$$P(s) = \frac{1}{s^2} + \sum_{i=1}^3 \frac{\alpha_i}{s^2 + 2\zeta_i\omega_i s + \omega_i^2} ,$$

where $[\alpha_1\ \alpha_2\ \alpha_3] = [5\ 10\ 20]$, $[\omega_1\ \omega_2\ \omega_3] = 2\pi\,[0.5\ 1\ 1.5]$ rad/s and $[\zeta_1\ \zeta_2\ \zeta_3] = [0.1\ 0.01\ 0.001]$. Clearly, the admissible r_{exp}'s are linear combination of steps, ramps and lightly-damped sinusoids. The vast majority of tracking problems restricts the references to to a linear combination of steps and ramps:

$$\{ r \mid r(t) = r_0 + r_1 t , \ r_0 \in \mathbb{R} , \ r_1 \in \mathbb{R} , \ t \ge 0 \} .$$

In order to show the efficiency of the proposed scheme, we will focus on actuation signals in $\mathcal{U}_T$, where $T \in [1,10]$s . Standard bang-bang actuation relying on the rigid-body approximation of P for rest-to-rest slewing over the interval $[1,10]$ s resulted in unsatisfactory outputs. We choose $N = 20$. All simulations were performed by sampling the plant P at 100 $\dots$. In order to have at least one sample instant added on for each time step ΔT , we choose $\Delta T = 0.2$s . We set up the linear programming problem, by constructing $\Gamma(T)$ from the matching conditions in Proposition 1 . For illustration purposes, we assume that the plant is initially at rest and the output is required to T-track steps and ramps only. We solve 46 linear programs along $\gamma = e_1$ and another 46 linear programs along $\gamma = e_2$. Let the reference trajectory r be as shown in Figure 1 (dashed line). The breakpoints and slopes in Figure 1 reveal that the sequence of inputs should satisfy the following increments in the residue-space denoted by the ordered pairs (r_0, r_1) : at $T = 0$, $(+2, 0)$; at $T = 5$, $(-2, -1)$; at $T = 12$, $(+7, +1)$. Using the one-hyperplane approximations to the 46 T-polytopes, the fastest tracking times for the sequence of residue increments are 3.2 , 4.6 and 7 s , respectively. Figure 1 shows the input and the associated output of P .

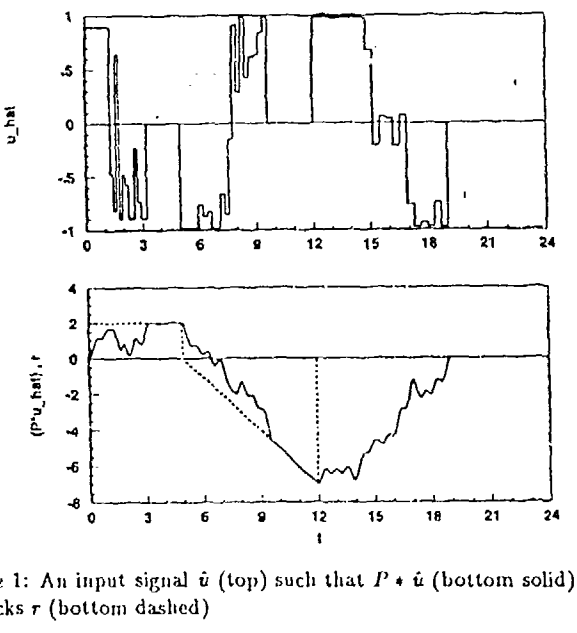

Figure 1: An input signal $\hat{u}$ (top) such that $P * \hat{u}$ (bottom solid) fast T-tracks r (bottom dashed)

References

[1] M. Athans and P. L. Falb, *Optimal Control: An Introduction to the Theory and Its Applications*, McGraw-Hill, 1966.

[2] J. Ben-Asher, J. A. Burns and E. M. Cliff, "Time-Optimal Slewing of Flexible Spacecraft," *Proc. of the IEEE Conference on Decision and Control*, pp. 524-528, Los Angeles, California, December 1987.

[3] S. P. Bhat and D. K. Miu, "Precise Point-to-Point Positioning Control of Flexible Structures," *Transactions of the ASME, Journal of Dynamic Systems, Measurement and Control*, vol. 112, no. 4, pp. 667-674, December 1990.

[4] S. F. Schmidt, *The Analysis and Design of Continuous and Sampled-Data Feedback Control Systems with a Saturation Type Nonlinearity*, Ph.D. Dissertation, Stanford University, June 1959.

[5] G. Singh, P. T. Kabamba and N. H. McClamroch, "Time-Optimal Slewing of a Rigid Body with Flexible Appendages," *Proceedings of the IEEE Conference on Decision and Control*, pp. 1441-1442, Los Angeles, California, December 1987.

[6] M. L. Workman, *Adaptive Proximate Time-Optimal Servomechanisms*, Ph.D. Dissertation, Stanford University, March 1987.

[7] M. L. Workman, R. L. Kosut and G. F. Franklin, "Adaptive Proximate Time-Optimal Control: Continuous-Time Case," *Proceedings of the Automatic Control Conference*, pp. 589-594, Minneapolis, Minnesota, June 1987.

[8] M. L. Workman, R. L. Kosut and G. F. Franklin, "Adaptive Proximate Time-Optimal Control: Discrete-Time Case," *Proceedings of the IEEE Conference on Decision and Control*, pp. 1548-1553, Los Angeles, California, December 1987.